

Alma Mater Studiorum – Università di Bologna

DOTTORATO DI RICERCA IN
INGEGNERIA DEI MATERIALI

Ciclo XXII

Settore scientifico-disciplinare di afferenza: ING-IND/22

**THE INCOMPLETE IONIZATION
OF SUBSTITUTIONAL DOPANTS
IN SILICON CARBIDE**

Presentata da: Raffaele Scaburri

Coordinatore Dottorato

Prof. Giorgio Timellini

Relatore

Prof.ssa Maria Chiara Bignozzi

Correlatori

Prof. Agostino Desalvo

Dott.ssa Roberta Nipoti

Esame finale anno 2011

To my family

Contents.

CONTENTS	v
INTRODUCTION	1
1. SILICON CARBIDE	3
1.1. History of Silicon Carbide	3
1.2. SiC crystalline structure and SiC polytypes	5
1.3. Band diagrams and effective masses	8
1.4. Main dopant impurities in SiC	12
2. OCCUPANCY OF ENERGY LEVELS	15
2.1. Occupation probability for discrete impurity levels	15
2.1.1. Occupancy of a monovalent impurity in its ground state	16
2.1.2. Occupancy of a monovalent impurity with excited states	19
2.2. Solution of the charge neutrality equation in some particular cases	21
2.3. General solution of the charge neutrality equation	24
Appendix. 2A. Useful properties of the space charge density function $\Phi(E_F)$	27
3. DOPANT IONIZATION ENERGY VARIATION	29
3.1. Experimental evidence for a dopant ionization energy variation	29
3.2. Pearson and Bardeen's model and its improvements	32
3.2.1. Pearson and Bardeen's model	32
3.2.2. Corrections to Pearson and Bardeen's model	35
3.2.3. Pearson and Bardeen's model as applied to SiC	36
3.3. A different model for the ionization energy variation	37

Contents

3.3.1. Static Coulomb screening	37
3.3.2. Evaluation of the screening radius	39
3.3.3. Approximate expression for the Fermi-Dirac integral of order -1/2	41
3.3.4. Eigenvalues of Schrödinger equation with a screened Coulomb potential	43
3.4. Simulation results	48
Appendix 3A. Debye-Hückel and Thomas-Fermi screening radius	55
Appendix 3B. Derivative of the ionized dopant concentration	59
Appendix 3C. Screening radius for a single donor level	61
Appendix 3D. Dimensionless Schrödinger equation	63
4. INCLUSION OF IMPURITY BANDS IN OUR MODEL	65
4.1. Formation of impurity bands	65
4.2. Our model for impurity bands	70
4.3. Occupancy of impurity bands	74
4.4. Simulation results and discussion	77
Appendix 4A. Calculation of the parameter σ from Eqs. (4.8)	83
Appendix 4B. Calculation of the energy transfer integral (Eq. 4.12)	85
Appendix 4C. Calculation of the averaged energy transfer integral (Eq. (4.14))	93
Appendix 4D. Asymptotic behavior of the two integrals $I_1(\beta)$ and $I_2(\beta)$	97
Appendix 4E. Approximate expressions for the two integrals $I_1(\beta)$ and $I_2(\beta)$	101
Appendix 4F. Asymptotic behavior of the averaged energy transfer integral (Eq. (4.17))	103
Appendix 4G. Ionization in an impurity band (Eq. (4.23))	107
CONCLUSIONS	113
BIBLIOGRAPHY	115
ACKNOWLEDGMENTS	123

Introduction.

Silicon Carbide is a polymorphic ceramic material which can be grown as a single crystal with electronic grade purity. Without doping SiC is semi-insulating, while with appropriate doping is a wide bandgap semiconductor. However, not all the dopant atoms in substitutional position contribute with an electron or a hole to the electrical conductivity due to their high ionization energy. The purpose of this thesis is to analyze theoretically the phenomenon of partial ionization of the substitutional dopants in SiC in the concentration range 10^{14} - 10^{21} atoms / cm^3 . A quantitative description of this phenomenon is crucial for both design of SiC devices and their characterization, activities which are both performed in CNR-IMM, Bologna, by the group led by Dr. Roberta Nipoti, group inside which I carried on this research.

In order to evaluate the degree of ionization of dopants, it is necessary to know the energy levels they generate and their dependence on both temperature and doping density. Simplified models exist in the literature which describe the variation of dopant ionization energies with dopant concentration. The aim of this thesis is to improve these models by taking into account many important aspects, in particular the effect of the screening of Coulomb potential of the ionized dopant atoms by free carriers and the formation of impurity bands at high concentrations. This problem can not be treated analytically, therefore numerical methods will be used to obtain quantitative predictions. However, in this work we shall proceed as long as possible (or reasonable) with purely analytical instruments.

The thesis is organized as follows:

- In Chapter 1 the properties of SiC of interest for this work are described.
- In Chapter 2 the distribution of electrons and holes between conduction and valence bands and impurity energy levels at thermal equilibrium is described,

Introduction

taking into account Fermi-Dirac statistics for the conduction and valence bands to allow the treatment of high doping levels.

- In Chapter 3 the variation of the impurity ionization energies with dopant concentration and temperature is analyzed by using a numerical solution of the Schrödinger equation for a screened Coulomb potential. A comparison of our calculations with experimental data for moderately doped SiC is carried out.
- In Chapter 4 the formation of impurity bands from single impurity levels with increasing impurity concentration and the occupancy of these bands when they overlap with the conduction or the valence band are analyzed. A preliminary comparison of the calculations with existing experiments on heavily doped SiC samples is finally carried out.

The chapters include many mathematical appendices which can be skipped at a first reading.

This thesis was fully granted by the institute CNR-IMM, Bologna, through the contracts 126.241.BS.1.2007 and IMM009/2010/BO.

Chapter 1.

Silicon Carbide.

In this chapter, after the presentation of a brief history of Silicon Carbide in section 1.1, the properties of Silicon Carbide of interest for the topic of this thesis will be presented. In particular, in section 1.2 a description of the polytypism of SiC is given. In section 1.3 the different band structures of various SiC polytypes are discussed, while in Sec. 1.4 the main dopant impurities used for doping Silicon Carbide are presented.

1.1. History of Silicon Carbide.

Silicon Carbide is one of the oldest natural compound semiconductor of the universe and it was among the first semiconductor materials taken into account for the fabrication of electronic components. In fact, SiC microcrystal powders have been found in the interstellar material that millions of years ago reached the earth. In 1824 the Swedish chemist J. J. Berzelius, the same who discovered Silicon, suggested the idea that there might be a chemical bond between Silicon and Carbon. This was the first time in history when there was talk of Silicon Carbide. However, this new material had to wait the invention of electric furnaces and their application to Carbon compounds. In 1891 E. G. Acheson fused a mass of Carbon and Aluminum Silicate in an attempt to obtain a material similar to Diamond; immediately after the mixture

Silicon Carbide

had cooled, he noticed that they had formed small shining blue crystals. Acheson thought to use these crystals, which were very hard, as an abrasive or cutting tools. He called this compound "*carborundum*" because it mistakenly believed he had achieved a compound between Aluminum and Carbon; only later his collaborators realized that the compound was composed of Silicon and Carbon. In 1905 H. Moisson discovered Silicon Carbide grains in some meteorites found in Diablo Canyon, Arizona, so that in its mineral form is also known as "moissanite".

Silicon Carbide was initially marketed as an abrasive because of its extreme hardness, later as a ceramic material resistant to high temperatures. Further later it was used in electronic applications, when in 1907 H. J. Round created the first LED (Light Emitting Diode) made of Silicon Carbide. In 1912 H. Baumhauer used for the first time the word polytypism, to describe the ability of Silicon Carbide to crystallize in different forms varying only in their stacking order in one direction. Research on Silicon Carbide for electronic applications received a boost in 1955 when Lely developed a technique of growing single crystals of Silicon Carbide, of high crystalline quality, in large slices, i.e. $\geq 1 \text{ cm}^2$. During those same years, however, another semiconductor material was spreading faster than Silicon Carbide: it was Silicon. Hence, the research on Silicon Carbide were put aside. In the late 70s the interest on Silicon Carbide was brought back to life in applications related to blue light LED, but soon was supplanted by direct gap semiconductors. Interest revived when researchers realized that Silicon technology is strongly limited for high temperature and high power applications, and therefore semiconductor materials with improved performance were required. Research on Silicon Carbide underwent a substantial acceleration with the birth of Cree Research in 1987, which made easier the availability of wafers of Silicon Carbide. The history of Silicon Carbide is illustrated in the timing diagram of Fig.1.1.

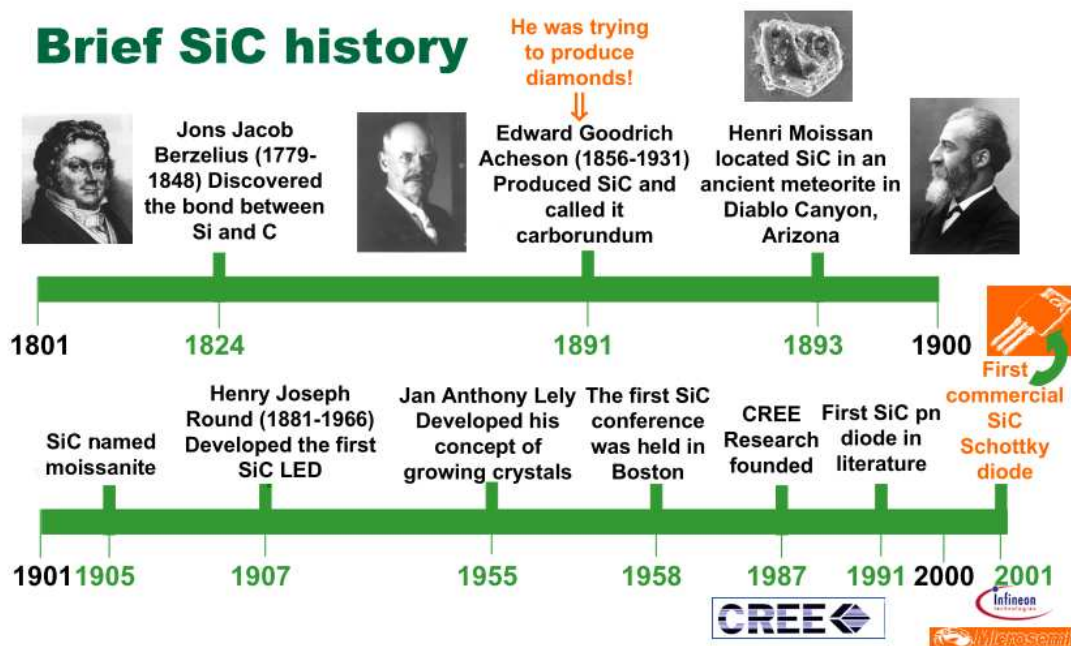


Fig.1.1. Time diagram of the Silicon Carbide history. From [Ozpineci02], p. 15.

1.2. SiC crystalline structure and SiC polytypes.

Silicon Carbide has the chemical formula SiC which corresponds to 50% atoms of Silicon (Si) and 50% of Carbon (C), that in terms of weight is a 70% content of Si and 30% of C. From a structural point of view, it falls within covalent compounds with each Carbon atom that binds to four Silicon atoms with tetrahedral bonds similar to those of Diamond. The basic unit of the SiC structure is the tetrahedron shown in Figure 1.2. The structure of single crystal SiC is given by the concatenation of these tetrahedrons, linked together by the vertices, with the Si-Si distance a and C-Si distance of 3.08 and of 1.89 Å, respectively.

SiC has several stable crystalline structures called polytypes. Polytypism is characterized by the fact that the atoms that are constituent of the material may have

Silicon Carbide

a different spatial arrangement along a direction but maintaining the same atomic ratio or atomic weight ratio per unit volume. Depending on the spatial sequence, the crystal symmetry varies. Among the SiC crystal symmetries, one of great interest for electronic application is the hexagonal one. The four axes reference system of an hexagonal crystal is shown in Fig.1.3. This system is aligned with respect to SiC tetrahedron so that the c -axis is parallel to a C-Si bond, while the a_1 , a_2 and a_3 axes, that are orthogonal to the c -axis and are placed at 120° one from the other, point to the position of the three Si atoms at the base of the tetrahedron, as can be seen from the comparison of Figs. 1.2 and 1.3.

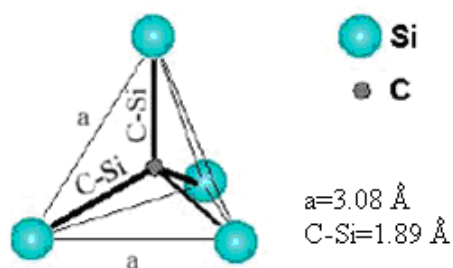


Fig. 1.2. Silicon Carbide tetrahedral cell.
From [Alampio10], p. 7.

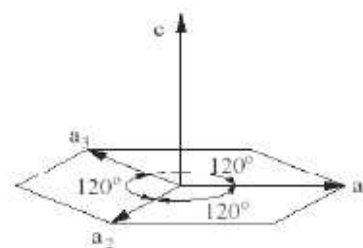


Fig. 1.3. Coordinate system with 4 axes for describing a hexagonal crystal structure.
From [Alampio10], p. 7.

The Si-C bi-layers along the c -axis can be ordered in more than 170 sequences. Fig. 1.4 shows that, with respect to the tetrahedral bond along the c -axis, the above "couple of Si-C planes" can occupy only three possible positions that are labeled A, B and C. The various polytypes of SiC result from a different stacking sequence of the Si-C planes pairs along the direction of c -axis. Often to indicate the various polytypes of SiC Ramsdell notation is used, consisting of a number followed by a letter. The number indicates the minimum number of layers beyond which the stacking of Si-C planes is repeated periodically. The letter indicates the symmetry of the crystal structure: C stands for cubic, H for hexagonal, and R for rhombohedral. Fig.1.4 shows the sequences of the cubic 3C-SiC, with a Zincblende type structure, and of the hexagonal 4H-SiC and 6H- SiC, with a Wurtzite type structure, but many

other have been grown and studied, among these the rhombohedral 15R-SiC and 21R-SiC and the hexagonal 2H-SiC. 3C-, 4H- and 6H-SiC are at present the more used SiC polytypes for manufacturing microelectronics devices.

The polytype 4H has ABAC stacking sequence (Fig. 1.4). Macroscopically it has hexagonal symmetry, but microscopically is composed half of cubic sites and half of hexagonal sites, equally distributed between Si and C atoms. To date it is the most widely polytype used for the construction of electronic devices and it can be grown into slices with diameter of 100 mm and has the highest and least anisotropic mobility than the other polytypes, the 6H, which can be grown in slices of equal size.

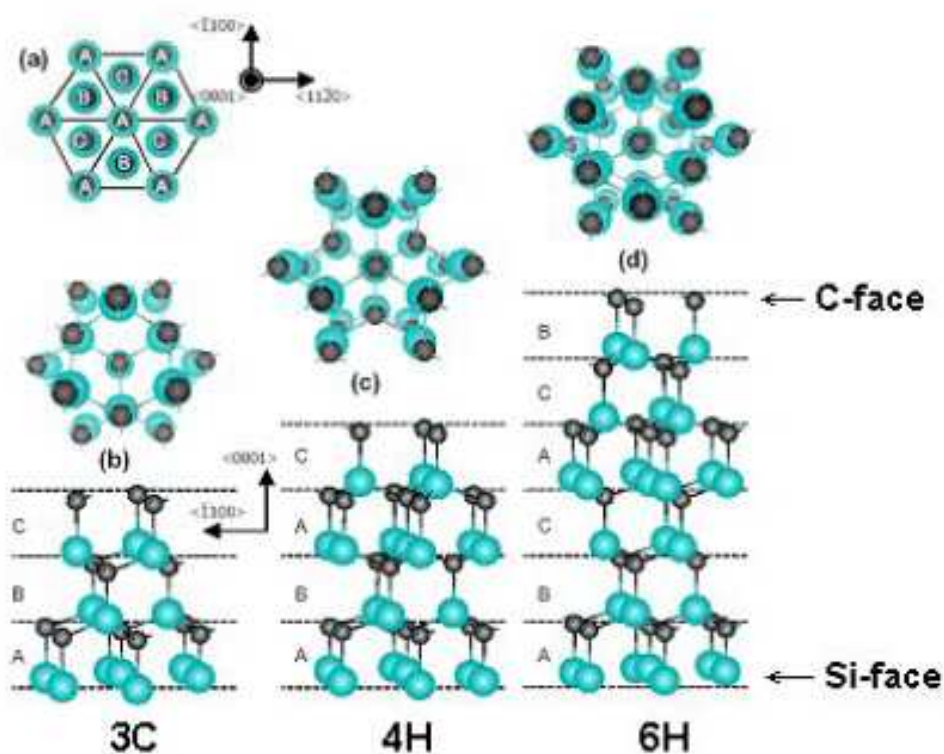


Fig. 1.4. Order of stacking of Silicon Carbide hexagonal planes.
From [Alampi10], p. 8.

1.3. Band diagrams and effective masses.

SiC is a wide bandgap semiconductor material. Calculations of Silicon Carbide band structure (see Figs. 1.5) show that SiC polytypes have an indirect bandgap between the maximum of the valence band and the minimum (or the equivalent minima) of the conduction band. Such a gap has a value which is significantly larger than that of the most common semiconductor, i.e. Silicon. Fig. 1.6 shows the bandgaps of the 4 most commonly used SiC polytypes. For comparison, also SiO₂ and Silicon are presented. It should be noted that the bandgap depends on temperature and pressure.

Of the polytypes of SiC, 4H has the widest bandgap. Due to this property, devices fabricated on 4H-SiC are able to sustain a higher electric field. This property, together with the fact that the native oxide of SiC is Silicon Dioxide, leads to the expectation that 4H-SiC will be a suitable substitute for Silicon in the production of power MOSFETs working in the harsh environments. Currently, the quality of SiC/SiO₂ interface is so improved that the first commercial SiC MOSFET has been launched by CREE Research Inc. [CREE11].

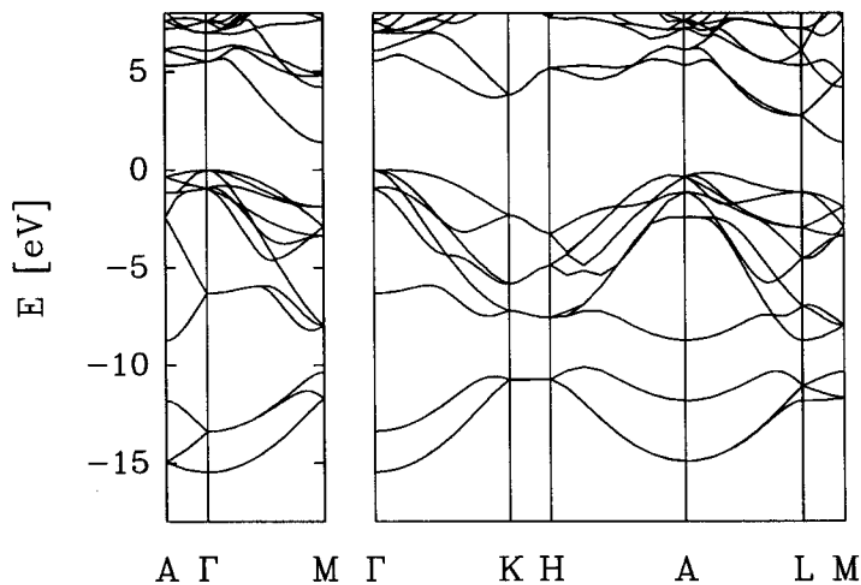


Fig. 1.5a. Band structure of 3C-SiC, from [Wellenhofer97].

Here and in the following Figs. 1.5b and 1.5c, the band above 0 eV is the conduction band and the other two below 0 eV are the p and the s valence electron bands.

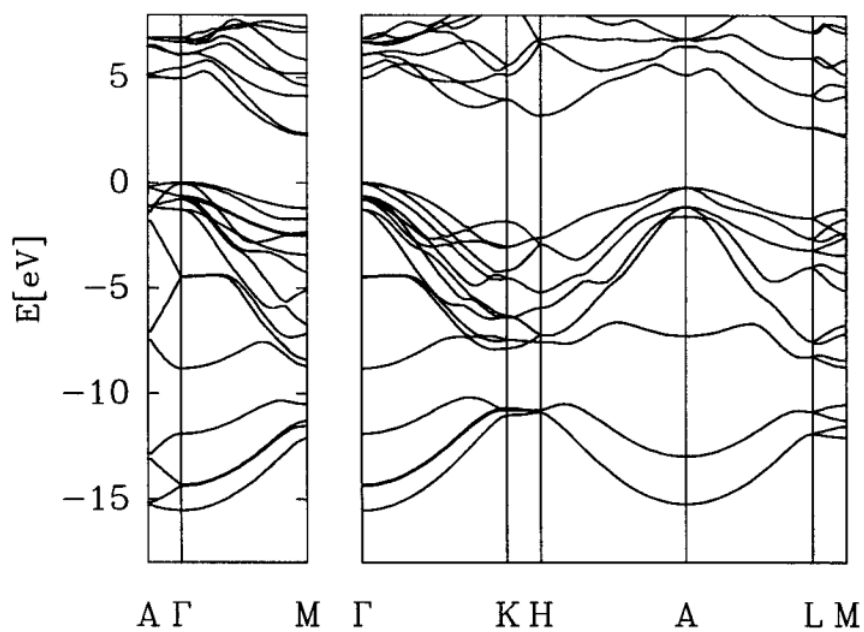


Fig. 1.5b. Band structure of 4H-SiC, from [Wellenhofer97].

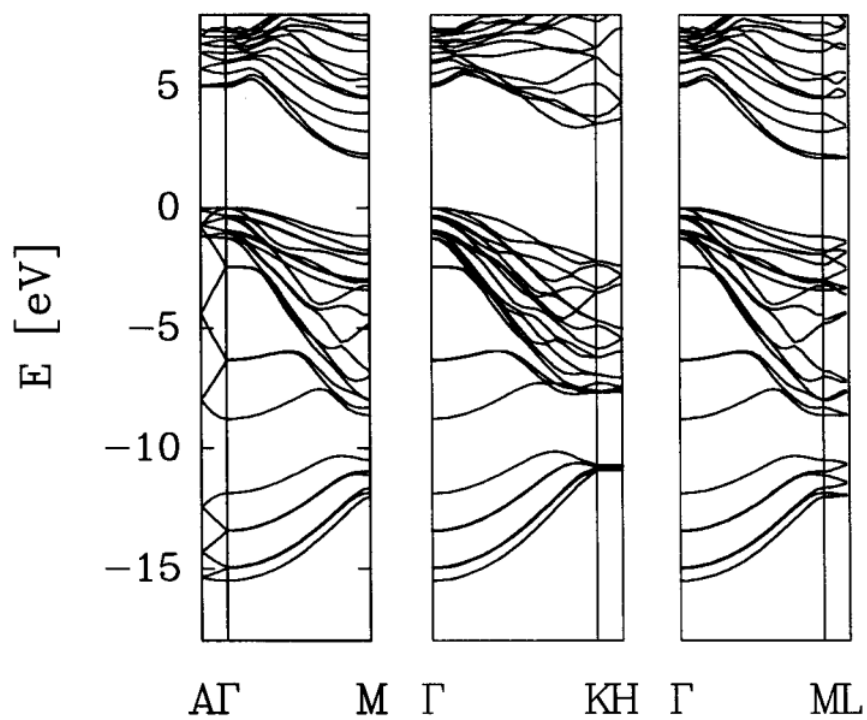


Fig. 1.5c. Band structure of 6H-SiC, from [Wellenhofer97].

Silicon Carbide

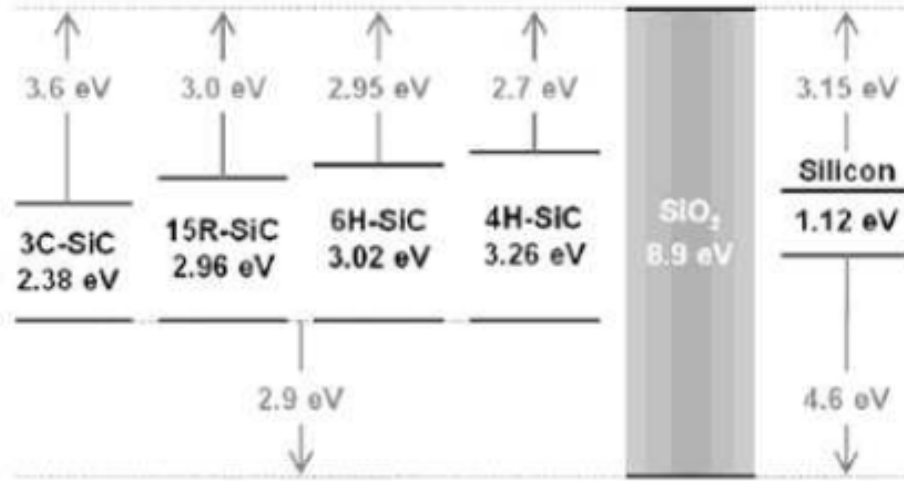


Fig. 1.6. Energy gaps and relative band offsets of Si, SiO₂ and common SiC polytypes, compiled from results by [Afanas'ev96]. From [Rozen08], p. 7.

Other quantities strictly related to the band structure of a semiconductor, and which will be essential in our simulations, are the effective mass of electrons and holes and the effective density of states (DOS) of the conduction and valence band. In particular we are interested in the latter, which are related to the effective mass of electrons m_e^* and of holes m_h^* , respectively, by the equations ([Sze07], p. 18):

$$N_C(T) = 2M_C \cdot \left(\frac{2\pi m_e^* k_B T}{h^2} \right)^{3/2} \quad (1.1a)$$

$$N_V(T) = 2M_V \cdot \left(\frac{2\pi m_h^* k_B T}{h^2} \right)^{3/2} \quad (1.1b)$$

where M_C and M_V are the number of equivalent minima of the conduction band and of maxima of the valence band, respectively, k_B is Boltzmann's constant, T the absolute temperature of the semiconductor and h Planck's constant. To be precise, in general the electron and hole effective masses are tensors and not scalars: in Eqs.

(1.1) two quantities enter which are appropriate averages of the principal components of such tensors, called DOS effective masses in one valley. In general they are functions of the temperature. For example, Wellenhofer and Rössler have calculated theoretically their values for 4H- and 6H-SiC [Wellenhofer97], see Figs. 1.7. For 3C-SiC the values $m_e^* = 0.35 m_0$ and $m_h^* = 0.6 m_0$ have been reported [NSM], where m_0 is the free electron mass. We report in Tab. 1.1 the number of equivalent valleys of the conduction and valence band for some SiC polytypes.

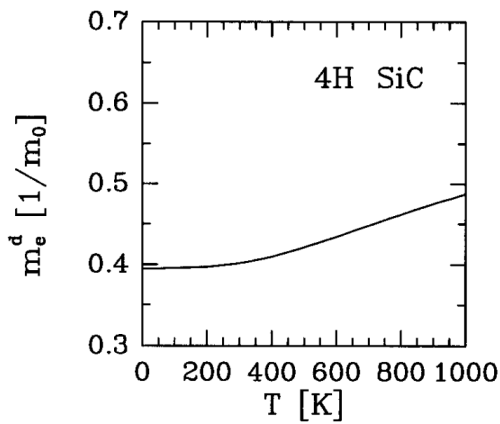


Fig. 1.7a. Electron DOS effective mass in 4H-SiC, from [Wellenhofer97].

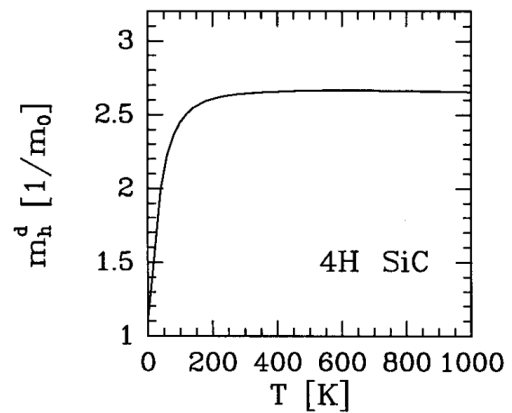


Fig. 1.7b. Hole DOS effective mass in 4H-SiC, from [Wellenhofer97].

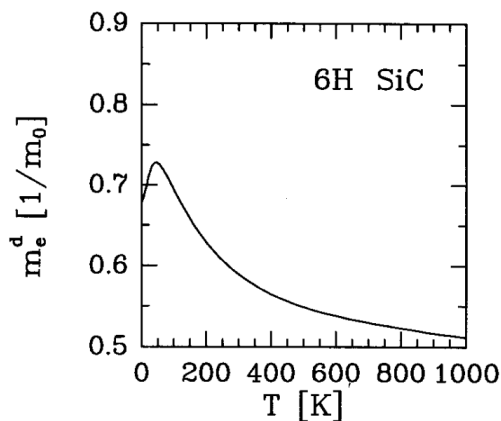


Fig. 1.7c. Electron DOS effective mass in 6H-SiC, from [Wellenhofer97].

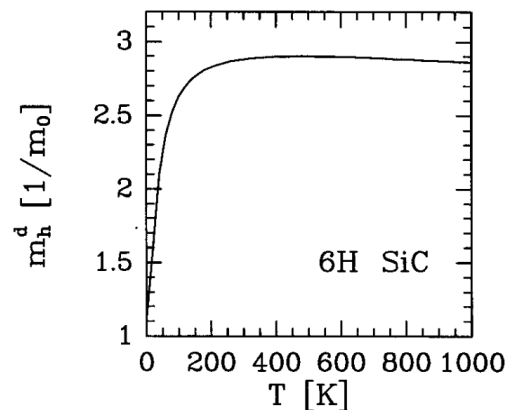


Fig. 1.7d. Hole DOS effective mass in 6H-SiC, from [Wellenhofer97].

Silicon Carbide

	M_C	M_V
3C-SiC	3	1
4H-SiC	3	1
6H-SiC	6	1

Tab. 1.1. Numbers of equivalent valleys in 3C, 4H- and 6H-SiC [NSM].

1.4. Main dopant impurities in SiC.

Doped semiconductors contain impurities, i.e. foreign atoms that are incorporated into the crystal structure of the semiconductor. These impurities can either be unintentional or they can be added on purpose to provide free carriers in the semiconductor. The generation of free carriers requires not only the presence of impurities, but also that such impurities are ionized to provide electrons to the conduction band (donors) or holes to the valence band (acceptors), in the latter case by effectively accepting an electron from the filled valence band. A semiconductor doped with impurities which are ionized (meaning that the impurity atoms either have donated or accepted an electron) will therefore contain free carriers.

Shallow impurities are impurities which require little energy – typically around the thermal energy at room temperature or less – to be ionized. Deeper impurities require energies higher than the thermal energy at room temperature to be ionized, so that, if present in a semiconductor, in practice only a fraction of them contributes to free carriers. In particular, deep states with energy levels more than five times the thermal energy away from either of band edges are very unlikely to be ionized at room temperature. These deep impurities can be effective recombination centers, in which electrons and holes recombine and annihilate each other. They are also called traps.

A semiconductor in which ionized donors provide free electrons is called *n*-type, while a semiconductor in which ionized acceptors provide free holes is referred

Chapter 1

to as a *p*-type semiconductor. The ionization of the impurities is dependent on the thermal energy and the position of the impurity level within the energy bandgap. Statistical thermodynamics can be used to obtain the probability that the impurity is ionized. The resulting expression is similar to the Fermi-Dirac probability function, except for a factor that accounts for the fact that the impurity can host only one electron or one hole, and also accounts for the degeneracy of the conduction or valence band. If shallow impurities are completely ionized, the majority carrier density equals their *net* impurity concentration (i.e. having subtracted the density of compensating centers, which capture the majority carriers), if the intrinsic carrier concentration is negligible.

In the case of SiC the most common donors are Nitrogen and Phosphorus. The former substitutes on Carbon sites and the latter on Silicon sites in the lattice. The most common acceptors are Aluminum and Boron. They all substitute on Silicon sites. The site on which these dopants substitute (i.e. C or Si site) is not polytype dependent, but their energy level depends on the particular polytype. Furthermore, due to the presence of several non-equivalent (cubic and hexagonal) lattice sites in almost all SiC polytypes, the same dopant species in general gives rise to more than one energy level, one for each kind of non-equivalent lattice site, with the exception of 3C- and 2H-SiC which are purely cubic and hexagonal, respectively ([Patrick62], [Ikeda79], [Ikeda80]). In Tab. 1.2 the stacking sequence together with the number of non-equivalent (cubic and hexagonal) lattice sites for the main SiC polytypes are given.

Ramsdell notation	ABC notation	No. of inequivalent sites	
		hexagonal-like	cubic-like
2H (wurzite)	AB	1	0
3C (zinc blende)	ABC	0	1
4H	ABAC	1	1
6H	ABCACB	1	2
15R	ABCACBCABACBCB	2	3

Tab. 1.2. Stacking sequence and relative number of non-equivalent lattice sites in some SiC polytypes. From [Ikeda80].

Silicon Carbide

Nitrogen, Phosphorus and Aluminum are the most common dopants. Such impurities may be intentionally introduced during the growth, via ion implantation technique or by diffusion. Diffusion is a common doping method of active layers. However, the diffusion coefficients of impurities in SiC are small, therefore ion implantation is frequently used in SiC device fabrication. The main drawbacks are the lattice damage caused during the ion bombardment and the occurrence of amorphous material in the ion implanted volume. Therefore, a post-implantation annealing is needed.

Purpose of this thesis is to model the ionization of both p - and n -type dopants in various SiC polytype versus doping concentration and material temperature, for homogeneous SiC samples at thermal equilibrium. The results so obtained can be used both for simulating SiC electrical behavior, in order to improve the design of various SiC devices, and for the interpretation of experimental data such as those of temperature dependent Hall effect measurements.

Chapter 2.

Occupancy of energy levels.

In this chapter we shall consider how electrons and holes are distributed between conduction and valence bands and the various energy levels provided by impurities in a homogeneously doped semiconductor at thermal equilibrium. In Sec. 2.1 we shall present the expressions which rule the incomplete ionization of discrete dopant levels, considering also the possibility of excited states and valley-orbit splitting. In Sec. 2.2 the charge neutrality equation will be analytically solved in the non-degenerate case, both for a single energy level in the gap, with or without compensation, and for the case of two energy levels in presence of compensation. In Sec. 2.3 we shall present a numerical method capable to solve the neutrality equation for an arbitrary number of energy levels (both donors and acceptors at the same time) also in the degenerate case.

2.1. Occupation probability for discrete impurity levels.

In this section we shall treat the thermodynamic nature of the incomplete ionization of substitutional dopants in semiconductors. In subsection 2.1.1 we shall treat the well established model proposed for describing incomplete ionization of the ground state of monovalent impurities (and in general of single discrete levels), while in

Chapter 2

subsection 2.1.2 we shall study the effect of excited states and of splitting of the ground state on the occupancy probability of impurity centers.

2.1.1. Occupancy of a monovalent impurity in its ground state.

For simplicity, let us consider a semiconductor containing N_D monovalent donor impurity atoms per unit volume. In these atoms all valence electrons, with the exception of the least tightly bound, are in paired valence bonds. Therefore, in the ground state each atom has only one electron trapped at a certain energy ΔE_D below the absolute minimum of the conduction band, with a wave function of purely s character. This electron can have spin up or down, so the ground state will be degenerate with a degeneracy factor of 2.

Note that, at a first approximation, a monovalent donor can not trap two electrons since, once one electron is trapped, electrostatic forces raise the remaining spin possibility to a higher energy, nearby or into the conduction band. Therefore, we will consider only electrically neutral donors (with one electron trapped at the energy $E_D = E_C - \Delta E_D$), whose density we shall indicate with N_D^0 , and ionized (unoccupied) donors with a density $N_D^+ = N_D - N_D^0$.

From statistical mechanics ([Kittel80], p. 138), the grand partition function of $N = N_D V$ donor atoms in a semiconductor of volume V is given by:

$$\mathcal{Z} = \sum_{M=0}^N \sum_{s(M;N)} \exp\left(\frac{ME_F - E_{s(M;N)}}{k_B T}\right),$$

where $s(M; N)$ represents any possible arrangement of M electrons between N donors, E_F is the Fermi level of the system, $E_{s(M;N)}$ is the total energy of the given configuration $s(M; N)$, k_B is Boltzmann's constant and T is the temperature of the system. Taking the absolute minimum of the conduction band E_C as the energy reference for *each* single donor state, and disregarding the effect of electrostatic interaction between charges on the energy level position with respect to E_C , we have:

Occupancy of energy levels

$$E_{s(M;N)} = M(E_C - \Delta E_D)$$

so that:

$$\begin{aligned} Z &= \sum_{M=0}^N \sum_{s(M;N)} \exp\left[\frac{ME_F - M(E_C - \Delta E_D)}{k_B T}\right] = \\ &= \sum_{M=0}^N \binom{N}{M} 2^M \exp\left(M \frac{E_F - E_C + \Delta E_D}{k_B T}\right) = \\ &= \left[1 + 2 \exp\left(\frac{E_F - E_C + \Delta E_D}{k_B T}\right)\right]^N, \end{aligned}$$

the term 2^M in the sum being due to the two possible spin orientations of each of the M electrons. The average number of occupied donors is given by the relation ([Kittel80], p. 139):

$$\langle N^0 \rangle = \frac{k_B T}{Z} \cdot \frac{\partial Z}{\partial E_F}$$

so that, substituting the grand partition function previously obtained, we have finally:

$$\langle N^0 \rangle = \frac{N}{1 + \frac{1}{2} \exp\left(\frac{E_C - E_F - \Delta E_D}{k_B T}\right)}.$$

The statistical degree of neutrality of the donors is therefore ([Blakemore62], p. 119):

$$\xi_D^0 \equiv \frac{N_D^0}{N_D} = \frac{\langle N^0 \rangle}{N} = \frac{1}{1 + \frac{1}{2} \exp\left(\frac{E_C - E_F - \Delta E_D}{k_B T}\right)},$$

while their statistical degree of ionization is:

Chapter 2

$$\xi_D^+ \equiv \frac{N_D^+}{N_D} = 1 - \xi_D^0 = \frac{1}{1 + 2 \exp\left(\frac{E_F - E_C + \Delta E_D}{k_B T}\right)}.$$

In general, the degeneracy g_D of the donor ground state will differ from 2, for example when the level is created by splitting off states from a conduction band with multiple or degenerate minima. Thus, for a donor level at energy $E_D = E_C - \Delta E_D$, the probability that this level will contain an electron is in general ([Blakemore62], p. 119):

$$\xi_D^0 = \frac{1}{1 + \frac{1}{g_D} \exp\left(\frac{E_C - E_F - \Delta E_D}{k_B T}\right)}, \quad (2.1a)$$

so the probability it will be ionized is:

$$\xi_D^+ = \frac{1}{1 + g_D \exp\left(\frac{E_F - E_C + \Delta E_D}{k_B T}\right)}. \quad (2.1b)$$

Similar expressions hold for a monovalent acceptor, for which:

$$\xi_A^0 \equiv \frac{N_A^0}{N_A} = \frac{1}{1 + \frac{1}{g_A} \exp\left(\frac{E_F - E_V - \Delta E_A}{k_B T}\right)} \quad (2.2a)$$

is its degree of neutrality and:

$$\xi_A^- \equiv \frac{N_A^-}{N_A} = \frac{1}{1 + g_A \exp\left(\frac{E_V - E_F + \Delta E_A}{k_B T}\right)} \quad (2.2b)$$

Occupancy of energy levels

is its ionization degree, ΔE_A being the ionization energy and g_A the spin degeneracy (or degeneracy factor) of its ground state, while N_A is the total concentration of substitutional acceptors, N_A^0 the density of the neutral ones and N_A^- that of the ionized ones

2.1.2. Occupancy of a monovalent impurity with excited states.

As is well known, an isolated hydrogen atom consists of an electron moving under the influence of a proton. The ground state of this system, the $1s$ state, has a spin degeneracy of 2, and an energy of 13.6 eV is required to ionize the atom. But there are also many possible excited states of this atom, the eight $2s$ and $2p$ states, the eighteen $3s$, $3p$ and $3d$ states, and so on. It is dangerous to press too far for the analogy between a hydrogen atom and a monovalent impurity center, but such analogies are useful in reminding us that a donor impurity is electrically neutral whether it has an electron bound in the ground state at $E_C - \Delta E_D$ or in an excited state closer to the conduction band. Let us denote by 1 the lowest (or ground) level of the donor, having a spin degeneracy of $g_{D,1}$. Groups of excited states in general have different degeneracy factors, say $g_{D,r}$ with $r > 1$, and lie at energies $\Delta E_{D,r}$ below the conduction band edge.

Within the same approximation of the previous subsection, a donor is capable of binding an electron in one of the $g_{D,r}$ states at energy $E_C - \Delta E_{D,r}$ only if it doesn't have an electron already bound in any other state, either at the same level or at a different one. Therefore, we finally obtain ([Blakemore62], p. 142-144):

$$\xi_D^+ = \frac{1}{1 + g_{D,1} \cdot [1 + F_{exc}(T)] \cdot \exp\left(\frac{E_F - E_C + \Delta E_{D,1}}{k_B T}\right)}, \quad (2.3)$$

where:

$$F_{exc}(T) = \frac{1}{g_{D,1}} \cdot \sum_{r=2}^{+\infty} g_{D,r} \exp\left(\frac{\Delta E_{D,r} - \Delta E_{D,1}}{k_B T}\right). \quad (2.4)$$

Chapter 2

It should be noted that the series (2.4) diverges for any finite temperature T . However, as Shifrin remarked ([Blakemore62], ref. 1944:1), it is only necessary to consider the first few terms of such a series since, for a finite donor density, the wave functions for the higher excited states will overlap quite strongly and these states will form part of the conduction band. At very low temperatures $F_{exc}(T) \ll 1$, so Eq. (2.3) reduces to Eq. (2.1b). At higher temperatures, however, excited states could no longer be neglected. Expressions similar to (2.3) and (2.4) hold, obviously, for the p -type case, and H. Matsuura applied them to the analysis of Al-doped SiC samples [Matsuura02].

Also the splitting of the ground state can affect the ionization degree of an impurity center. For example, as a consequence of the six equivalent conduction band minima, the $1s$ state of Phosphorus in Silicon is compounded of six states, each with a spin degeneracy of 2, or twelve states in all. Two of these states have wave functions which do not vanish at the donor nucleus (completely symmetrical states), whereas the wave functions of the other ten do vanish at this point. As a consequence, the two completely symmetrical states lie at a considerably lower energy than the remaining $1s$ states. Let us call ΔE_{vo} the energy difference between the two lowest and the other ten $1s$ states. The spin degeneracy g_D must be substituted in Eq. (2.1b) by a temperature dependent effective degeneracy factor ([Blakemore62], p. 148):

$$g_{D,eff}(T) = 2 + 10 \exp\left(-\frac{\Delta E_{vo}}{k_B T}\right),$$

taking as ΔE_D the ionization energy of the two deeper states. A similar result holds, for example, for substitutional Nitrogen donors at the hexagonal sites in 4H-SiC, for which:

$$g_{D,eff}(T) = 2 + 4 \exp\left(-\frac{\Delta E_{vo}}{k_B T}\right),$$

Occupancy of energy levels

where $\Delta E_{vo} = 7.6$ meV [Götz93].

In the following part of our thesis, for simplicity we shall not take into account the presence of excited states or of ground state splitting.

2.2. Solution of the charge neutrality equation in some particular cases.

Eqs. (2.1) and (2.2) have a general validity for a semiconductor at thermal equilibrium. However, they depend on the Fermi energy E_F so they are not immediately useful for a comparison with experimental data. To this purpose the Fermi level has to be eliminated, in order to obtain expressions depending only from measurable parameters such as the dopant concentrations, their energy levels and the system temperature. For a homogeneously doped semiconductor, the charge neutrality equation holds ([Sze07], p. 22):

$$N_D^+(E_F) + p(E_F) = N_A^-(E_F) + n(E_F) , \quad (2.5)$$

where p and n are the free hole and electron concentrations, respectively, so permitting theoretically to eliminate E_F and express the ionization degree of the various dopant species in terms of well known or measurable parameters.

Let us consider the n -type case, for simplicity. For a wide range of temperatures, the minority carrier concentration p can be neglected in Eq. (2.5). Furthermore, if the acceptor levels are sufficiently below the Fermi level in the band gap (as it is often the case), they can be considered fully ionized so that Eq. (2.5) becomes:

$$N_D^+(E_F) = N_A + n(E_F) . \quad (2.6)$$

In the non-degenerate case, the free carrier concentrations can be expressed as:

Chapter 2

$$n = N_C \exp\left(\frac{E_F - E_C}{k_B T}\right) \quad (2.7a)$$

$$p = N_V \exp\left(\frac{E_V - E_F}{k_B T}\right), \quad (2.7b)$$

N_C and N_V being the effective density of states in the conduction and valence band, respectively. Therefore, substituting Eq. (2.1b) into Eq. (2.6) gives, for a single donor species present in the semiconductor:

$$\frac{N_D}{1 + g_D \frac{n}{N_C} \exp\left(\frac{\Delta E_D}{k_B T}\right)} = N_A + n. \quad (2.8)$$

This is a second-order polynomial equation in the variable n , which can easily be solved.

In absence of compensation ($N_A = 0$), the physically meaningful solution of Eq. (2.8) is ([Blakemore62], p. 122):

$$n = N_D^+ = \frac{2N_D}{1 + \sqrt{1 + 4g_D \frac{N_D}{N_C} \exp\left(\frac{\Delta E_D}{k_B T}\right)}},$$

thus giving:

$$\xi_D^+ \equiv \frac{N_D^+}{N_D} = \frac{-1 + \sqrt{1 + 4g_D \frac{N_D}{N_C} \exp\left(\frac{\Delta E_D}{k_B T}\right)}}{2g_D \frac{N_D}{N_C} \exp\left(\frac{\Delta E_D}{k_B T}\right)}.$$

Such an expression has been proposed for Silicon Carbide [Ruff94], also for the cases like 4H- and 6H-SiC in which there are several non-equivalent lattice sites in

Occupancy of energy levels

the crystal, ΔE_D being an effective energy level intermediate between the real ones and N_D their total concentration ([ISE04], p. 15.164). If compensation is present, the physically meaningful solution of Eq. (2.8) is given in [Blakemore62], p. 134.

Similar expressions hold for the p -type case. We stress that their applicability is limited to the non-degenerate case and when only one dominant energy level is present in the bandgap or it is sufficient for describing the electrical behavior of the system. For example, in Al-doped Silicon Carbide also in the case of several non-equivalent lattice sites (such as in 4H- and 6H-SiC) only one acceptor energy level can often be solved by temperature dependent Hall effect data analysis [Pensl93], seeming to be sufficient for electrical behavior description.

However, for n -type 4H-SiC two energy levels have to be considered, one corresponding to a donor substituting in a hexagonal site and the other to a donor substituting in a cubic site, levels that are well solvable by temperature dependent Hall effect data analysis [Pensl93]. Again using Boltzmann approximation (2.7), Eq. (2.6) becomes:

$$\frac{N_{D,h}}{1 + g_{D,h} \frac{n}{N_C} \exp\left(\frac{\Delta E_{D,h}}{k_B T}\right)} + \frac{N_{D,k}}{1 + g_{D,k} \frac{n}{N_C} \exp\left(\frac{\Delta E_{D,k}}{k_B T}\right)} =$$

$$= N_A + n , \tag{2.9}$$

the letters h and k corresponding to a donor substituting in a hexagonal and cubic site, respectively. Eq. (2.9) gives rise to a third order polynomial equation in the variable n , whose exact solution in presence of compensation is given in [Rutsch99].

2.3. General solution of the charge neutrality equation.

In general, however, more than two dominant energy levels are present in the energy gap, due to non-equivalent lattice sites or to deep dopants. In this case, the charge neutrality equation takes the general form:

$$\sum_{j=1} \frac{N_{A,j}}{1 + g_{A,j} \exp\left(\frac{E_V - E_F + \Delta E_{A,j}}{k_B T}\right)} + N_V \cdot \mathcal{F}_{1/2}\left(\frac{E_V - E_F}{k_B T}\right) =$$

$$= \sum_{i=1} \frac{N_{D,i}}{1 + g_{D,i} \exp\left(\frac{E_F - E_C + \Delta E_{D,i}}{k_B T}\right)} + N_C \cdot \mathcal{F}_{1/2}\left(\frac{E_F - E_C}{k_B T}\right)$$

(2.10)

$\mathcal{F}_{1/2}(x)$ being the Fermi-Dirac integral of order 1/2 (see [Blakemore62], App. A), while the letters i and j correspond to the i -th and j -th kind of donor and acceptor level, respectively. Here we have used the expressions ([Blakemore62], p. 79):

$$n = N_C \cdot \mathcal{F}_{1/2}\left(\frac{E_F - E_C}{k_B T}\right)$$

(2.11a)

$$p = N_V \cdot \mathcal{F}_{1/2}\left(\frac{E_V - E_F}{k_B T}\right)$$

(2.11b)

which, unlike Eqs. (2.7), hold also in the case of degeneration. Therefore, the results we shall obtain here can be applied also to the study of degenerate semiconductors.

Unfortunately, Eq. (2.10) can not be solved analytically, therefore a numerical method must be used for obtaining the dopant ionization degrees. To this purpose, looking at Eq. (2.10), let us define the function:

Occupancy of energy levels

$$\Phi(E_F) \equiv \sum_{j=1} \frac{N_{A,j}}{1 + g_{A,j} \exp\left(\frac{E_V - E_F + \Delta E_{A,j}}{k_B T}\right)} + N_V \cdot \mathcal{F}_{1/2}\left(\frac{E_V - E_F}{k_B T}\right) - \sum_{i=1} \frac{N_{D,i}}{1 + g_{D,i} \exp\left(\frac{E_F - E_C + \Delta E_{D,i}}{k_B T}\right)} - N_C \cdot \mathcal{F}_{1/2}\left(\frac{E_F - E_C}{k_B T}\right).$$

It can be demonstrated (see App 2A) that the function $\Phi(E_F)$ is continuous and monotonic in E_F and that it passes through the value zero if the values of the parameters $N_{A,j}$, $g_{A,j}$, $N_{D,i}$ and $g_{D,i}$ are non-negative and N_V and N_C are strictly positive (the only physically meaningful values they can assume). Therefore, the simple bisection method can be used for solving the charge neutrality equation $\Phi(E_F) = 0$, being sure that the value of E_F so obtained is its *unique* solution and necessarily the physically correct one. To this purpose, we have chosen the approximate expression for $\mathcal{F}_{1/2}(x)$ given by [AymerichHumet81] which represents a good compromise between accuracy and computational time, having to be used in an iterative method that often includes poorly accurate parameters, such as the empirical values of impurity concentrations. Once the correct value of E_F is obtained in such a manner, it can be substituted into Eqs. (2.11), (2.1) and (2.2) for giving the corresponding values of n , p , $\xi_{D,i}^+$ and $\xi_{A,j}^-$. This method can be applied also in the presence of very deep compensating centers, whose ionization can no longer be assumed as complete if their level is localized in the neighborhood of the main dopant levels or of the Fermi energy.

To this purpose, sufficiently accurate values for the ionization energy of the dopant levels should be known. However, the empirical values obtained for example by temperature dependent Hall effect data analysis span over large ranges, making questionable the choice of a certain value to the detriment of another in the same range. Besides, these ionization energies show a clear dependence on dopant concentration. This is exactly the topic which will be treated in the next chapter.

Chapter 2

Appendix 2A. Useful properties of the space charge density function $\Phi(E_F)$.

In Sec. 2.3 we have introduced the function:

$$\Phi(E_F) \equiv \sum_{j=1} \frac{N_{A,j}}{1 + g_{A,j} \exp\left(\frac{E_V - E_F + \Delta E_{A,j}}{k_B T}\right)} + N_V \cdot \mathcal{F}_{1/2}\left(\frac{E_V - E_F}{k_B T}\right) - \sum_{i=1} \frac{N_{D,i}}{1 + g_{D,i} \exp\left(\frac{E_F - E_C + \Delta E_{D,i}}{k_B T}\right)} - N_C \cdot \mathcal{F}_{1/2}\left(\frac{E_F - E_C}{k_B T}\right)$$

corresponding to the space charge density ρ as a function of the Fermi energy E_F . To be physically meaningful, the parameters $N_{D,i}$, $N_{A,j}$, $g_{D,i}$ and $g_{A,j}$ must be non-negative, while N_C , N_V and T must be strictly positive. First of all, we have to note that the function $\Phi(E_F)$ is continuous in the variable E_F , being the sum of continuous functions (for the properties of $\mathcal{F}_{1/2}(x)$ see [Blakemore62], App. A). Let us now study the asymptotic behavior of $\Phi(E_F)$. Being:

$$\lim_{x \rightarrow -\infty} \mathcal{F}_{1/2}(x) = 0$$

$$\lim_{x \rightarrow +\infty} \mathcal{F}_{1/2}(x) = +\infty ,$$

we have:

$$\lim_{E_F \rightarrow -\infty} \Phi(E_F) = +\infty$$

$$\lim_{E_F \rightarrow +\infty} \Phi(E_F) = -\infty$$

Chapter 2

being N_C , N_V and T positive.

Furthermore, the first derivative of $\Phi(E_F)$ is:

$$\begin{aligned} \frac{\partial \Phi(E_F)}{\partial E_F} = & -\frac{1}{k_B T} \cdot \sum_{j=1} \frac{g_{A,j} N_{A,j}}{\left[1 + g_{A,j} \exp\left(\frac{E_V - E_F + \Delta E_{A,j}}{k_B T}\right) \right]^2} - \frac{N_V}{k_B T} \cdot \mathcal{F}_{-1/2}\left(\frac{E_V - E_F}{k_B T}\right) - \\ & - \frac{1}{k_B T} \cdot \sum_{i=1} \frac{g_{D,i} N_{D,i}}{\left[1 + g_{D,i} \exp\left(\frac{E_F - E_C + \Delta E_{D,i}}{k_B T}\right) \right]^2} - \frac{N_C}{k_B T} \cdot \mathcal{F}_{-1/2}\left(\frac{E_F - E_C}{k_B T}\right) < 0, \end{aligned}$$

being ([Blakemore62], App. A):

$$\mathcal{F}_{-1/2}(x) = \frac{d\mathcal{F}_{1/2}(x)}{dx} > 0 .$$

We have thus established that, with physically meaningful values of its parameters:

- 1) $\Phi(E_F)$ is a continuous function;
- 2) $\Phi(E_F)$ is a monotonically decreasing function;
- 3) $\Phi(E_F)$ assumes a positive value as E_F tends to $-\infty$, and assumes a negative value as E_F tends to $+\infty$.

Therefore, there exist, and it is unique, a value of E_F for which $\Phi(E_F) = 0$. Due to the continuity and monotonicity of $\Phi(E_F)$, such a value can easily be found numerically by using the bisection method (Newton method turned out to be not always convergent for such a problem).

Chapter 3.

Dopant ionization energy variation.

In this chapter we shall treat the observed variation of the dopant ionization energies with dopant concentration, and we shall suggest their indirect dependence also from temperature. In Sec. 3.1 we shall present an empirical evidence for this variation, based in particular on measurements of the majority carrier concentration for different values of substitutional dopant densities. In Sec. 3.2 we shall present the traditional approach to this topic, based on the article by G. L. Pearson and J. Bardeen written in 1949 and then improved by different authors, together with its recent application to SiC. In Sec. 3.3 we shall discuss the limits of such an approach and propose a model based on a screened Coulomb potential due to the redistribution of free carriers around the dopant cores and the solution of the Schrödinger equation with such a potential. Results of simulations implementing such a model for SiC will be presented and discussed in Sec. 3.4, and compared to experimental data.

3.1. Experimental evidence for a dopant ionization energy variation.

As is well known, from temperature dependent Hall effect measurements it is possible to obtain the majority carrier concentration in a homogeneous sample at different temperatures and, fitting these data with the charge neutrality equation, the dopant densities and ionization energies can be extracted, together with the total

concentration of the compensating centers ([Blood92], Chap. 3) The accuracy of this procedure depends on several preconditions (such as the knowledge of the Hall scattering factor and homogeneity of the sample, for example) and shrewdness in performing the experiment ([Blood92], Chap. 3) A consequence of these results, however, seems to be undeniable: in a given semiconductor material, for a given dopant species and compensating center concentration, the ionization energies $\Delta E_{d,i}$ decrease with increasing substitutional dopant concentration N_d . This result is universal, i.e. it holds for all types of semiconductors and dopant species. In particular, we report in Figs. 3.1 some results of the analysis of temperature dependent Hall effect data corresponding to both n - and p -type 3C- and 4H-SiC samples ([Segall86], [Achatz08], [Rao06], [Kagamihara04]).

This phenomenon is well known from more than half a century, and several models have been proposed to explain it. In the next section we shall analyze the most important of them, which has been most largely used for fitting experimental ionization energies and for simulating the electrical behavior of semiconductor samples and devices (see [SILVACO00], p. 3-10, [ISE04], p. 15.163).

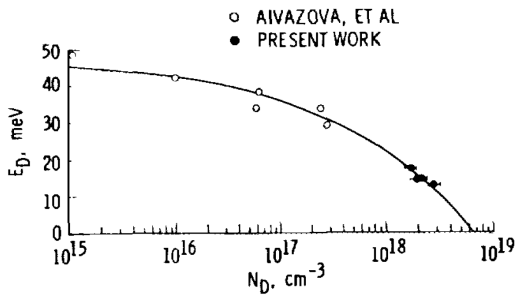


Fig. 3.1(a). Nitrogen donor ionization energy in 3C-SiC as a function of N density. “Present work” refers to [Segall86], from which this image is taken. In this and the following figures, the solid or dashed lines are fits of the experimental data following Pearson and Bardeen’s model (see next section).

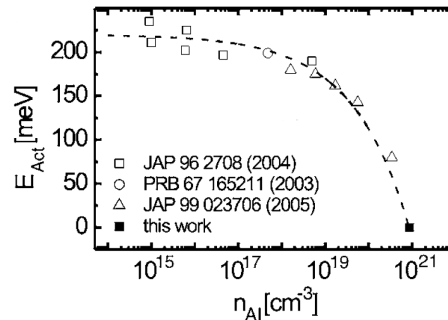


Fig. 3.1(b). Aluminum acceptor ionization energy in 4H-SiC as a function of Al density. “This work” refers to [Achatz08], from which this image is taken.

Dopant ionization energy variation

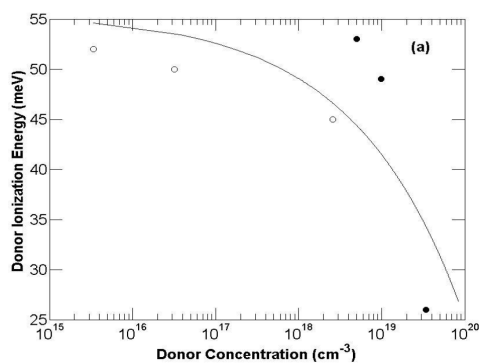


Fig. 3.1(c). Phosphorus donor ionization energy in the hexagonal sites of 4H-SiC as a function of P density, from [Rao06]. In this and next figure, full circles correspond to [Rao06] while open circles to [Wang02] and [Laube02] experimental results.

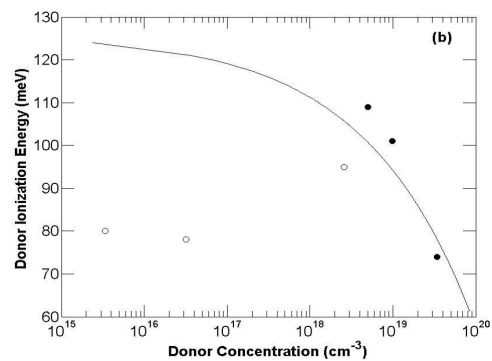


Fig. 3.1(d). Phosphorus donor ionization energy in the cubic sites of 4H-SiC as a function of P density, from [Rao06].

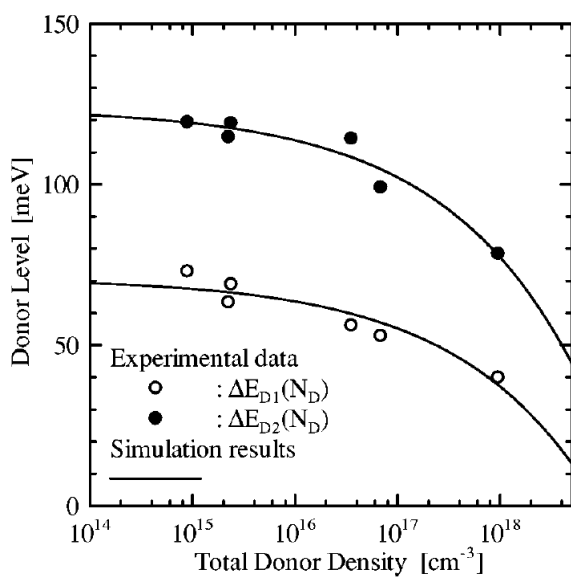


Fig. 3.1(e). Nitrogen donor ionization energies in cubic and hexagonal sites of 4H-SiC as a function of N density, from [Kagamihara04].

3.2. Pearson and Bardeen's model and its improvements.

Chronologically, the first model suggested for describing the variation of the ionization energy of dopants in a semiconductor material was proposed by K. S. Shifrin in 1944 (see [Lehman55], note 1), then improved by G. L. Pearson and J. Bardeen in 1949 ([Pearson49], [Pearson50]). It was so successful that it is still largely used, with only little variations in order to take into account the effect of compensation. The main reasons of such a generalized application of this model are essentially two: its ability to fit the experimental energy data together with its great simplicity. In Sec. 3.2.1 we shall describe this model, while in Sec. 3.2.2 we shall see the variations proposed by other authors in order to improve it and in Sec. 3.2.3 its application to 3C- and 4H-SiC.

3.2.1. Pearson and Bardeen's model.

Pearson and Bardeen studied the case of uncompensated Silicon, in which the lattice sites are equivalent, homogeneously doped with monovalent impurities (P or B) at the thermodynamic equilibrium. They suggested that the decrease in ionization energy of a substitutional dopant atom with increasing concentration results from a decrease in the average potential energy of an electron or a hole. The energy decrease is taken to be inversely proportional to the average distance of separation between impurities, i.e. proportional to $N_d^{1/3}$, where N_d is the substitutional dopant concentration. Thus, one might expect the ionization energy to vary with concentration as:

$$\Delta E_d(N_d) = \Delta E_d(0) - \alpha_d \cdot N_d^{1/3} \quad (3.1)$$

where, following a simple model *à la* Bohr:

$$\Delta E_d(0) = \frac{m^* e^4}{8\epsilon^2 h^2} \quad (3.2)$$

Dopant ionization energy variation

is the ionization energy for an isolated impurity center, m^* being the effective mass of majority carriers, e the absolute value of electron charge, ϵ the dielectric permittivity of the semiconductor and h Planck's constant. The value of α_d depends on the exact form of the potential energy [Pearson49].

The authors observed that an accurate calculation of the potential energy term is very difficult, so they attempted only very rough considerations and left α_d to be determined by a fit of the experimental data. It has been theoretically evaluated only in order to see if the empirical value they obtained was or not of reasonable magnitude.

In order to estimate the value of α_d , Pearson and Bardeen observed that the impurities are probably distributed more or less at random, and the mobile charges are distributed in such a way to shield the dopant ions from one another. They maintained that, following the method of Wigner and Seitz [Wigner33], it should be possible to draw a spherical region about each ion which is electrically neutral. The average radius, r_s , of such a sphere (Wigner-Seitz radius) is given by:

$$\frac{4\pi}{3} r_s^3 = N_d^{-1}$$

so that:

$$r_s = \left(\frac{3}{4\pi N_d} \right)^{1/3} \approx 0.6204 \cdot N_d^{-1/3} . \quad (3.3)$$

Assuming the mobile charges uniformly distributed throughout the sphere and all electron or holes as mobile (complete ionization), they found a variation in the ionization energy given by:

$$-1.646 \cdot \frac{e^2}{4\pi\epsilon r_s} . \quad (3.4)$$

Substituting for r_s from the Eq. (3.3), this becomes [Pearson49]:

$$-2.653 \cdot \frac{e^2 N_d^{1/3}}{4\pi\epsilon}$$

Therefore:

$$\alpha_d = 2.653 \cdot \frac{e^2}{4\pi\epsilon} = \frac{3.82 \cdot 10^{-7}}{\epsilon_r} \text{ eV} \cdot \text{cm} , \quad (3.5)$$

where ϵ_r is the relative dielectric permittivity of the host semiconductor. The value given by (3.5) resulted to be about 2/3 of the empirical one obtained by Pearson and Bardeen for Si ($\epsilon_r \approx 13$) doped with P or B, thus justifying on a qualitative theoretical basis the experimental results.

One important feature of Pearson and Bardeen's model is that, as N_d reaches the critical value:

$$N_{cr} \equiv \left[\frac{\Delta E_d(0)}{\alpha_d} \right]^3 ,$$

ΔE_d becomes zero and all substitutional dopants are ionized. In this case, the sample will behave like a metal, presenting a finite conductivity in the limit of zero temperature and a weak dependence on temperature of both conductivity and free carrier concentration. This effect has been observed experimentally in all semiconductors, Silicon Carbide included [FerreiraDaSilva06], and it is known as the Mott transition (although the latter includes a larger set of phenomena [Mott74]). Another feature is that ionization energies, following this model, are independent of the temperature T , having assumed a complete ionization of dopants at all temperatures and therefore a concentration of mobile carriers independent of T .

3.2.2. Corrections to Pearson and Bardeen's model.

As pointed out before, Pearson's and Bardeen's model has been largely used although with some corrections due to several authors. In this subsection we will make a survey of this variations.

The first correction is due to the observed difference between the empirical ionization energies of several dopants in their high dilution limit and the values predicted by (3.2) ([Milnes73], p. 6). So $\Delta E_d(0)$ is treated as an empirical parameter in expressions like Eq. (3.1) instead of using Eq. (3.2).

Similarly, the factor:

$$\alpha_d = 2.653 \cdot \frac{e^2}{4\pi\epsilon}$$

appears to be unfit to predict the experimental values, so also α_d is treated as an empirical parameter to be obtained by a fit of the experimental ionization energy values with the expression (3.1).

A subtler correction to Pearson and Bardeen's model aims to take into account the effect of compensation on the ionization energy values of dopants. Several models have been proposed to this purpose, but all seems to lead to an expression like [Shklovskii80]:

$$\alpha_d(K) = \frac{e^2}{4\pi\epsilon} \cdot f(K) , \quad (3.6)$$

where:

$$K \equiv \frac{N_{comp}}{N_d} \quad (3.7)$$

is the compensation degree, N_{comp} being the total concentration of compensating centers, while $f(K)$ is a universal dimensionless function of K . In Pearson and Bardeen's model:

$$f(K) = 2.653 ,$$

i.e. it is a constant, while for some authors [Leloup78]:

$$f(K) = B \cdot (1 - K)^{1/3} , \quad (3.8a)$$

where B is a dimensionless constant, so that:

$$\Delta E_d(N_d - N_{comp}) = \Delta E_d(0) - \frac{Be^2}{4\pi\epsilon} \cdot (N_d - N_{comp})^{1/3} . \quad (3.8b)$$

For other authors, instead, $f(K)$ is a much more complex function of K , which can be expressed analytically only in some limiting cases [Shklovskii80].

3.2.3. Pearson and Bardeen's model as applied to SiC.

Pearson and Bardeen's model, with the corrections discussed in the preceding subsection, has been applied also to different polytypes of Silicon Carbide. We report in Tab. 3.1 some results published in the literature, corresponding to some of the fits plotted in Figs. 3.1.

polytype	dopant	$\Delta E_{d,1}$ [eV]	$\alpha_{d,1}$ [eV cm]	$\Delta E_{d,2}$ [eV]	$\alpha_{d,2}$ [eV cm]	reference
3C-SiC	N	0.048	$2.6 \cdot 10^{-8}$	-	-	[Segal186]
4H-SiC	N	0.0709	$3.38 \cdot 10^{-8}$	0.1237	$4.65 \cdot 10^{-8}$	[Kagamihara04]
4H-SiC	Al	0.220	$2.32 \cdot 10^{-8}$	-	-	[Achatz08]

Tab. 3.1. Parameters for the concentration dependence of some substitutional dopant energy levels in 3C- and 4H-SiC.

3.3. A different model for the ionization energy variation.

As the same Pearson and Bardeen suggested in [Pearson49], the majority carriers may be concentrated more in the neighborhood of the dopant ions than they assumed, so the assumption of an ionization energy independent of the degree of ionization of the impurities can be considered only an approximation. In fact, on the average, only a part of the majority carriers become free due to thermal activation, while the remaining ones are localized in the neighborhood of the dopant ions in a bound state, so the concentration of *mobile* carriers that shield the impurity ion potential is minor than the total substitutional dopant density: in this case, N_d should be substituted by N_D^+ or N_A^- in Eq. (3.1), thus giving a temperature dependent ionization energy. Moreover, as we shall see in the next subsection, the mobile carriers rearrange themselves more in the neighborhood of the dopant charged cores, so the hypothesis of a uniform mobile charge distribution falls down. These observations led us to search for a model of the ionization energy variation more realistic than Pearson and Bardeen's one.

3.3.1. Static Coulomb screening.

In order to find a more physically correct model for the variation of the dopant ionization energy, we concentrated our attention on the variation of the potential energy of a charge carrier due to a dopant ion in the presence of mobile carriers. Such a potential energy $U(\mathbf{r})$ is given by the solution of Poisson's equation ([Sze07], p. 62) multiplied by $\mp e$, the minus sign holding for electrons and the plus sign for holes:

$$\Delta_{\mathbf{r}}U(\mathbf{r}) = \pm \frac{e^2}{\epsilon} \cdot \rho(\mathbf{r}) , \quad (3.9)$$

where $\Delta_{\mathbf{r}}$ is the Laplacian operator and $\rho(\mathbf{r})$ is the space charge density, the plus sign holding for electrons and the minus sign for holes. Considering here the n -type case and calling E_C the absolute minimum of the conduction band, we require the potential energy $U(\mathbf{r})$ of an electron in the presence of a donor ion (placed at the origin of the coordinate system) to satisfy the constraints:

$$\lim_{|\mathbf{r}| \rightarrow \infty} U(\mathbf{r}) = E_C \quad (3.10a)$$

and:

$$\lim_{|\mathbf{r}| \rightarrow 0} \{ |\mathbf{r}| \cdot [U(\mathbf{r}) - E_C] \} = -\frac{e^2}{4\pi\epsilon} \quad (3.10b)$$

in order to be physically meaningful. The first constraint means that, taking E_C as the energy reference, the potential energy tends to zero at infinite distance from the donor ion, while the second constraint means that, in the very neighborhood of the dopant ion, the latter exercises on electrons an ordinary (i.e. unscreened) Coulomb attraction.

The solution of Eq. (3.9) subject to the constraints (3.10) is, within the linear screening approximation ([Shklovskiĭ84], Sec. 11.1):

$$U(\mathbf{r}) = E_C - \frac{e^2}{4\pi\epsilon} \cdot \frac{\exp(-r/r_{sc})}{r}, \quad (3.11)$$

where $r \equiv |\mathbf{r}|$ and the screening radius, r_{sc} , is given by:

$$\frac{1}{r_{sc}^2} = -\frac{e^2}{\epsilon} \cdot \frac{d\rho}{dE_F}, \quad (3.12)$$

where E_F is the Fermi level of the system. In the next subsection we shall search for an acceptable expression for the screening radius r_{sc} .

3.3.2. Evaluation of the screening radius.

In the literature several expressions for the screening radius, r_{sc} , can be found. The most simple of them neglect both the minority carrier and the ionized dopant concentration, i.e. they simplify the space charge density taking into account only the majority carrier concentration in the right side of Eq. (3.12). Then, in the n -type case:

$$\frac{1}{r_{sc}^2} = \frac{e^2}{\epsilon} \cdot \frac{dn}{dE_F}, \quad (3.13)$$

where n is the free electron concentration.

In the two limiting cases of non-degeneration and strong degeneration of electrons in the conduction band, two very simple expressions for r_{sc} can be obtained. In the first case Boltzmann statistic can be used, thus giving (see App. 3A) the so called Debye-Hückel radius ([Fistul'69], p. 93-94):

$$r_{DH} = \sqrt{\frac{\epsilon k_B T}{e^2 n}}. \quad (3.14)$$

In the opposite case, we obtain (see App. 3A) the so called Thomas-Fermi radius ([Fistul'69], p. 93-94):

$$r_{TF} = \sqrt{\frac{\hbar^2 \epsilon}{4m_e^* e^2} \cdot \left(\frac{1}{3\pi^2 M_c^2 n}\right)^{1/3}}. \quad (3.15)$$

For having a unique general expression for r_{sc} , W.A. Harrison suggested to use ([Harrison99], p. 289):

$$r_{sc} \approx \sqrt{r_{DH}^2 + r_{TF}^2}, \quad (3.16)$$

but this is a very rough expression which doesn't satisfy us. In fact, the correct expression is given by ([Fistul'69], p. 93-94):

$$\frac{1}{r_{sc}^2} = \frac{e^2 N_C}{\epsilon k_B T} \cdot \mathcal{F}_{-1/2} \left(\frac{E_F - E_C}{k_B T} \right), \quad (3.17)$$

where N_C is the effective density of states in the conduction band and $\mathcal{F}_{-1/2}(x)$ is the Fermi-Dirac integral of order $-1/2$. Using tabulated values of the functions $\mathcal{F}_{1/2}(x)$ and $\mathcal{F}_{-1/2}(x)$ [Cloutman89], we have verified that the expression (3.16) gives values of r_{sc} far until 11% from the correct ones for values of E_F in the neighborhood of E_C . Therefore, an approximate expression for the function $\mathcal{F}_{-1/2}(x)$ have to be used, but we shall discuss its choice in the next subsection.

A further improvement in the expression for r_{sc} can be obtained considering not only the contribution to the space charge density of the free majority carriers, but also that of the ionized dopant atoms. Considering the compensating centers completely ionized, their concentration results to be independent of the Fermi energy and Eq. (3.12) becomes:

$$\frac{1}{r_{sc}^2} = \frac{e^2}{\epsilon} \cdot \frac{d(n - N_D^+)}{dE_F}, \quad (3.18)$$

where N_D^+ is the total concentration of ionized donors:

$$N_D^+ = \sum_i \frac{N_{D,i}}{1 + g_{D,i} \cdot \exp\left(\frac{\Delta E_{D,i}}{k_B T}\right) \cdot \exp\left(\frac{E_F - E_C}{k_B T}\right)},$$

$N_{D,i}$ being the concentration, $g_{D,i}$ the degeneracy factor and $\Delta E_{D,i}$ the ionization energy of the i -th substitutional donor level, respectively. In the case a single donor species is present, $i = 1$ for 3C-, $i = 1, 2$ for 4H- and $i = 1, 2, 3$ for 6H-SiC, due to non-equivalent lattice sites (see Tab. 1.2). By defining the ionization degree of the i -th donor level as:

Dopant ionization energy variation

$$\xi_{D,i}^+ = \frac{1}{1 + g_{D,i} \cdot \exp\left(\frac{\Delta E_{D,i}}{k_B T}\right) \cdot \exp\left(\frac{E_F - E_C}{k_B T}\right)}$$

(see Eq. (2.1b)), we find (see App. 3B):

$$\frac{1}{r_{sc}^2} = \frac{e^2}{\epsilon k_B T} \cdot \left[N_C \cdot \mathcal{F}_{-1/2}\left(\frac{E_F - E_C}{k_B T}\right) + \sum_i N_{D,i} \cdot \xi_{D,i}^+ \cdot (1 - \xi_{D,i}^+) \right] \quad (3.19a)$$

which, in the case of a single donor level, assumes the well known form (see [Pernot01] for the non-degenerate case):

$$\frac{1}{r_{sc}^2} = \frac{e^2}{\epsilon k_B T} \cdot \left[N_C \cdot \mathcal{F}_{-1/2}\left(\frac{E_F - E_C}{k_B T}\right) + \frac{(N_A + n) \cdot (N_D - N_A - n)}{N_D} \right], \quad (3.19b)$$

where N_A is the total compensating acceptor concentration (see App. 3C). Therefore, the expression (3.19a) can be considered as the generalization of (3.19b) for more than one dopant level. Similar expressions hold for the p -type case.

3.3.3. Approximate expression for the Fermi-Dirac integral of order $-1/2$.

We have seen in the preceding subsection that for calculating the screening radius, r_{sc} , we need an expression for the Fermi-Dirac integral of order $-1/2$, $\mathcal{F}_{-1/2}(x)$. Such a function cannot be expressed in terms of simpler known functions, so we need to use an approximate expression for $\mathcal{F}_{-1/2}(x)$. In the literature exist several accurate procedures for calculating this function with a very high precision ([Jog79], [VanHalen85], [Sagar91], [VanCong91], [VanCong92], [Goano93], [MacLeod98], [Lether00]) but in general they are too complex for the limited precision we need, requiring a certain unnecessary computational time, and converging only in a part of the whole domain of the function. An expression exists, however, which has a form

similar to that we used for calculating $F_{1/2}(x)$ [AymerichHumet81] and represents a good compromise between accuracy and simplicity [AymerichHumet83]. It is unique over the entire range of its variable, so avoiding unnatural discontinuities in the simulation results. Therefore, we believe it is a good starting point.

The expression proposed in [AymerichHumet83] is:

$$F_{-1/2}(x) = \frac{1}{\sqrt{\frac{\pi/2}{x+b+(|x-b|^c+a)^{1/c}} + \exp(-x)}}, \quad (3.20)$$

which with the values proposed by the authors for the parameters a , b , c reaches a maximum relative error (in its absolute value) of 1.2%. However, it is possible to improve its precision with a better choice of the three parameters a , b , c . For example, we found that using the values:

$$a = 10.05912$$

$$b = 1.63692$$

(3.21)

$$c = 4.44581$$

it is possible to reach a maximum relative error (in its absolute value) of less than 0.8% (see Fig. 3.2), thus obtaining a maximum relative error (in its absolute value) of less than 0.4% for the screening radius (3.19a). We will use the approximate function (3.20) with the parameters (3.21) in our simulations.

Dopant ionization energy variation

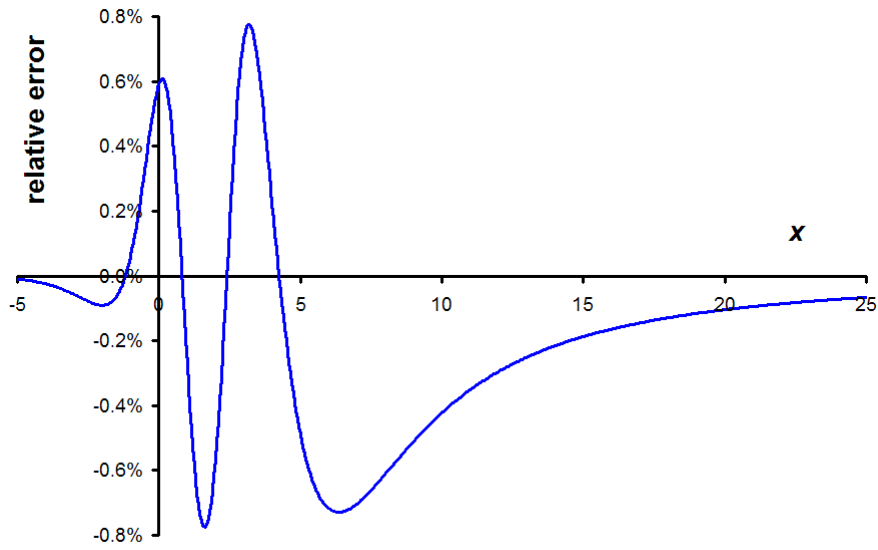


Fig. 3.2. Relative error of our fit of $F_{-1/2}(x)$ with function (3.20) and parameters (3.21).

3.3.4. Eigenvalues of Schrödinger equation with a screened Coulomb potential.

Now we have all the instruments for determining numerically the potential energy (3.11) or, to be more precise, the difference $U(\mathbf{r}) - E_C$. At this point, what should we do with this function?

It is evident that the hydrogenic model for a substitutional donor atom can no longer be used, and something else should take its place. The hydrogenic model was obtained by solving the Schrödinger equation with a simple (unscreened) Coulomb potential, while now a static screened Coulomb potential has to be considered. In other words, we have to solve the Schrödinger equation:

$$\frac{\hbar^2}{2m^*} \Delta_r \Psi + \left[-\Delta E_D + \frac{e^2}{4\pi\epsilon} \cdot \frac{\exp(-r/r_{sc})}{r} \right] \cdot \Psi = 0, \quad (3.22)$$

where Ψ is the wave function of the system, $\hbar \equiv h / 2\pi$ is the reduced Planck's constant and m^* is the effective mass of electrons or holes, but not necessarily the

conduction or valence band free carrier effective mass, respectively. In fact, it seems to be more useful to introduce the binding mass m_B [Martinez02]:

$$m_B = \epsilon_r^2 \cdot \frac{\Delta E_D(0)}{\Delta E_H} \cdot m_0, \quad (3.23)$$

where $\Delta E_D(0)$ is the measured ionization energy of the donor in the high dilution limit (so without screening), $\Delta E_H = 13.6$ eV is the ionization energy of the hydrogen atom in vacuum and m_0 is the free electron mass. In such a manner, the solution of Eq. (3.22) with $m^* = m_B$ and without screening gives the correct empirical result $\Delta E_D = \Delta E_D(0)$ in the high dilution limit.

We now assume, as a simplifying hypothesis, that the donor atom can be described by Eq. (3.22) with a constant effective mass $m^* = m_B$, which is considered unaffected by screening effects. We then introduce the effective Bohr radius of the donor atom in the high dilution limit [Martinez02]:

$$r_D(0) \equiv \frac{\epsilon_r m_0}{m_B} \cdot a_H = \frac{1}{\epsilon_r} \cdot \frac{\Delta E_H}{\Delta E_D(0)} \cdot a_H, \quad (3.24)$$

where $a_H = 0.529$ Å is the Bohr radius of a hydrogen atom in vacuum. Let us now define the dimensionless variable:

$$\rho \equiv \frac{r}{r_D(0)}$$

and the dimensionless parameters:

$$\chi_D \equiv \frac{r_D(0)}{r_{sc}} \quad (3.25a)$$

$$\Delta \epsilon_D \equiv \frac{\Delta E_D}{\Delta E_D(0)}. \quad (3.25b)$$

Dopant ionization energy variation

With some passages the Schrödinger equation (3.22) becomes (see App. 3D):

$$\Delta_{\rho} \Psi + \left[-\Delta \varepsilon_D + \frac{2}{\rho} \exp(-\chi_D \rho) \right] \cdot \Psi = 0 , \quad (3.26)$$

where $\Delta_{\rho} \equiv r_D(0)^2 \Delta_r$ is the reduced Laplacian operator. Therefore, in our model, the reduced energy $\Delta \varepsilon_D$ turns out to be a universal function of the parameter χ_D alone. Let us search for such a function.

Fortunately, we are interested only in the eigenvalues $\Delta \varepsilon_D$ of Eq. (3.26) in the ground state of the system: we don't need to know also the corresponding wave functions. Several authors ([Rogers70], [Singh84], [Holubec90], [Diaz91]) had solved numerically such an equation for a discrete set of values of χ_D , finding also its critical value [Diaz91]:

$$\chi_{cr} = 1.190612421060618$$

above which $\Delta \varepsilon_D < 0$ and no more bound states exist. In the latter case, all donors of the examined type turn out to be ionized, as in Pearson and Bardeen's model.

Eq. (3.26) is not analytically solvable. In order to find an approximate expression for the universal function $\Delta \varepsilon_D(\chi_D)$ corresponding to the $1s$ state, we have performed a fit of the numerical results obtained in [Holubec90], [Diaz91] in the interval $[0, \chi_{cr}]$ through a fourth order polynomial:

$$f(\chi) \equiv c_0 + c_1 \cdot \chi + c_2 \cdot \chi^2 + c_3 \cdot \chi^3 + c_4 \cdot \chi^4 \quad (3.27)$$

subjected to the four constraints:

- 1) $f(0) = 1$ (by the definition of $\Delta \varepsilon_D$)
- 2) $f'(0) = -2$ (by perturbation theory [Smith64])

3) $f(\chi_{cr}) = 0$ (by definition of χ_{cr} [Diaz91])

4) $f'(\chi_{cr}) = 0$ (by looking at the behavior of $\Delta\epsilon_D(\chi)$ in the neighborhood of χ_{cr}),

requiring also that $f(\chi) \geq 0$ in its domain $[0, \chi_{cr}]$. The optimal parameters we obtained are:

$$c_0 = 1$$

$$c_1 = -2$$

$$c_2 = 1.399971475167$$

(3.28)

$$c_3 = -0.489054015737$$

$$c_4 = 0.110522145823$$

The universal function $\Delta\epsilon_D(\chi_D) \approx f(\chi_D)$ is plotted in Fig. 3.3a, while Fig. 3.3b illustrates the relative error (in its absolute value) of our fit.

For $\chi_D > \chi_{cr}$ we have to set $g_D = 0$ in the expression for the ionization degree of the donor; this corresponds physically to the absence of bound donor states and gives numerically $N_D^+ = N_D$. This makes superfluous the knowledge of the (reasonably negative) ionization energy of the corresponding donor state, therefore we can set it arbitrarily equal to zero in our simulations and in the graphical representations of our results (see Fig. 3.4b in the next section for an example).

Dopant ionization energy variation

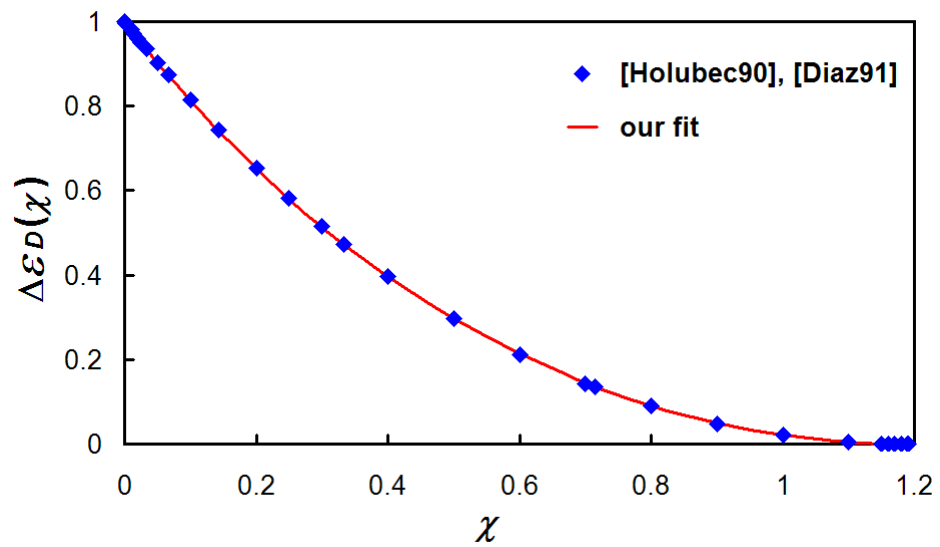


Fig. 3.3a. Fit of numerical values given by [Holubec90] and [Diaz91] using Eq. (3.27) with parameters (3.28).

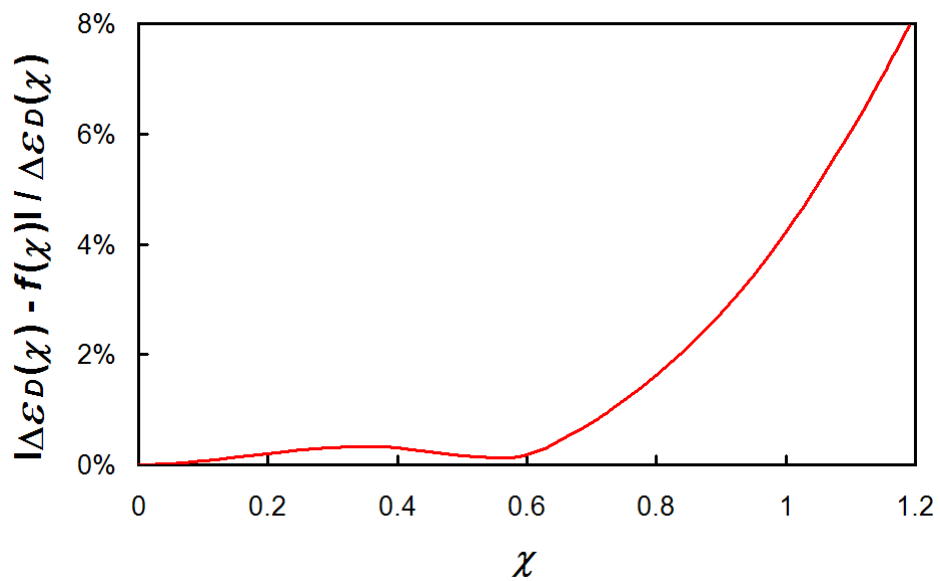


Fig. 3.3b. Relative error (in its absolute value) of our fit using Eq. (3.27) with parameters (3.28).

It should be stressed that, while the screening radius assumes a *unique* value for all donors or acceptors present in the system, a *different* value of the parameter χ_d will correspond to *each* kind of dopant state due to the different ionization energies of the same dopant species substituting in non-equivalent lattice sites, or of different dopant species contemporarily present (see Eqs. (3.24) and (3.25a)). Therefore it happens that when a certain dopant state becomes completely ionized, i.e. when its energy level touches the conduction or valence band edge, all the other states with deeper energy levels in general continue to exist with finite ionization energies also if they correspond to the same chemical species. For example, as we shall see in the next section, P substituting in *hexagonal* sites in 4H-SiC is completely ionized at room temperature at a phosphorus concentration for which P substituting in *cubic* sites is still partially ionized, because of its deeper energy level and therefore a lower value of χ_d (see Eqs. (3.24) and (3.25a)).

3.4. Simulation results.

The model we have elaborated in the preceding sections has been implemented in a simulation program written in VBA (*Visual Basic for Applications*), which treats in a self-consistent way the solution of the charge neutrality equation together with the screening problem. Here and in the next chapter we simulate 4H-SiC behavior because for this polytype *all* the physical parameters required by our model are well established in the literature. However, our model can be applied also to the other SiC polytypes, thus giving at least semi-quantitative results.

We illustrate in Figs. 3.4 our simulation results for uncompensated 4H-SiC:P at room temperature ($T = 300$ K), having taken as parameters those given in Tab. 3.2, so that the effective density of states of the conduction band at room temperature results to be $N_C(300 \text{ K}) = 1.87 \cdot 10^{19} \text{ cm}^{-3}$. For comparison, we have plotted in Fig. 3.4a also our solution of the charge neutrality equation without screening, i.e. with concentration independent ionization energies, by using again the parameters of Tab. 3.2, and in particular the same ionization energies relative to the high dilution limit.

Dopant ionization energy variation

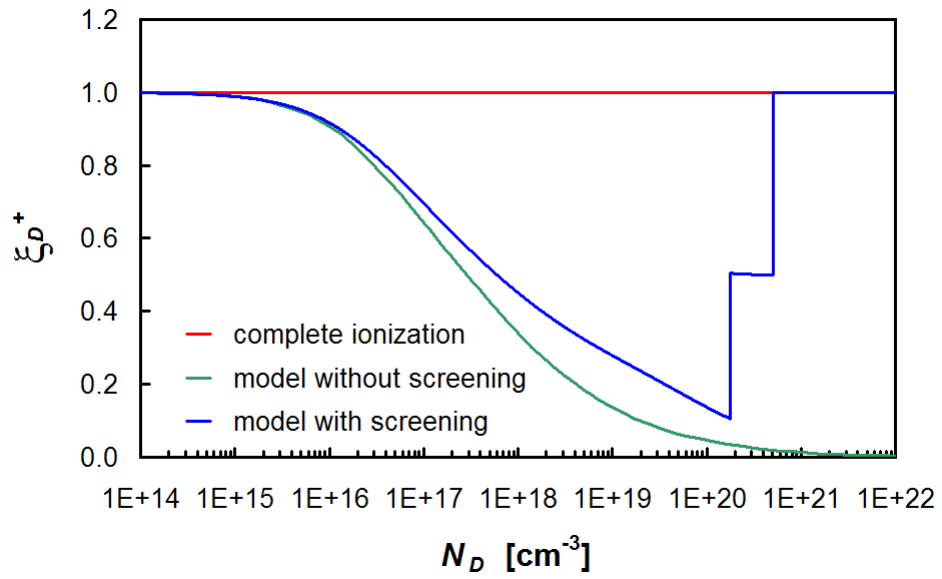


Fig. 3.4a. Ionization degree of substitutional Phosphorus in uncompensated 4H-SiC at room temperature.

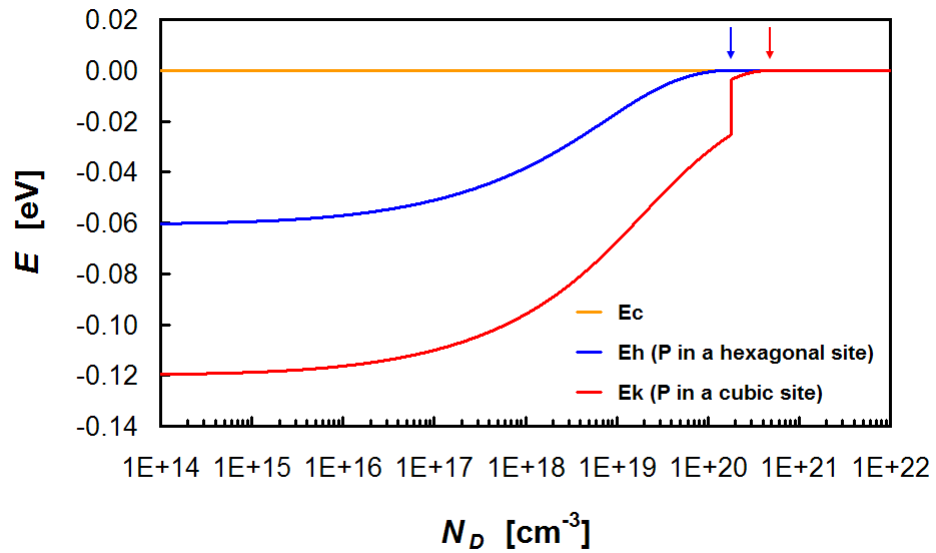


Fig. 3.4b. Energy levels of substitutional Phosphorus in uncompensated 4H-SiC at room temperature, taking the conduction band edge E_C as energy reference. An arrow indicates when the bound state plotted with the same color vanishes.

$m_e^* = 0.394 m_0$	DOS effective mass of electrons in one valley of the conduction band	[Wellenhofer97]
$M_C = 3$	number of equivalent valleys in the conduction band	[Persson97]
$\epsilon_r = 9.78$	static dielectric constant	[Koizumi09]
$g_{P,h} = g_{P,k} = 4$	degeneracy factor of hexagonal and cubic P donor bound states	[GreulichWeber97]
$\Delta E_{P,h}(0) = 60.7 \text{ meV}$	ionization energy of P substituting on hexagonal sites: high dilution limit	[Ivanov05]
$\Delta E_{P,k}(0) = 120 \text{ meV}$	ionization energy of P substituting on cubic sites: high dilution limit	[Ivanov05]
$N_{P,h} = N_{P,k}$	repartition of substitutional P between hexagonal and cubic sites	[Kagamihara04]

Tab. 3.2. Parameters used for simulating Phosphorus doped 4H-SiC behavior.

In the first line, m_0 is the free electron mass.

As we can see from Fig. 3.4a, the main difference between unscreened and screened dopant model is that the former predicts a monotonically decreasing ionization degree of Phosphorus with increasing concentration, while the latter, after a similar decrease for moderately doped 4H-SiC, predicts a P complete ionization for sufficiently high substitutional Phosphorus concentrations. The model including screening reproduces better the experimental results in the heavy doping region, where for example an electron concentration of about $1.2 \cdot 10^{20} \text{ cm}^{-3}$ was measured for a 4H-SiC sample with a P implant concentration equal to $2.0 \cdot 10^{20} \text{ cm}^{-3}$ [Laube02]. By assuming a complete activation of the implanted donors and the absence of compensating centers, the ionization degree of P in such a sample is 0.6. The model with constant energy levels predicts an ionization degree value equal to 0.03, which is really too low, while the model including screening predicts a value of

Dopant ionization energy variation

0.5; the latter model seems to respect at least the order of magnitude of the experimental data.

However, as it is apparent from Fig. 3.4a, our model predicts unnatural discontinuities in the degree of ionization, each discontinuity corresponding to an ionization energy becoming zero; in this case, for P substituting in a hexagonal site first and in a cubic site successively, as we can see from Fig. 3.4b. This is due to the fact that when an ionization energy becomes zero, the dopants to whom it corresponds are “suddenly” completely ionized because of the discrete nature of their energy level. In order to avoid such discontinuities, we must consider an important phenomenon typical of heavily doped semiconductors, i.e. the broadening of dopant energy levels into impurity bands [Morgan65]. This topic will be discussed in detail in the next chapter.

Another feature of our model is the dependence of energy levels on temperature, due to the decrease of free carrier concentration with decreasing T and the consequent increase of the screening radius. To give an example, we have plotted in Fig. 3.5 the Phosphorus donor energy levels as functions of T for 4H-SiC doped with 10^{20} P atoms / cm^3 and 10% compensated. As we can see from this figure, between liquid Nitrogen temperature (77 K) and 150 K the P energy levels result to be strongly temperature dependent, tending to their high dilution limits as T tends to the absolute zero (the latter being a general characteristic of our model, because at very low temperatures the screening becomes negligible). This temperature dependence of energy levels increases in magnitude with increasing dopant concentration, because the difference between the high temperature and the low temperature limit of energy levels increases with concentration due to screening effects. But the low temperature region is crucial for extracting just the dopant ionization energies from standard temperature dependent Hall effect data analysis ([Blood92], p. 101), which assumes energy levels independent of T . Therefore, the values obtained from such an analysis result to be at least questionable for samples with a not too low dopant density, if our model is correct. This makes very difficult a comparison of our model with the experimental data found in the literature.

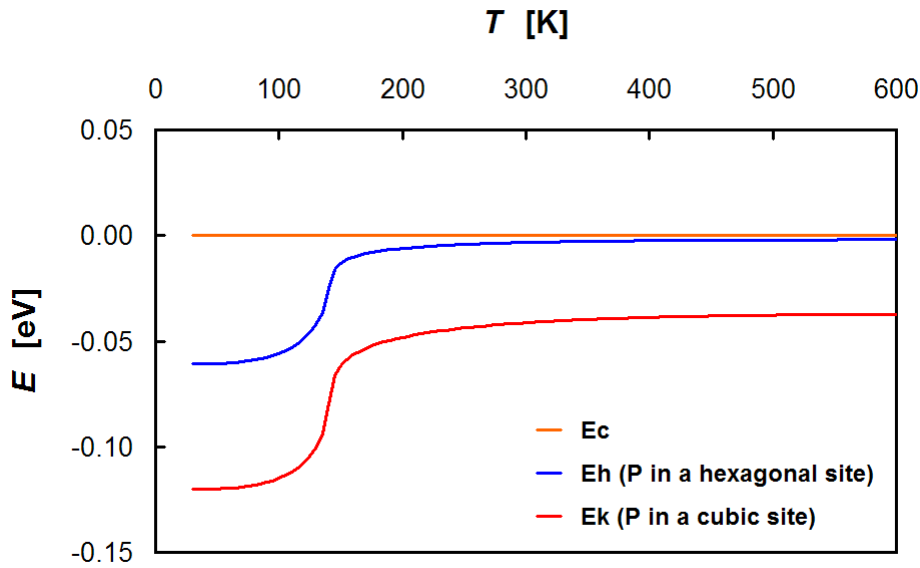


Fig. 3.5. Energy levels of substitutional P in 10^{20} cm^{-3} Phosphorus doped 4H-SiC, 10% compensated, taking the conduction band edge E_C as energy reference.

For this reason, we made a comparison with the literature data obtained by *moderately doped* SiC samples, for which the ionization energy variation with temperature can be neglected. In Fig. 3.6 we present computed versus experimental values (the latter taken from [Laube02], [Handy00] and [Rao06]) of the free electron concentration n for a few different couples of P donors and compensating center densities (N_D , N_{comp}) in 4H-SiC at room temperature. The couples of experimental N_D and N_{comp} values are those given by [Laube02], [Handy00] and [Rao06], while the substitutional Phosphorus ionization energies are calculated self-consistently during our simulation. The parameters used in our computation are the same of Tab. 3.2. As we can see from Fig. 3.6, our model reproduces well the measured values of n in all the examined cases. We presented these results at the 8th European Conference on Silicon Carbide and Related Materials (ECSCRM 2010) [Scaburri].

Dopant ionization energy variation

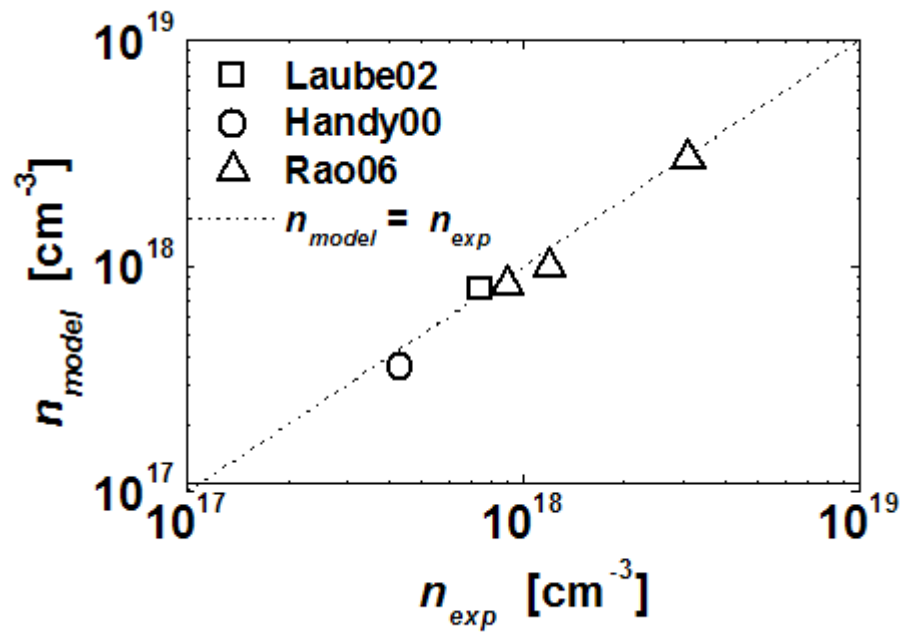


Fig. 3.6. Simulated versus experimental free electron concentration in partially compensated 4H-SiC:P at room temperature.

Chapter 3

Appendix 3A. Debye-Hückel and Thomas-Fermi screening radius.

We have seen that, considering only the screening due to free carriers and neglecting the minority carrier density, in the n -type case the screening radius is given by (3.13):

$$\frac{1}{r_{sc}^2} = \frac{e^2}{\epsilon} \cdot \frac{dn}{dE_F}, \quad (3A.1)$$

where (see Eq. 2.11a):

$$n(E_F) = N_C \cdot \mathcal{F}_{1/2} \left(\frac{E_F - E_C}{k_B T} \right) \quad (3A.2)$$

is the free electron concentration. Let us now calculate the screening radius in two limiting cases: the non-degenerate and the strongly degenerate one.

1) In the case of non-degeneration:

$$\frac{E_F - E_C}{k_B T} \ll -1$$

and therefore (see [\[Blakemore62\]](#), App. A):

$$\mathcal{F}_{1/2} \left(\frac{E_F - E_C}{k_B T} \right) \approx \exp \left(\frac{E_F - E_C}{k_B T} \right).$$

Hence Boltzmann approximation can be used, (3A.2) becoming:

$$n(E_F) = N_C \cdot \exp \left(\frac{E_F - E_C}{k_B T} \right),$$

to give:

$$\begin{aligned} \frac{1}{r_{sc}^2} &= \frac{e^2}{\epsilon} \cdot \frac{d}{dE_F} \left[N_C \cdot \exp\left(\frac{E_F - E_C}{k_B T}\right) \right] = \\ &= \frac{e^2 N_C}{\epsilon} \cdot \frac{1}{k_B T} \exp\left(\frac{E_F - E_C}{k_B T}\right) = \\ &= \frac{e^2}{\epsilon k_B T} \cdot n . \end{aligned}$$

Hence, we obtain the Debye-Hückel radius (3.14):

$$r_{DH} = \sqrt{\frac{\epsilon k_B T}{e^2 n}} .$$

2) In the case of strong degeneration:

$$\frac{E_F - E_C}{k_B T} \gg 1$$

and therefore (see [\[Blakemore62\]](#), App. A):

$$\mathcal{F}_{1/2}\left(\frac{E_F - E_C}{k_B T}\right) \approx \frac{4}{3\sqrt{\pi}} \cdot \left(\frac{E_F - E_C}{k_B T}\right)^{3/2} .$$

Hence Thomas-Fermi approximation can be used, being:

$$n = \frac{4N_C}{3\sqrt{\pi}} \cdot \left(\frac{E_F - E_C}{k_B T}\right)^{3/2} .$$

Substituting Eq. (1.1a) we have:

Dopant ionization energy variation

$$\begin{aligned}
 n &\approx \frac{4}{3\sqrt{\pi}} \cdot 2M_C \cdot \left(\frac{2\pi m_e^* k_B T}{h^2} \right)^{3/2} \left(\frac{E_F - E_C}{k_B T} \right)^{3/2} = \\
 &= \frac{8\pi M_C}{3h^3} \cdot [2m_e^* (E_F - E_C)]^{3/2}
 \end{aligned} \tag{3A.3}$$

which, by inversion, gives:

$$E_F - E_C = \frac{1}{8m_e^*} \left(\frac{3n}{\pi M_C} \right)^{2/3} . \tag{3A.4}$$

Substituting (3A.3) in (3A.1) gives:

$$\begin{aligned}
 \frac{1}{r_{sc}^2} &= \frac{e^2}{\epsilon} \cdot \frac{d}{dE_F} \left\{ \frac{8\pi M_C}{3h^3} \cdot [2m_e^* (E_F - E_C)]^{3/2} \right\} = \\
 &= \frac{8\pi M_C e^2}{3h^3 \epsilon} (2m_e^*)^{3/2} \cdot \frac{3}{2} (E_F - E_C)^{1/2} = \\
 &= \frac{4\pi M_C e^2}{h^3 \epsilon} (2m_e^*)^{3/2} (E_F - E_C)^{1/2}
 \end{aligned}$$

which, substituting (3A.4), becomes:

$$\begin{aligned}
 \frac{1}{r_{sc}^2} &= \frac{4\pi M_C e^2}{h^3 \epsilon} (2m_e^*)^{3/2} \left[\frac{1}{8m_e^*} \left(\frac{3n}{\pi M_C} \right)^{2/3} \right]^{1/2} = \\
 &= \frac{4m_e^* e^2}{h^3 \epsilon} \cdot (3\pi^2 M_C^2 n)^{1/3} .
 \end{aligned}$$

Therefore:

$$r_{sc} = \sqrt{\frac{h^3 \epsilon}{4m_e^* e^2} \cdot \frac{1}{(3\pi^2 M_C^2 n)^{1/3}}},$$

i.e. the Thomas-Fermi radius (3.15).

Out of any approximation, being (see [\[Blakemore62\]](#), App. A):

$$\frac{d}{dx} \mathcal{F}_{1/2}(x) = \mathcal{F}_{-1/2}(x),$$

Eqs. (3A.1) and (3A.2) give:

$$\begin{aligned} \frac{1}{r_{sc}^2} &= \frac{e^2}{\epsilon} \cdot \frac{d}{dE_F} \left[N_C \cdot \mathcal{F}_{1/2} \left(\frac{E_F - E_C}{k_B T} \right) \right] = \\ &= \frac{e^2 N_C}{\epsilon k_B T} \cdot \mathcal{F}_{-1/2} \left(\frac{E_F - E_C}{k_B T} \right), \end{aligned}$$

i.e. Eq. (3.17).

Appendix 3B. Derivative of the ionized dopant concentration.

Eq. (3.18) for the screening radius requires the knowledge of the derivative of:

$$N_D^+ = \sum_i \frac{N_{D,i}}{1 + g_{D,i} \cdot \exp\left(\frac{\Delta E_{D,i}}{k_B T}\right) \cdot \exp\left(\frac{E_F - E_C}{k_B T}\right)}$$

with respect to E_F . The ionization degree of the i -th kind of donor being:

$$\xi_{D,i}^+ = \frac{1}{1 + g_{D,i} \cdot \exp\left(\frac{\Delta E_{D,i}}{k_B T}\right) \cdot \exp\left(\frac{E_F - E_C}{k_B T}\right)}, \quad (3A.1)$$

we have:

$$N_D^+ = \sum_i N_{D,i} \cdot \xi_{D,i}^+$$

so that, the concentrations $N_{D,i}$ being independent of E_F , we have:

$$\frac{dN_D^+}{dE_F} = \sum_i N_{D,i} \cdot \frac{d\xi_{D,i}^+}{dE_F}. \quad (3A.2)$$

By taking the derivative of Eq. (3A.1) we obtain:

$$\frac{d\xi_{D,i}^+}{dE_F} = - \frac{\frac{d}{dE_F} \left[1 + g_{D,i} \cdot \exp\left(\frac{\Delta E_{D,i}}{k_B T}\right) \cdot \exp\left(\frac{E_F - E_C}{k_B T}\right) \right]}{\left[1 + g_{D,i} \cdot \exp\left(\frac{\Delta E_{D,i}}{k_B T}\right) \cdot \exp\left(\frac{E_F - E_C}{k_B T}\right) \right]^2} =$$

Chapter 3

$$\begin{aligned}
 &= -\frac{1}{k_B T} \cdot \frac{g_{D,i} \cdot \exp\left(\frac{\Delta E_{D,i}}{k_B T}\right) \cdot \exp\left(\frac{E_F - E_C}{k_B T}\right)}{\left[1 + g_{D,i} \cdot \exp\left(\frac{\Delta E_{D,i}}{k_B T}\right) \cdot \exp\left(\frac{E_F - E_C}{k_B T}\right)\right]^2} = \\
 &= -\frac{1}{k_B T} \cdot \xi_{D,i}^+ (1 - \xi_{D,i}^+) ,
 \end{aligned}$$

so substituting in (3A.2) and then in (3.18) gives the expression (3.19a) for the screening radius.

Appendix 3C. Screening radius for a single donor level.

In Eq. (3.19a) the term:

$$\sum_i N_{D,i} \cdot \xi_{D,i}^+ \cdot (1 - \xi_{D,i}^+)$$

occurs, which, in the case of only one dopant level, becomes:

$$N_D \cdot \xi_D^+ \cdot (1 - \xi_D^+) .$$

Multiplying and dividing this term by N_D , we have:

$$\begin{aligned} N_D \cdot \xi_D^+ \cdot (1 - \xi_D^+) &= \frac{(N_D \cdot \xi_D^+) \cdot (N_D - N_D \cdot \xi_D^+)}{N_D} = \\ &= \frac{N_D^+ \cdot (N_D - N_D^+)}{N_D} . \end{aligned} \tag{3C.1}$$

However, by neglecting the minority carriers and considering completely ionized the compensating centers (of acceptor type), the charge neutrality equation becomes:

$$N_D^+ = N_A + n .$$

Substituting in (3C.1), we finally obtain:

$$N_D \cdot \xi_D^+ \cdot (1 - \xi_D^+) = \frac{(N_A + n) \cdot (N_D - N_A - n)}{N_D}$$

which, substituted in Eq. (3.19a), gives Eq. (3.19b).

Chapter 3

Appendix 3D. Dimensionless Schrödinger equation.

By introducing the binding mass (3.23) and the dimensionless parameters:

$$\rho \equiv \frac{r}{r_D(0)}$$

and:

$$\chi_D \equiv \frac{r_D(0)}{r_{sc}}$$

the Schrödinger equation (3.22) can be rewritten as:

$$\frac{\hbar^2}{2m_B[r_D(0)]^2} \cdot \Delta_\rho \Psi + \left[-\Delta E_D + \frac{e^2}{4\pi\epsilon r_D(0)} \cdot \frac{\exp(-\chi_D \rho)}{\rho} \right] \cdot \Psi = 0$$

or, multiplying by $\frac{2m_B[r_D(0)]^2}{\hbar^2}$, as:

$$\Delta_\rho \Psi + \left[-\frac{2m_B[r_D(0)]^2 \Delta E_D}{\hbar^2} + \frac{2m_B r_D(0) e^2}{4\pi\epsilon \hbar^2} \cdot \frac{\exp(-\chi_D \rho)}{\rho} \right] \cdot \Psi = 0 .$$

From the definitions (3.23) and (3.24) we have:

$$\begin{aligned} \frac{2m_B[r_D(0)]^2 \Delta E_D}{\hbar^2} &= \frac{2\Delta E_D}{\hbar^2} \cdot \epsilon_r^2 \frac{\Delta E_D(0)}{\Delta E_H} m_0 \cdot \left[\frac{1}{\epsilon_r} \cdot \frac{\Delta E_H}{\Delta E_D(0)} \cdot a_H \right]^2 = \\ &= \frac{\Delta E_D}{\Delta E_D(0)} \cdot \frac{2m_0 a_H^2 \Delta E_H}{\hbar^2} = \frac{\Delta E_D}{\Delta E_D(0)} , \end{aligned}$$

taking into account that:

$$\Delta E_H = \frac{\hbar^2}{2m_0 a_H^2} . \quad (3D.1)$$

Furthermore:

$$\begin{aligned} \frac{2m_B r_D(0)e^2}{4\pi\epsilon\hbar^2} &= \frac{2e^2}{4\pi\epsilon_r\epsilon_0\hbar^2} \cdot \epsilon_r^2 \frac{\Delta E_D(0)}{\Delta E_H} m_0 \cdot \frac{1}{\epsilon_r} \cdot \frac{\Delta E_H}{\Delta E_D(0)} \cdot a_H = \\ &= 2 \cdot \frac{m_0 e^2 a_H}{4\pi\epsilon_0\hbar^2} = 2 , \end{aligned}$$

taking into account that:

$$a_H = \frac{4\pi\epsilon_0\hbar^2}{m_0 e^2} . \quad (3D.2)$$

Therefore Eq. (3.22) takes the form (3.26):

$$\Delta_\rho \Psi + \left[-\Delta\epsilon_D + \frac{2}{\rho} \exp(-\chi_D \rho) \right] \cdot \Psi = 0 ,$$

being by definition (3.25b):

$$\Delta\epsilon_D \equiv \frac{\Delta E_D}{\Delta E_D(0)} .$$

Chapter 4.

Inclusion of impurity bands in our model.

In this chapter we shall treat the impurity band formation and insert it into our model for incomplete ionization of substitutional dopants. In Sec. 4.1 we shall discuss the physical origin of impurity bands and present the model of this phenomenon proposed by T. F. Lee and T. C. McGill in 1975 for lightly doped semiconductors. In Sec. 4.2 we shall modify Lee and McGill's model in order to extend it also to heavily doped semiconductors. In Sec. 4.3 we shall discuss how to treat the effect of impurity bands on the degree of ionization of substitutional dopants. In Sec. 4.4 we shall present the results of our simulations for Silicon Carbide and compare them with experimental results.

4.1. Formation of impurity bands.

With increasing doping concentration in a semiconductor material, dopant discrete energy levels in the bandgap split into quasi-continuous bands. This is due to two independent phenomena, which however happen at the same time. The first one is the gradual overlapping of wave functions of charge carriers bound with *equal* binding energies to dopant cores as the average distance between these latter decreases, following the model of Kronig and Penney [[Kronig31](#)]: it has a purely quantum mechanical nature. The second phenomenon consists in increasing

Chapter 4

potential fluctuations by ionized impurities distributed at random in the host lattice, which has the effect of spreading out the densities of states in the energy diagram [Kane63]: it has a purely statistical nature. As previously said, the combination of these two phenomena determines the formation of impurity bands.

An enormous number of papers in the literature has been devoted to this topic. We have chosen to start from the relatively simple model proposed by T. F. Lee and T. C. McGill [Lee75] for impurity bands, which includes Morgan's model for the effect of potential fluctuations on impurity levels [Morgan65]. For a quantitative treatment of the quantum mechanical broadening of a dopant level, Lee and McGill considered a dopant concentration sufficiently low so that the tight binding model can be used. Therefore, the energy level broadening results to be proportional to the energy transfer integral [Lee75]:

$$J_d \left(\left| \mathbf{R}_i - \mathbf{R}_j \right| \right) = \int_{\mathbb{R}^3} V(\mathbf{r} - \mathbf{R}_i) \phi_{d,0}(\mathbf{r} - \mathbf{R}_i) \phi_{d,0}(\mathbf{r} - \mathbf{R}_j) d^3\mathbf{r} ,$$

where:

$$V(\mathbf{r}) = -\frac{e^2}{4\pi\epsilon_r\epsilon_0 r}$$

is the unscreened Coulomb potential energy and:

$$\phi_{d,0}(\mathbf{r}) = \frac{1}{\sqrt{\pi[r_d(0)]^3}} \exp\left[-\frac{r}{r_d(0)}\right] \quad (4.1)$$

is the dopant ground state wave function, being ϵ_r the relative dielectric permittivity of the host semiconductor and $r_d(0)$ a ground state effective Bohr radius of the dopant atom (different than ours). Due to the symmetry of the problem, the energy transfer integral can be rewritten as:

$$J_d(R) = \int_{\mathbb{R}^3} V(\mathbf{r}) \phi_{d,0}(\mathbf{r}) \phi_{d,0}(\mathbf{r} - \mathbf{R}) d^3\mathbf{r} \quad (4.2)$$

Inclusion of impurity bands in our model

to give [Lee75]:

$$J_d(R) = -\frac{e^2}{4\pi\epsilon_r\epsilon_0 r_d(0)} \left[1 + \frac{R}{r_d(0)} \right] \exp\left[-\frac{R}{r_d(0)} \right],$$

where R is the distance between nearest dopant neighbors. Since the doping atoms are randomly distributed in space, the distance R to the nearest dopant neighbor and the energy transfer integral $J_d(R)$ vary from one doping atom to another. If the dopants are absolutely randomly distributed in semiconductors, they should follow a Poisson distribution. In a Poisson distribution, the probability that the nearest dopant neighbor lies at a distance R in a spherical shell between R and $R + dR$ is given by:

$$4\pi N_d \exp\left(-\frac{4\pi}{3} N_d R^3\right) R^2 dR,$$

where N_d is the concentration of dopants with the same energy level E_d . Therefore, the average energy transfer integral between a doping atom and its nearest dopant neighbor is equal to [Lee75]:

$$\langle J_d(R) \rangle = 4\pi N_d \int_0^{+\infty} J_d(R) \exp\left(-\frac{4\pi}{3} N_d R^3\right) R^2 dR. \quad (4.3)$$

In the tight binding model, the total bandwidth is:

$$B_d = 2z_d |J_d(R)|, \quad (4.4)$$

where z_d is the number of nearest neighbors. With a Poisson distribution, there is only one nearest neighbor to every dopant atom and, therefore, $z_d = 1$. Hence, by defining the impurity band half-width $W_d \equiv B_d / 2$, we have [Lee75]:

$$W_d = |J_d(R)|.$$

Chapter 4

The quantity of interest is the impurity band density of states $\rho_{d,0}(E)$, which is in general a very complicated function of energy. However, for their purposes, Lee and McGill assumed $\rho_{d,0}(E)$ to be a constant over the bandwidth B_d , i.e. (see Fig. 4.1):

$$\rho_{d,0}(E) = \begin{cases} \frac{N_d}{2W_d} & |E - E_d| \leq W_d \\ 0 & |E - E_d| > W_d \end{cases} \quad (4.5)$$

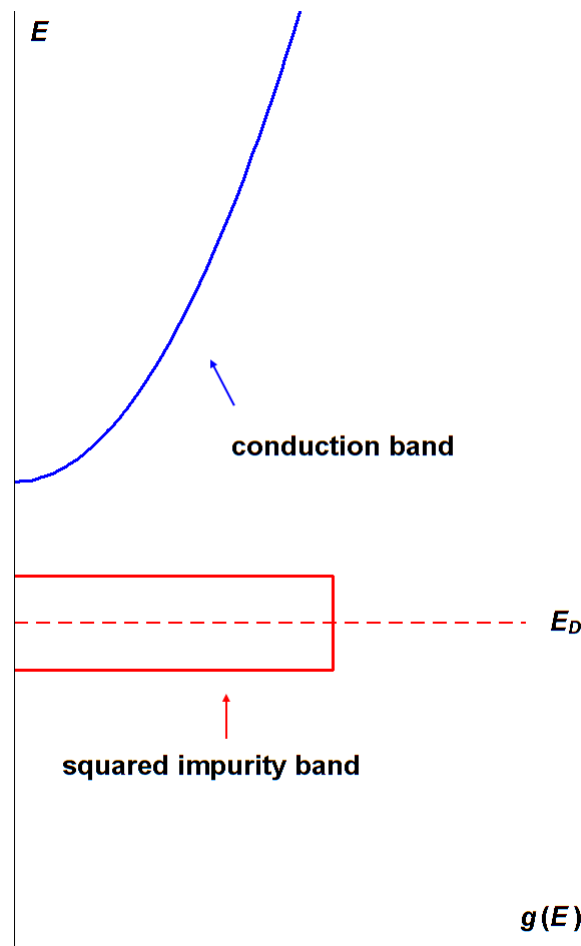


Fig. 4.1. Density of states described by (4.5).

Inclusion of impurity bands in our model

As we have mentioned before, the random distribution of ionized dopants generates spatial fluctuations in the potential, so that the dopant ground state results to be spread in energy. For having a dopant density of states $\rho_d(E)$ including both the fluctuation-induced broadening and the broadening due to a finite energy transfer integral, Lee and McGill proposed to average $\rho_{d,0}(E)$ over the value of the local potential. Therefore [Lee75]:

$$\rho_d(E) = \int_{-\infty}^{+\infty} \rho_{d,0}(E-V) p(V) dV , \quad (4.6)$$

where:

$$p(V) = \frac{1}{\sigma\sqrt{2\pi}} \exp\left(-\frac{V^2}{2\sigma^2}\right) . \quad (4.7)$$

Eq. (4.7) has been taken directly from the work of T.N. Morgan, where σ is the solution of the system [Morgan65]:

$$\begin{cases} \sigma^2 = 1.07 \cdot \frac{2\pi e^4 r_{sc}}{(4\pi\epsilon_r\epsilon_0)^2} \cdot \sum_d N_d^\pm Z_d^2 \exp\left(-\frac{2R_d}{r_{sc}}\right) \\ \frac{|Z_d|e^2}{4\pi\epsilon_r\epsilon_0 R_d} \cdot \exp\left(-\frac{R_d}{r_{sc}}\right) = 2.3\sigma , \end{cases} \quad (4.8)$$

where r_{sc} is the screening radius (the calculation was made by Morgan for the case of a screened Coulomb potential), N_d^\pm is the concentration of ionized dopants of the d -th type, Z_d is their charge (in e units) and R_d is a variable with the dimension of a length to be obtained together with σ by solving the system (4.8). It is apparent from the second of Eqs. (4.8) that the same value of R_d holds for all ionized dopants with the same charge (in its absolute value) $|Z_d|e$. Moreover, if we consider only monovalent dopants, i.e. $|Z_d| = 1$, it can be demonstrated (see App. 4A) that:

$$\sigma \approx \frac{e^2}{\epsilon_r \epsilon_0} \sqrt{\frac{r_{sc} (N_D^+ + N_A^-)}{8\pi}} \cdot \exp \left[-\frac{1}{6\sqrt{r_{sc}^3 (N_D^+ + N_A^-)}} \right]. \quad (4.9)$$

This is the model for impurity bands elaborated by Lee and McGill, who – it has to be remarked – used values for $r_d(0)$, r_{sc} and σ different from ours, the latter ones being given by Eqs. (3.19a) (or its equivalent for the p -type case), (3.24) and (4.9) respectively.

4.2. Our model for impurity bands.

We have seen that Lee and McGill obtained their value for the bandwidth B_d in the case of an unscreened Coulomb potential, which is consistent with their assumption of a moderate dopant concentration. However, we have seen in the preceding chapter that it has to be substituted by a screened Coulomb potential if we want to describe the behavior of a heavily doped semiconductor. This choice affects also the form of the ground state wave function to be put into the energy transfer integral (4.2). As a first approximation, we assume the correct ground state wave function to have the same form (4.1), but with an effective Bohr radius r_d given by:

$$r_d(\chi_d) = \begin{cases} r_d(0) \cdot \frac{\Delta E_d(0)}{\Delta E_d(\chi_d)} & \chi_d < \chi_{cr} \\ +\infty & \chi_d \geq \chi_{cr} \end{cases} \quad (4.10)$$

consistently with the $1s$ hydrogenic wave function (4.1) we chose and the value of the ionization energy $\Delta E_d(\chi_d)$, with χ_d given by (3.25a). Therefore, by defining the dimensionless parameters:

Inclusion of impurity bands in our model

$$\alpha_d \equiv \frac{r_d(\chi_d)}{r_{sc}} = \frac{\chi_d}{\Delta E_d(\chi_d)} \approx \frac{\chi_d}{f(\chi_d)} \quad (4.11a)$$

(see the definition (3.25b) and Eqs. (3.27) and (3.28)) and:

$$x \equiv \frac{R}{r_d(\chi_d)}, \quad (4.11b)$$

the energy transfer integral turns out to be (see App. 4B):

$$J_d(R) = J_d(r_d x) = -\frac{8\Delta E_d}{2 + \alpha_d} \cdot \frac{\exp(-x)}{\alpha_d^2 x} \cdot \left\{ \alpha_d x - \frac{2}{2 + \alpha_d} \cdot [1 - \exp(-\alpha_d x)] \right\}. \quad (4.12)$$

(in the following part of this chapter, the dependence of r_d , ΔE_d and α_d on χ_d will be implied). By defining the dimensionless parameter:

$$\beta_d \equiv \frac{4\pi}{3} N_d r_d^3 \quad (4.13)$$

and substituting Eq. (4.12) into (4.3), we thus obtain (see App. 4C):

$$\langle J_d(R) \rangle = -\frac{24\beta_d \Delta E_d}{(2 + \alpha_d) \alpha_d^2} \cdot \left\{ \frac{2}{2 + \alpha_d} \cdot \left[\frac{1}{(1 + \alpha_d)^2} \cdot I_1 \left(\frac{\beta_d}{(1 + \alpha_d)^3} \right) - I_1(\beta_d) \right] + \alpha_d \cdot I_2(\beta_d) \right\}$$

(4.14)

where:

Chapter 4

$$I_n(\beta) \equiv \int_0^{+\infty} x^n \exp(-x - \beta x^3) dx \quad (\beta \geq 0). \quad (4.15)$$

Unfortunately, the integrals (4.15) can not be expressed in terms of other known functions. Therefore we have to find approximated expressions for them, at least for the two integrals $I_1(\beta)$ and $I_2(\beta)$ which appear in (4.14). We shall explain in App. 4E the two approximate expressions we found. At this point, it is more important to stress on the asymptotic behavior of $I_1(\beta)$ and $I_2(\beta)$ as β tends to infinity, i.e. as χ_d approaches χ_{cr} so that r_d tends to infinity (see App. 4D):

$$I_1(\beta) \approx \frac{\Gamma(2/3)}{\beta^{2/3}}$$

$$I_2(\beta) \approx \frac{1}{\beta}.$$

It is easy to verify (see App. 4F) that, in the same limiting case:

$$\langle J_d(R) \rangle \approx -24 \Delta E_d(0) \frac{r_d(0) r_{sc}^2}{r_d^3},$$

i.e. in the heavy doping limit, when χ_d reaches χ_{cr} and r_d become infinite, if z_d is still equal to 1 in Eq. (4.4), the bandwidth tends to zero. But this makes no physical sense and is in contrast with all experimental results. However, the assumption $z_d = 1$ holds only in the high dilution limit: when the extension r_d of a dopant state becomes infinite, *all* other dopants become nearest neighbors. Therefore, we suggest to replace $z_d = 1$ with the expression:

$$z_d = 1 + \zeta \cdot \frac{4\pi}{3} N_d r_d^3, \quad (4.16)$$

Inclusion of impurity bands in our model

where ζ is a dimensionless constant of the order of unity. This means that in the high dilution limit $z_d \approx 1$, but the probability to have *more than one* nearest neighbor increases proportionally to the dopant concentration and to the “volume” of the dopant state, in such a manner that the number of nearest neighbors becomes infinite as the dopant state extends to infinity. In this case, we have from (4.4):

$$\lim_{r_d \rightarrow \infty} W_d = \lim_{r_d \rightarrow \infty} z_d \left| \langle J_d(R) \rangle \right| = 32\pi \zeta N_d r_d(0) r_{sc}^2 \Delta E_d(0), \quad (4.17)$$

which is finite, as it should be (see App. 4F). We propose to use (4.17) for all values $\chi_d \geq \chi_{cr}$, this expression having been obtained for infinite r_d , which is characteristic of *all* extended states. For simplicity, in our simulations we shall use $\zeta = 1$, but we think that its correct value could be obtained from probabilistic considerations.

Now we have all the instruments needed for the calculation of the impurity band half-width W_d . For simplicity we assume, as Lee and McGill, that the impurity band density of states due to the overlapping of dopant state wave functions still has the rectangular form (4.5). We have now to treat the effect of potential fluctuations due to randomly distributed ionized impurities. Instead of using the expression (4.6), we propose to keep the rectangular form also for the resulting density of states $\rho_d(E)$, but with an effective half-bandwidth:

$$W_{d,eff} = \sqrt{W_d^2 + \sigma^2}, \quad (4.18)$$

with σ given by Eq. (4.9).

At this point, our model for the impurity band density of states seems to be complete. However, we have not yet said anything about the position of the center E_d of the impurity band once χ_d exceeds its critical value χ_{cr} . When $\chi_d = \chi_{cr}$, the ionization energy ΔE_d becomes zero, i.e. $E_d = E_C$ or $E_d = E_V$ for a donor or acceptor case, respectively. But what happens to E_d once $\chi_d > \chi_{cr}$? We have not given an answer to this question in the preceding chapter, because we considered there only discrete states becoming completely ionized when $\chi_d \geq \chi_{cr}$, the exact value of the (negative or zero) ionization energy thus being not influential. But in the case of

Chapter 4

impurity bands the position of E_d is of crucial importance, governing the concentration of free carriers. At the moment, however, we have not a quantitative model for this topic. Therefore, considering that the function (3.27) presents a minimum at $\chi_d = \chi_{cr}$, we assume *arbitrarily* in our simulations that:

$$\Delta\varepsilon_d(\chi_d) = f(\chi_d) \cdot \text{sign}(\chi_{cr} - \chi_d) , \quad (4.19)$$

because we expect that E_d continues to penetrate into the conduction or valence band, and Eq. (4.19) is the simplest function which extends monotonically the function (3.27) to all the positive real axis while keeping a continuous first derivative. We hope to find a better expression in the future based on more physical considerations. From this point of view, the model of band edge displacements elaborated for 3C-, 4H- and 6H-SiC by U. Lindefelt [Lindefelt98] seems to be well promising, but it is still limited to the uncompensated case and can cause problems of convergence in our simulation software.

4.3. Occupancy of impurity bands.

Having established a model for the impurity band density of states, now we have to explain how its energy levels are occupied by electrons or holes. Let us consider the n -type case for simplicity. As we have done for discrete energy levels in Chap. 3, we shall consider completely ionized all donor states with energy $E \geq E_C$, while we ask the donor states with energy $E < E_C$ to follow the ordinary Fermi-Dirac statistics (2.1). Therefore, we assume:

$$N_D^+ = N_D^+(E < E_C) + N_D(E \geq E_C) , \quad (4.20)$$

where:

Inclusion of impurity bands in our model

$$N_D(E \geq E_C) = \int_{E_C}^{+\infty} \rho_D(E) dE \quad (4.21a)$$

$$N_D^+(E < E_C) = \int_{-\infty}^{E_C} \frac{\rho_D(E)}{1 + g_D \exp\left(\frac{E_F - E}{k_B T}\right)} dE, \quad (4.21b)$$

$\rho_D(E)$ being the density of states (4.5) but with half-width given by Eq. (4.18). Let us define the dimensionless function:

$$F(x) \equiv \begin{cases} 1 & x > 1 \\ x & |x| \leq 1 \\ -1 & x < -1 \end{cases} \quad (4.22)$$

Hence we obtain (see App. 4G):

$$N_D^+ = \frac{N_D k_B T}{2 W_{D,eff}} \cdot \ln \left\{ \frac{\exp\left[\frac{W_{D,eff}}{k_B T} \cdot F\left(\frac{\Delta E_D}{W_{D,eff}}\right)\right] + g_D \exp\left(\frac{E_F - E_C + \Delta E_D}{k_B T}\right)}{\exp\left(-\frac{W_{D,eff}}{k_B T}\right) + g_D \exp\left(\frac{E_F - E_C + \Delta E_D}{k_B T}\right)} \right\} +$$

$$+ \frac{N_D}{2} \cdot \left[1 - F\left(\frac{\Delta E_D}{W_{D,eff}}\right) \right] \quad (4.23)$$

which is the value to be put into the charge neutrality equation (2.5). A similar expression holds for the *p*-type case.

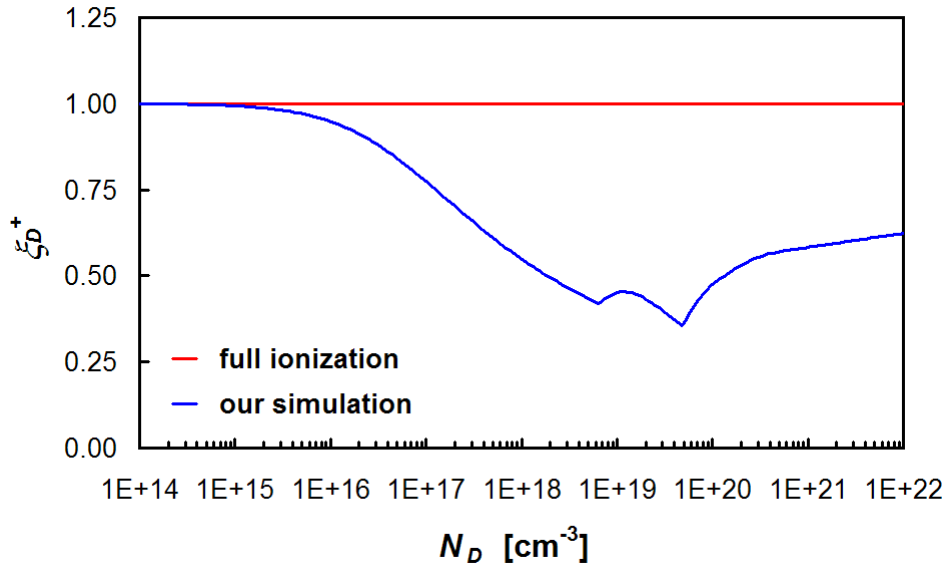


Fig. 4.2. Phosphorus donor ionization degree in uncompensated 4H-SiC at room temperature. The pure rectangular model has been used.

We have implemented such a model in a self-consistent iterative program, and we have found that slope discontinuities appear when $\Delta E_D = \pm W_{D,eff}$ (see Fig. 4.2, where we have used the same parameters given in Tab. 3.2, p. 50 of this thesis). These slope discontinuities are mathematical artifacts and have no physical meaning: they are due only to the oversimplified rectangular model (4.5) for the impurity band density of states. In order to avoid them, we have decided to substitute the function (4.22) into (4.23) with the more smoothed function:

$$F(x) \equiv \frac{1}{1 + \exp(-2x)}, \quad (4.24)$$

which has the same asymptotic behavior of (4.22) as $|x|$ tends to infinity and has the same derivative in $x = 0$ (see Fig. 4.3 for a comparison). In such a manner all slope discontinuities disappeared, as can be seen from the figures in the next section. Such a smoothing is qualitatively consistent with Eqs. (4.6) and (4.7), which spread the density of states (4.5) of well defined width B_d over all the real axis of the energies.

Inclusion of impurity bands in our model

As a consequence, the resulting density of states is *finite* also at a large distance from E_d , although small for low impurity concentrations.

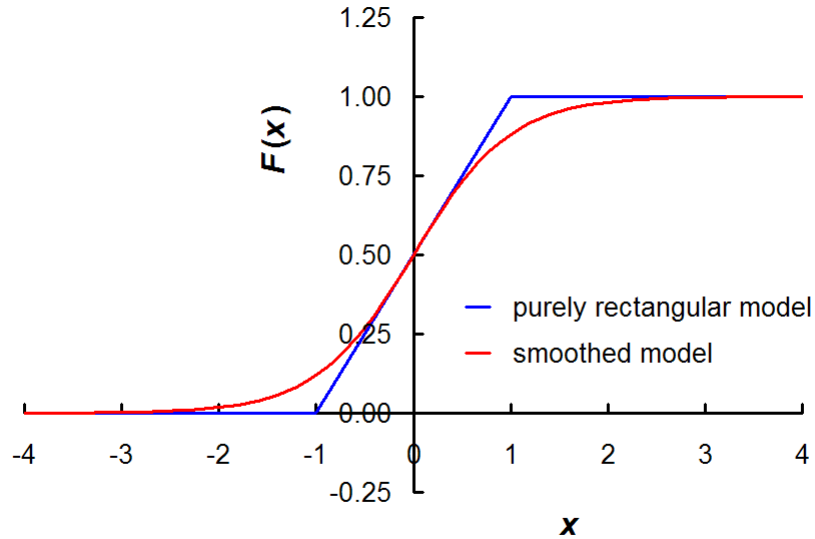


Fig. 4.3. Functions (4.22) and (4.24) for impurity band modeling.

4.4. Simulation results and discussion.

We illustrate in Fig. 4.4 our simulation results for Phosphorus-doped uncompensated 4H-SiC at room temperature obtained by using the function (4.24) instead of (4.22) and the same parameters given in Tab. 3.2, p. 50 of this thesis. As we can see from Fig. 4.4a, the unnatural slope discontinuities we obtained by using (4.22) vanished. We must point out that, in comparison with Fig. 3.4a, the ionization degree does not go to one for high concentrations, i.e. the ionization is not complete. In Fig. 4.4b we have plotted the corresponding energy diagram, in which we have used $B_{D,eff}$ as a measure of the impurity band amplitude.

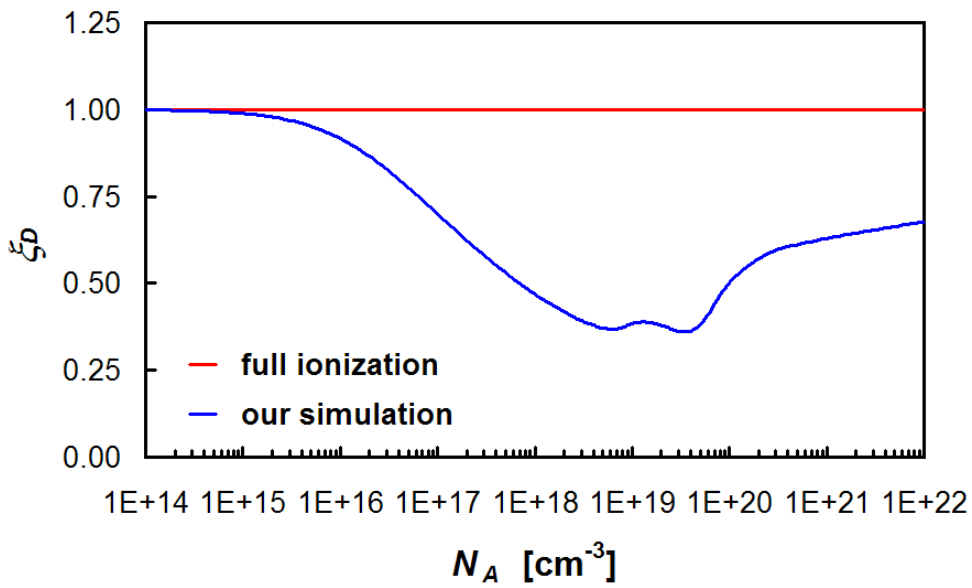


Fig. 4.4a. Phosphorus donor ionization degree in uncompensated 4H-SiC at room temperature. The smoothed impurity band model has been used.

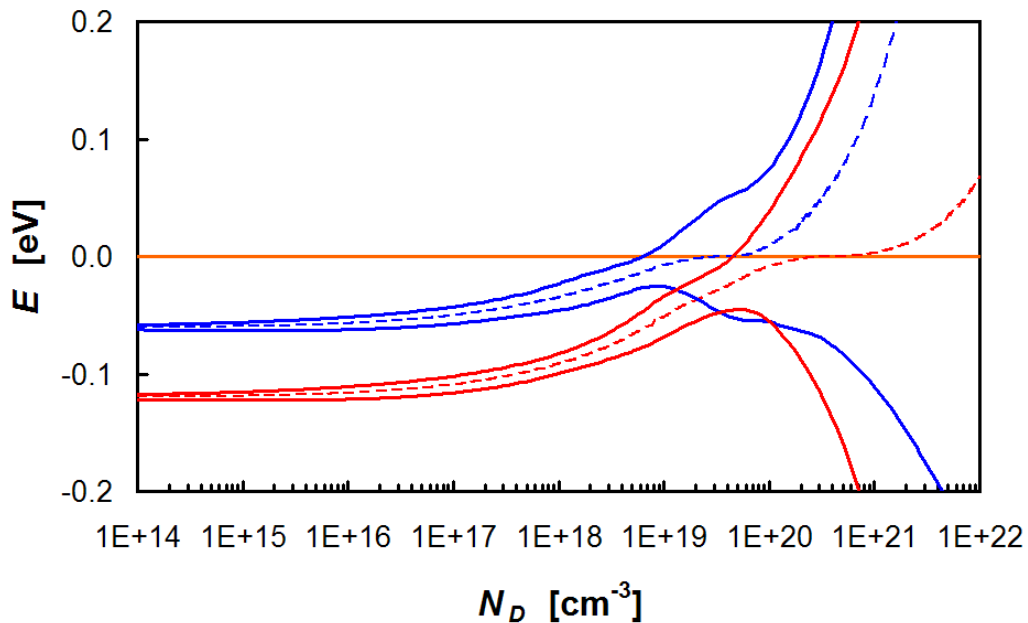


Fig. 4.4b. Phosphorus impurity band formation in uncompensated 4H-SiC at room temperature, taking the conduction band edge E_C as energy reference. The dashed lines represent the center E_D of each impurity band. Blue color refers to the hexagonal site and red color to the cubic one. The smoothed impurity band model has been used.

Inclusion of impurity bands in our model

To test our model, we have simulated the free electron concentration as a function of temperature for Phosphorus doped 10% compensated 4H-SiC for different values of P concentration (from 10^{14} to 10^{21} cm^{-3} , as explained in Tab. 4.1), which could be obtained from a temperature dependent Hall effect measurement. For comparison, we have performed the same simulation also following the model with discrete energy levels both without screening (as seen in Chap. 2) and taking it into account (as seen in Chap. 3). Figs. 4.5 illustrate our results. As we can see, the main difference between the model including impurity bands and the others is that it predicts more and more high carrier concentrations at low temperatures with increasing P concentration. As a consequence, between 10^{19} and $5 \cdot 10^{19}$ P atoms / cm^3 (for a compensation degree $K = 0.1$), a passage from a semiconducting to a metallic behavior is predicted. Such a behavior has been observed experimentally, as can be seen in [Laube02]. M. Laube and coworkers explained such a behavior by invoking the onset of impurity conduction, i.e. a movement of electrons through impurities without thermal activation from donors to CB ([Hung50], [Hung54]). In our model, however, such a metallic behavior is entirely due to electrons *in the conduction band*, made free from impurity levels lying over the CB edge (see Fig. 4.4b), while impurity conduction has been completely neglected. If our model is correct, it is therefore not necessary to invoke the onset of impurity conduction for explaining such a metallic behavior. As a consequence, our model could be used for analyzing temperature dependent Hall effect data also for those samples which are degenerate and present a metallic behavior, analysis that can not be performed by using the standard discrete-energy-level-based fitting procedure.

To give an example of such a possibility, we have plotted in Fig. 4.5 the experimental values obtained by Laube and coworkers for the electron concentration in three Phosphorus-implanted and then annealed 4H-SiC samples together with our simulation curves, the latter obtained by using the parameters given in Tab. 3.2 and P concentrations equal to those effectively implanted: $N_P = 2.6 \cdot 10^{18}$ cm^{-3} for sample P1, $N_P = 5 \cdot 10^{19}$ cm^{-3} for sample P2 and $N_P = 2 \cdot 10^{20}$ cm^{-3} for sample P3 [Laube02]. The compensation degree has been adjusted manually in order to achieve a fairly good agreement with the experimental data. We obtained a degree of compensation equal to 15%, 14% and 0% for samples P1, P2 and P3, respectively.

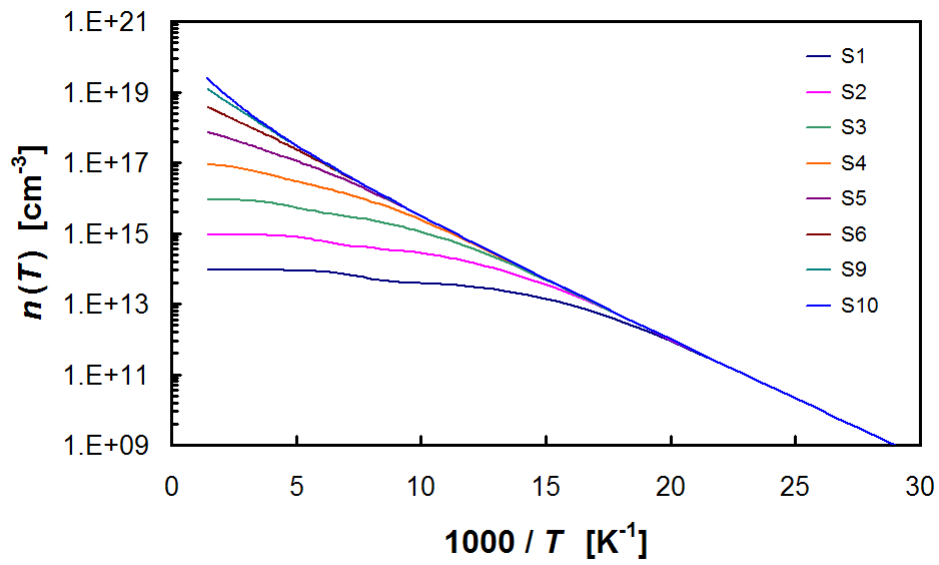


Fig. 4.5a. Electron concentrations from simulation with constant discrete energy levels.

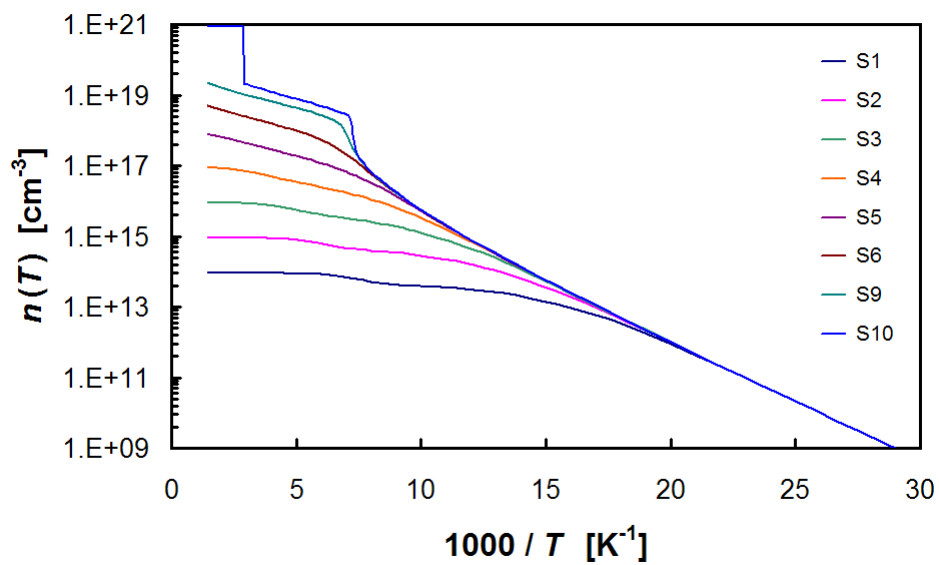


Fig. 4.5b. Electron concentrations from simulation with discrete energy levels in presence of screening.

Inclusion of impurity bands in our model

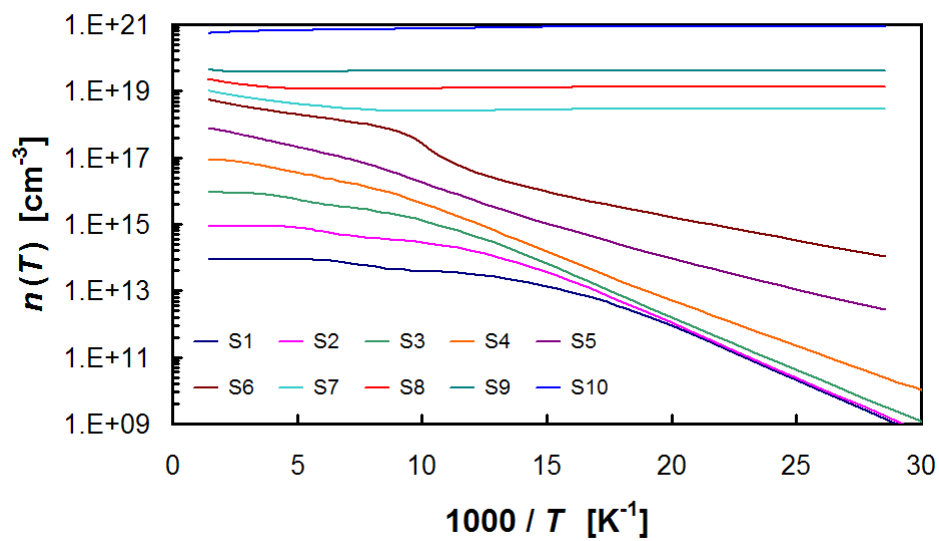


Fig. 4.5c. Electron concentrations from simulation with smoothed impurity bands.

identifier name	substitutional P concentration [cm^{-3}]
S1	10^{14}
S2	10^{15}
S3	10^{16}
S4	10^{17}
S5	10^{18}
S6	10^{19}
S7	$2 \cdot 10^{19}$
S8	$5 \cdot 10^{19}$
S9	10^{20}
S10	10^{21}

Tab. 4.1. Concentrations used for the simulations illustrated in Figs. 4.5.

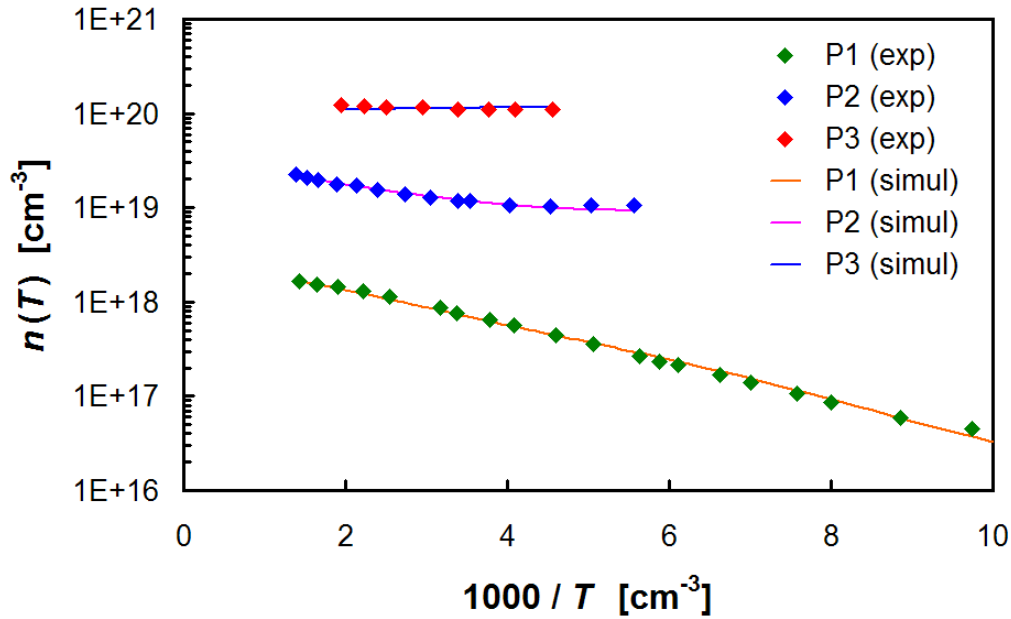


Fig. 4.5. Manual fit of [Laube02] experimental results by using our model.

While the first two results are reasonable for implanted samples, the third is not: a compensation degree of the order of 10% is expected from the experience. Furthermore, as we can see from Fig. 4.5, the agreement of our curves with the experimental data is rather good, but, also if it is not evident from the figure, their derivatives with respect to inverse temperature don't correspond to those of the empirical data. Therefore, we think that our model has to be further refined in order to get a better agreement with the experimental results. On the other side, it has demonstrated to be a very good instrument for analyzing temperature dependent Hall effect measurement data of SiC samples, in particular those corresponding to the most heavily doped samples, which could not be analyzed by using the standard methods.

Appendix 4A. Calculation of the parameter σ from Eqs. (4.8).

Let us rewrite the system (4.8) by substituting the second equation with its square:

$$\begin{cases} \sigma^2 = 1.07 \cdot 2\pi r_{sc} \cdot \sum_d N_d^\pm \frac{Z_d^2 e^4}{(4\pi\epsilon_r \epsilon_0)^2} \exp\left(-\frac{2R_d}{r_{sc}}\right) \\ \frac{Z_d^2 e^4}{(4\pi\epsilon_r \epsilon_0 R_d)^2} \cdot \exp\left(-\frac{2R_d}{r_{sc}}\right) = (2.3)^2 \sigma^2 . \end{cases} \quad (4A.1)$$

From the second equation:

$$\frac{Z_d^2 e^4}{(4\pi\epsilon_r \epsilon_0)^2} \cdot \exp\left(-\frac{2R_d}{r_{sc}}\right) = (2.3R_d)^2 \sigma^2$$

which, substituted into the first equation of the system, gives:

$$\sigma^2 = 1.07 \cdot 2\pi r_{sc} \cdot \sum_d N_d^\pm (2.3R_d)^2 \sigma^2 .$$

Hence:

$$r_{sc} \cdot \sum_d N_d^\pm R_d^2 = \frac{1}{2\pi \cdot 1.07 \cdot (2.3)^2} \approx 0.028 . \quad (4A.2)$$

If ions of only one value of $|Z|$ are present, like our case in which $|Z| = 1$ (monovalent centers), from the second equation of (4A.1) results that there will be a unique value of R_d for both $Z = +1$ and $Z = -1$. Therefore, (4A.2) gives:

$$R_d = \frac{1}{\sqrt{2\pi \cdot 1.07 \cdot (2.3)^2 r_{sc} \cdot (N_D^+ + N_A^-)}} \approx \sqrt{\frac{0.028}{r_{sc} \cdot (N_D^+ + N_A^-)}} \approx \frac{1}{6\sqrt{r_{sc} \cdot (N_D^+ + N_A^-)}}$$

Chapter 4

which, substituted into the second equation of the system (4.8) with $|Z_d| = 1$, gives:

$$\begin{aligned}
 \sigma &= \frac{e^2}{2.3 \cdot 4\pi\epsilon_r\epsilon_0 R_d} \cdot \exp\left(-\frac{R_d}{r_{sc}}\right) \approx \\
 &\approx \frac{e^2 \sqrt{2\pi \cdot 1.07 \cdot (2.3)^2 r_{sc} \cdot (N_D^+ + N_A^-)}}{2.3 \cdot 4\pi\epsilon_r\epsilon_0} \cdot \exp\left(-\frac{1}{6r_{sc}\sqrt{r_{sc} \cdot (N_D^+ + N_A^-)}}\right) \approx \\
 &\approx \frac{e^2}{\epsilon_r\epsilon_0} \sqrt{\frac{r_{sc}(N_D^+ + N_A^-)}{8\pi}} \cdot \exp\left[-\frac{1}{6\sqrt{r_{sc}^3(N_D^+ + N_A^-)}}\right],
 \end{aligned}$$

i.e. Eq. (4.9). In the last passage we assumed $1.07 \approx 1$.

Appendix 4B. Calculation of the energy transfer integral (Eq. (4.12)).

We have to calculate the energy transfer integral (4.2):

$$J_d(R) = \int_{\mathbb{R}^3} V(\mathbf{r}) \phi_d(\mathbf{r}) \phi_d(\mathbf{r} - \mathbf{R}) d^3\mathbf{r} \quad (4B.1)$$

with:

$$V(\mathbf{r}) = -\frac{e^2}{4\pi\epsilon_r\epsilon_0 r} \exp\left(-\frac{r}{r_{sc}}\right)$$

and:

$$\phi_d(\mathbf{r}) = \frac{1}{\sqrt{\pi r_d^3}} \exp\left(-\frac{r}{r_d}\right).$$

The integral (4B.1) can be written extensively as:

$$\begin{aligned} J_d(R) &= -\frac{e^2}{4\pi^2\epsilon_r\epsilon_0 r_d^3} \int_{\mathbb{R}^3} \frac{\exp(-r/r_{sc})}{r} \cdot \exp\left(-\frac{r}{r_d}\right) \cdot \exp\left(-\frac{|\mathbf{r}-\mathbf{R}|}{r_d}\right) d^3\mathbf{r} = \\ &= -\frac{e^2}{4\pi^2\epsilon_r\epsilon_0 r_d^3} \cdot \int_{\mathbb{R}^3} \frac{1}{r} \cdot \exp\left[-\left(\frac{r}{r_{sc}} + \frac{r+|\mathbf{r}-\mathbf{R}|}{r_d}\right)\right] d^3\mathbf{r}. \end{aligned}$$

Let us define the dimensionless variable:

$$\mathbf{q} \equiv \frac{\mathbf{r}}{r_d}$$

and the dimensionless parameters:

$$\mathbf{x} \equiv \frac{\mathbf{R}}{r_d} \quad (4B.2a)$$

$$\alpha \equiv \frac{r_d}{r_{sc}} . \quad (4B.2b)$$

(see Eqs. (4.11)). Hence, the energy transfer integral becomes:

$$\begin{aligned} J_d(R(x)) &= -\frac{e^2}{4\pi^2 \epsilon_r \epsilon_0 r_d} \cdot \int_{\mathbb{R}^3} \frac{r_d}{r} \cdot \exp\left[-\left(\frac{r_d}{r_{sc}} \cdot \frac{r}{r_d} + \frac{r + |\mathbf{r} + \mathbf{R}|}{r_d}\right)\right] \frac{d^3 \mathbf{r}}{r_d^3} = \\ &= -\frac{e^2}{4\pi^2 \epsilon_r \epsilon_0 r_d} \cdot \int_{\mathbb{R}^3} \frac{1}{q} \cdot \exp\left[-(\alpha q + q + |\mathbf{q} + \mathbf{x}|)\right] d^3 \mathbf{q} . \end{aligned}$$

Taking the z axis parallel to \mathbf{x} , i.e. to \mathbf{R} , the result being independent of the \mathbf{R} direction for reasons of symmetry, and introducing the spherical coordinates (q, θ, φ) , we obtain:

$$\begin{aligned} J_d(R(x)) &= -\frac{e^2}{4\pi^2 \epsilon_r \epsilon_0 r_d} \cdot \int_0^{+\infty} \int_0^\pi \int_0^{2\pi} \frac{1}{q} \cdot \exp\left[-(\alpha q + q) + \right. \\ &\quad \left. + \sqrt{q^2 + x^2 + 2xq \cdot \cos \theta}\right] \cdot q^2 \sin \theta d\varphi d\theta dx = \\ &= -\frac{e^2}{2\pi \epsilon_r \epsilon_0 r_d} \cdot \int_0^{+\infty} \int_0^\pi \exp\left[-(\alpha q + q + \sqrt{q^2 + x^2 + 2xq \cdot \cos \theta})\right] \\ &\quad \cdot q \sin \theta d\theta dq , \end{aligned}$$

the integrand being independent of the variable φ . Therefore, by defining:

$$j(x) \equiv -\frac{2\pi \epsilon_r \epsilon_0 r_d}{e^2} \cdot J_d(R(x)) = -\frac{1}{4} \cdot \frac{J_d(R(x))}{\Delta E_d} \quad (4B.3)$$

Inclusion of impurity bands in our model

(see Eqs. (4.10), (3.24), (3D.1) and (3D.2) for the equivalence of the second and the third term of (4B.3)), Eq. (4B.1) becomes simply:

$$j(x) = \int_0^{+\infty} \int_0^\pi \exp\left[-\left(\alpha q + q + \sqrt{q^2 + x^2 + 2xq \cdot \cos \theta}\right)\right] \cdot q \sin \theta \, d\theta \, dq .$$

In order to calculate explicitly such an integral, let us make the change of variable:

$$z \equiv -\cos \theta ,$$

from which:

$$dz = -\sin \theta \, d\theta$$

and therefore:

$$j(x) = \int_0^{+\infty} \int_{-1}^{+1} \exp\left[-\left(\alpha q + q + \sqrt{q^2 + x^2 - 2xq \cdot z}\right)\right] \cdot q \, dz \, dq .$$

Let us define also the new variable:

$$t^2 \equiv q^2 + x^2 - 2xq \cdot z , \quad t \geq 0 .$$

Hence:

$$2t \, dt = -2xq \, dz \quad \Leftrightarrow \quad dz = -\frac{t \, dt}{xq}$$

and:

Chapter 4

$$\begin{aligned}
 j(x) &= \int_0^{+\infty} \int_{|q-x|}^{q+x} \exp [-(\alpha q + q + t)] \cdot q \frac{t dt}{xq} dq = \\
 &= \frac{1}{x} \cdot \int_0^{+\infty} \left\{ \exp [-(1 + \alpha) q] \cdot \int_{|q-x|}^{q+x} t \cdot \exp (-t) dt \right\} dq .
 \end{aligned}$$

Taking into account that:

$$\int t \cdot \exp (-\xi t) dt = -\left(\frac{t}{\xi} + \frac{1}{\xi^2} \right) \cdot \exp (-\xi t) + \text{const.} , \quad (4B.4)$$

we can thus write (ξ being here equal to 1):

$$\begin{aligned}
 j(x) &= \frac{1}{x} \cdot \int_0^{+\infty} \left\{ \exp [-(1 + \alpha) q] \cdot \left[(|q-x| + 1) \cdot \exp (-|q-x|) - \right. \right. \\
 &\quad \left. \left. -(q+x+1) \cdot \exp (-q-x) \right] \right\} dq .
 \end{aligned}$$

In order to eliminate the modulus functions, let us split the range of integration into two intervals, $[0, y]$ and $[y, +\infty]$. Let us therefore write:

$$x \cdot j(x) = I_1(x) + I_2(x) - I_3(x) , \quad (4B.5)$$

where:

$$\begin{aligned}
 I_1(x) &\equiv \int_0^x \exp [-(1 + \alpha) q] \cdot (x - q + 1) \cdot \exp (q - x) dq = \\
 &= \exp (-x) \cdot \int_0^x \exp (-\alpha q) \cdot (x - q + 1) dq \\
 I_2(x) &\equiv \int_x^{+\infty} \exp [-(1 + \alpha) q] \cdot (q - x + 1) \cdot \exp (x - q) dq = \\
 &= \exp (x) \cdot \int_x^{+\infty} \exp [-(2 + \alpha) q] \cdot (q - x + 1) dx
 \end{aligned}$$

Inclusion of impurity bands in our model

$$\begin{aligned}
 I_3(x) &\equiv \int_0^{+\infty} \exp[-(1+\alpha)q] \cdot (q+x+1) \cdot \exp(-q-x) \, dq = \\
 &= \exp(-x) \cdot \int_0^{+\infty} \exp[-(2+\alpha)q] \cdot (q+x+1) \, dq .
 \end{aligned}$$

By remembering Eq. (4B.4), we can split the integral $I_1(x)$ itself into two parts:

$$\begin{aligned}
 I_1(x) &= \exp(-x) \cdot \left[(x+1) \cdot \int_0^x \exp(-\alpha q) \, dq - \int_0^x q \cdot \exp(-\alpha q) \, dq \right] = \\
 &= \exp(-x) \cdot \left[(x+1) \cdot \frac{1 - \exp(-\alpha x)}{\alpha} + \left(\frac{x}{\alpha} + \frac{1}{\alpha^2} \right) \cdot \exp(-\alpha x) - \frac{1}{\alpha^2} \right] .
 \end{aligned}$$

Hence:

$$I_1(x) = \exp(-x) \cdot \left[\left(\frac{x+1}{\alpha} - \frac{1}{\alpha^2} \right) + \left(-\frac{1}{\alpha} + \frac{1}{\alpha^2} \right) \cdot \exp(-\alpha x) \right] . \quad (4.B6a)$$

Similarly:

$$\begin{aligned}
 I_2(y) &= \exp(x) \cdot \left\{ (1-x) \cdot \int_x^{+\infty} \exp[-(2+\alpha)q] \, dq + \right. \\
 &\quad \left. + \int_x^{+\infty} q \cdot \exp[-(2+\alpha)q] \, dq \right\} = \\
 &= \exp(x) \cdot \left\{ (1-x) \cdot \frac{\exp[-(2+\alpha)x]}{2+\alpha} + \right. \\
 &\quad \left. + \left[\frac{x}{2+\alpha} + \frac{1}{(2+\alpha)^2} \right] \cdot \exp[-(2+\alpha)x] \right\} ,
 \end{aligned}$$

and therefore:

Chapter 4

$$I_2(y) = \left[\frac{1}{2+\alpha} + \frac{1}{(2+\alpha)^2} \right] \cdot \exp [-(1+\alpha)x] . \quad (4B.6b)$$

Finally:

$$I_3(x) = \exp (-x) \cdot \left\{ (x+1) \cdot \int_0^{+\infty} \exp [-(2+\alpha)q] dq + \right. \\ \left. + \int_0^{+\infty} q \cdot \exp [-(2+\alpha)q] dq \right\} ,$$

hence:

$$I_3(x) = \exp (-x) \cdot \left[\frac{x+1}{2+\alpha} + \frac{1}{(2+\alpha)^2} \right] . \quad (4B.6c)$$

We can therefore write, from (4B.5):

$$x \cdot j(x) = \exp (-x) \cdot \left\{ \left(\frac{x+1}{\alpha} - \frac{1}{\alpha^2} \right) + \left(-\frac{1}{\alpha} + \frac{1}{\alpha^2} \right) \cdot \exp (-\alpha x) + \right. \\ \left. + \left[\frac{1}{2+\alpha} + \frac{1}{(2+\alpha)^2} \right] \cdot \exp (-\alpha x) - \left[\frac{x+1}{2+\alpha} + \frac{1}{(2+\alpha)^2} \right] \right\} = \\ = \exp (-x) \cdot \left\{ \left[\frac{x+1}{\alpha} - \frac{1}{\alpha^2} - \frac{x+1}{2+\alpha} - \frac{1}{(2+\alpha)^2} \right] + \right. \\ \left. + \left[-\frac{1}{\alpha} + \frac{1}{\alpha^2} + \frac{1}{2+\alpha} + \frac{1}{(2+\alpha)^2} \right] \cdot \exp (-\alpha x) \right\} ,$$

which can be rewritten as:

Inclusion of impurity bands in our model

$$\begin{aligned}
 j(x) &= \frac{\exp(-x)}{(2+\alpha)\alpha^2 x} \cdot \left\{ \left[(2+\alpha)\alpha(x+1) - (2+\alpha) - \alpha^2(x+1) - \frac{\alpha^2}{2+\alpha} \right] + \right. \\
 &\quad \left. + \left[(2+\alpha)(-\alpha+1) + \alpha^2 + \frac{\alpha^2}{2+\alpha} \right] \cdot \exp(-\alpha x) \right\} = \\
 &= \frac{\exp(-x)}{(2+\alpha)\alpha^2 x} \cdot \left\{ \left[\alpha(2+\alpha-\alpha)(x+1) - (2+\alpha) - \frac{\alpha^2}{2+\alpha} \right] + \right. \\
 &\quad \left. + \frac{(2+\alpha)^2(-\alpha+1) + (2+\alpha)\alpha^2 + \alpha^2}{2+\alpha} \cdot \exp(-\alpha x) \right\} = \\
 &= \frac{\exp(-x)}{(2+\alpha)\alpha^2 x} \cdot \left[\left(2\alpha x + \alpha - 2 - \frac{\alpha^2}{2+\alpha} \right) + \right. \\
 &\quad \left. + \frac{(4+4\alpha+\alpha^2)(-\alpha+1) + 2\alpha^2 + \alpha^3 + \alpha^2}{2+\alpha} \cdot \exp(-\alpha x) \right] = \\
 &= \frac{\exp(-x)}{(2+\alpha)\alpha^2 x} \cdot \left[\left(2\alpha x + \frac{\alpha^2 - 4 - \alpha^2}{2+\alpha} \right) + \right. \\
 &\quad \left. + \frac{4+4\alpha+\alpha^2-4\alpha-4\alpha^2-\alpha^3+3\alpha^2+\alpha^3}{2+\alpha} \cdot \exp(-\alpha x) \right] = \\
 &= \frac{\exp(-x)}{(2+\alpha)\alpha^2 x} \cdot \left[\left(2\alpha x - \frac{4}{2+\alpha} \right) + \frac{4}{2+\alpha} \cdot \exp(-\alpha x) \right].
 \end{aligned}$$

Therefore:

$$j(x) = \frac{2 \exp(-x)}{(2+\alpha)\alpha^2 x} \cdot \left\{ \alpha x - \frac{2}{2+\alpha} \cdot [1 - \exp(-\alpha x)] \right\},$$

which becomes Eq. (4.12) taking into account Eq. (4B.3) and comparing the definitions (4B.2) to (4.11).

Chapter 4

Appendix 4C. Calculation of averaged energy transfer integral (Eq. (4.14)).

The average (4.3) of the energy transfer integral (4.12) is:

$$\begin{aligned} \langle J_d(R) \rangle &= 4\pi N_d \int_{\mathbb{R}^3} J_d(R) \exp\left(-\frac{4\pi}{3} N_d R^3\right) R^2 dR = \\ &= -\frac{32\pi N_d \Delta E_d}{(2+\alpha_d) \alpha_d^2} \cdot \int_{\mathbb{R}^3} \frac{r_d}{R} \cdot \exp\left(-\frac{R}{r_d}\right) \left\{ \alpha_d \frac{R}{r_d} - \frac{2}{2+\alpha_d} \cdot \right. \\ &\quad \left. \cdot \left[1 - \exp\left(-\alpha_d \frac{R}{r_d}\right) \right] \right\} \cdot \exp\left(-\frac{4\pi}{3} N_d R^3\right) R^2 dR . \end{aligned}$$

By introducing the dimensionless variable;

$$x \equiv \frac{R}{r_d} ,$$

it becomes:

$$\begin{aligned} \langle J_d(R) \rangle &= -\frac{32\pi N_d \Delta E_d}{(2+\alpha_d) \alpha_d^2} \cdot r_d^3 \int_0^{+\infty} \frac{\exp(-x)}{x} \left\{ \alpha_d x - \frac{2}{2+\alpha_d} \cdot [1 - \exp(-\alpha_d x)] \right\} \cdot \\ &\quad \cdot \exp\left(-\frac{4\pi}{3} N_d r_d^3 x^3\right) x^2 dx \end{aligned}$$

and, by defining the dimensionless parameter (4.13):

$$\beta_d \equiv \frac{4\pi}{3} N_d r_d^3 ,$$

Chapter 4

we have:

$$\begin{aligned} \langle J_d(R) \rangle = & -\frac{24\beta_d \Delta E_d}{(2+\alpha_d)\alpha_d^2} \cdot \int_0^{+\infty} x \exp(-x) \left\{ \alpha_d x - \frac{2}{2+\alpha_d} \cdot [1 - \exp(-\alpha_d x)] \right\} \\ & \cdot \exp(-\beta x^3) dx . \end{aligned} \quad (4C.1)$$

Let us study the dimensionless integral:

$$\begin{aligned} I(\alpha, \beta) \equiv & \int_0^{+\infty} x \exp(-x) \left\{ \alpha x - \frac{2}{2+\alpha} \cdot [1 - \exp(-\alpha x)] \right\} \\ & \cdot \exp(-\beta x^3) dx . \end{aligned} \quad (4C.2)$$

We can split it into three parts:

$$I(\alpha_d, \beta_d) = \alpha_d \cdot I_2(\beta_d) - \frac{2}{2+\alpha_d} \cdot I_1(\beta_d) + \frac{2}{2+\alpha_d} \cdot J_1(\alpha_d, \beta_d)$$

by defining the three integrals:

$$I_1(\beta) \equiv \int_0^{+\infty} x \cdot \exp(-x - \beta x^3) dx$$

$$I_2(\beta) \equiv \int_0^{+\infty} x^2 \cdot \exp(-x - \beta x^3) dx$$

$$J_1(\alpha, \beta) \equiv \int_0^{+\infty} x \cdot \exp[-(1+\alpha)x - \beta x^3] dx .$$

However, the third integral $J_1(\alpha, \beta)$ can be expressed in terms of the first one by means of the change of variable:

Inclusion of impurity bands in our model

$$t \equiv (1 + \alpha) x .$$

As a matter of fact, we have:

$$\begin{aligned} J_1(\alpha, \beta) &= \frac{1}{(1 + \alpha)^2} \cdot \int_0^{+\infty} (1 + \alpha) x \cdot \exp \left\{ -(1 + \alpha) x - \frac{\beta}{(1 + \alpha)^3} \cdot [(1 + \alpha) x]^3 \right\} \\ &\quad d[(1 + \alpha) x] \\ &= \frac{1}{(1 + \alpha)^2} \cdot \int_0^{+\infty} t \cdot \exp \left[-t - \frac{\beta}{(1 + \alpha)^3} \cdot t^3 \right] dt = \\ &= \frac{1}{(1 + \alpha)^2} \cdot I_1 \left(\frac{\beta}{(1 + \alpha)^3} \right) . \end{aligned}$$

Therefore, the integral (4C.2) can be written as:

$$\begin{aligned} I(\alpha, \beta) &= \alpha \cdot I_2(\beta) - \frac{2}{2 + \alpha} \cdot I_1(\beta) + \frac{2}{2 + \alpha} \cdot \frac{1}{(1 + \alpha)^2} \cdot I_1 \left(\frac{\beta}{(1 + \alpha)^3} \right) = \\ &= \frac{2}{2 + \alpha} \cdot \left[\frac{1}{(1 + \alpha)^2} \cdot I_1 \left(\frac{\beta}{(1 + \alpha)^3} \right) - I_1(\beta) \right] + \alpha \cdot I_2(\beta) , \end{aligned}$$

which, substituted in (4C.1), gives Eq. (4.14).

Chapter 4

Appendix 4D. Asymptotic behavior of the two integrals $I_1(\beta)$ and $I_2(\beta)$.

We want to study here the asymptotic behavior of the integral;

$$I_n(\beta) \equiv \int_0^{+\infty} x^n \exp(-x - \beta x^3) dx, \quad \beta \geq 0, \quad n > -1 \quad (4D.1)$$

in the two extreme cases $\beta \ll 1$ and $\beta \gg 1$. For $\beta \ll 1$ we can write:

$$\begin{aligned} I_n(\beta) &= \int_0^{+\infty} x^n \exp(-x) [1 - \beta x^3 + O(\beta^2)] dx = \\ &= \Gamma(n+1) - \beta \cdot \Gamma(n+4) + O(\beta^2). \end{aligned}$$

Therefore:

$$I_1(\beta) = 1 - 24\beta + O(\beta^2) \quad (4D.2)$$

$$I_2(\beta) = 2 - 120\beta + O(\beta^2).$$

In the opposite case, $\beta \gg 1$, we can rewrite the integral (4D.1) as:

$$\begin{aligned} I_n(\beta) &= \int_0^{+\infty} \left(\frac{\beta^{1/3} x}{\beta^{1/3}} \right)^n \exp\left(-\frac{\beta^{1/3} x}{\beta^{1/3}} - \beta x^3 \right) \frac{d(\beta^{1/3} x)}{\beta^{1/3}} = \\ &= \frac{1}{\beta^{(n+1)/3}} \cdot \int_0^{+\infty} (\beta^{1/3} x)^n \exp\left(-\frac{\beta^{1/3} x}{\beta^{1/3}} - \beta x^3 \right) d(\beta^{1/3} x) \end{aligned}$$

and introduce the new variable:

Chapter 4

$$t \equiv \beta^{1/3} x ,$$

so that:

$$I_n(\beta) = \frac{1}{\beta^{(n+1)/3}} \cdot \int_0^{+\infty} t^n \exp\left(-\frac{t}{\beta^{1/3}} - t^3\right) dt . \quad (4D.3)$$

By introducing now another variable:

$$z \equiv t^3$$

so that:

$$t = z^{1/3}$$

$$dt = \frac{dz}{3z^{2/3}} ,$$

the integral (4D.3) becomes:

$$\begin{aligned} I_n(\beta) &= \frac{1}{3\beta^{(n+1)/3}} \cdot \int_0^{+\infty} z^{(n-2)/3} \exp\left[-\left(\frac{z}{\beta}\right)^{1/3} - z\right] dz = \\ &= \frac{1}{3\beta^{(n+1)/3}} \cdot \left[\int_0^{+\infty} z^{(n-2)/3} \exp(-z) dz - \right. \\ &\quad \left. - \frac{1}{\beta^{1/3}} \cdot \int_0^{+\infty} z^{(n-1)/3} \exp(-z) dz + O\left(\frac{1}{\beta^{2/3}}\right) \right] = \\ &= \frac{\Gamma\left(\frac{n+1}{3}\right)}{3\beta^{(n+1)/3}} - \frac{\Gamma\left(\frac{n+2}{3}\right)}{3\beta^{(n+2)/3}} + O\left(\frac{1}{\beta^{n/3+1}}\right) . \end{aligned}$$

Inclusion of impurity bands in our model

Therefore:

$$I_1(\beta) = \frac{\Gamma(2/3)}{3\beta^{2/3}} - \frac{1}{3\beta} + O\left(\frac{1}{\beta^{4/3}}\right)$$

(4D.4)

$$I_2(\beta) = \frac{1}{3\beta} - \frac{\Gamma(4/3)}{3\beta^{4/3}} + O\left(\frac{1}{\beta^{5/3}}\right).$$

Chapter 4

Appendix 4E. Approximate expressions for the two integrals $I_1(\beta)$ and $I_2(\beta)$.

Starting from the asymptotic behaviors (4D.2) and (4D.4) we have found in App. 4D, let us define the two functions:

$$f_1(x) \equiv \left\{ \frac{1 + b_1^3 \cdot x^2}{(1 + 24 \cdot x)^3 + \left[\frac{3b_1}{\Gamma(2/3)} \cdot x \right]^3 \cdot \left[x^{1/3} + \frac{1}{\Gamma(2/3)} \right]^3} \right\}^{\frac{1}{3}}$$

$$f_2(x) \equiv \left\{ \frac{2^6 + b_2^6 \cdot x^2}{(1 + 60 \cdot x)^6 + (3b_2 \cdot x)^6 \cdot \left[x^{1/3} + \Gamma(4/3) \right]^6} \right\}^{\frac{1}{6}}$$

and set the parameters b_1 and b_2 to:

$$b_1 = 9.55276$$

$$b_2 = 9.08726$$

Let us now define the function:

$$g(x; \lambda, \sigma, \mu) \equiv 1 + \lambda \cdot \exp \left[-\sigma \cdot (\ln x - \mu)^2 \right]$$

The two integrals $I_1(x)$ and $I_2(x)$ can be well approximated by the two functions:

Chapter 4

$$I_1(x) \approx \frac{f_1(x)}{g(x; \lambda_{1a}, \sigma_{1a}, \mu_{1a}) \cdot g(x; \lambda_{1b}, \sigma_{1b}, \mu_{1b})} \quad (4B.1a)$$

$$I_2(x) \approx \frac{f_2(x)}{g(x; \lambda_{2a}, \sigma_{2a}, \mu_{2a}) \cdot g(x; \lambda_{2b}, \sigma_{2b}, \mu_{2b}) \cdot g(x; \lambda_{2c}, \sigma_{2c}, \mu_{2c})} \quad (4B.1b)$$

with the parameters given in Tabs. 4B.1. In such a manner, we have approximated the integrals $I_1(x)$ and $I_2(x)$ with a maximum relative error (in its absolute value) of about 0.5% and 0.14%, respectively.

	λ	σ	μ
1a	0.0534	0.1042	-1.343
1b	-0.0783	0.5292	-3.797

Tab. 4B.1a. Parameters to be used in (4.1a).

	λ	σ	μ
2a	0.05138	0.07266	0.3626
2b	-0.079	0.27	-0.92
2c	-0.03362	0.5454	-4.79084

Tab. 4B.1b. Parameters to be used in (4.1b).

Appendix 4F. Asymptotic behavior of the averaged energy transfer integral (Eq. (4.17)).

We have seen that the averaged energy transfer integral is given by (see Eq. (4.14)):

$$\langle J_d(R) \rangle = -\frac{24\beta_d \Delta E_d}{(2+\alpha_d)\alpha_d^2} \cdot \left\{ \frac{2}{2+\alpha_d} \cdot \left[\frac{1}{(1+\alpha_d)^2} \cdot I_1\left(\frac{\beta_d}{(1+\alpha_d)^3}\right) - I_1(\beta_d) \right] + \alpha_d \cdot I_2(\beta_d) \right\}, \quad (4F.1)$$

where:

$$\alpha_d \equiv \frac{r_d}{r_{sc}} \quad (4F.2a)$$

$$\beta_d \equiv \frac{4\pi}{3} N_d r_d^3 \quad (4F.2b)$$

(see definitions (4.11a) and (4.13)) and the relation:

$$\Delta E_d = \frac{\Delta E_d(0) r_d(0)}{r_d} \quad (4F.2c)$$

holds (see (4.10)).

Here we want to study the behavior of $\langle J_d(R) \rangle$ as r_d tends to infinity, i.e. when the dopant ionization energy tends to zero (see (4F.2c)) and the corresponding states become delocalized. This happens for finite values of the dopant concentration N_d and of the screening radius r_{sc} . Hence, substituting Eqs. (4F.2) into (4F.1), we have:

Chapter 4

$$\langle J_d(R) \rangle \approx -\frac{24\beta_d \Delta E_d}{\alpha_d^3} \cdot \left\{ \frac{2}{\alpha_d} \cdot \left[\frac{1}{\alpha_d^2} \cdot I_1\left(\frac{\beta_d}{\alpha_d^3}\right) - I_1(\beta_d) \right] + \alpha_d \cdot I_2(\beta_d) \right\}$$

because both α_d and β_d tends to infinity in such a limit (see (4F.2a) and (4F.2b)).

Being:

$$\frac{\beta_d}{\alpha_d^3} = \frac{4\pi}{3} N_d r_{sc}^3$$

finite, from Eqs. (4D.4) we have:

$$\begin{aligned} \frac{2}{\alpha_d} \cdot \left[\frac{1}{\alpha_d^2} \cdot I_1\left(\frac{\beta_d}{\alpha_d^3}\right) - I_1(\beta_d) \right] + \alpha_d \cdot I_2(\beta_d) &\approx \\ &\approx \frac{2}{\alpha_d} \cdot \left[\frac{1}{\alpha_d^2} \cdot I_1\left(\frac{4\pi}{3} N_d r_{sc}^3\right) - \frac{\Gamma(2/3)}{\beta_d^{2/3}} \right] + \frac{\alpha_d}{\beta_d} = \\ &= \frac{2r_{sc}}{r_d} \cdot \left[\frac{r_{sc}^2}{r_d^2} \cdot I_1\left(\frac{4\pi}{3} N_d r_{sc}^3\right) - \frac{\Gamma(2/3)}{r_d^2} \cdot \left(\frac{3}{4\pi N_d}\right)^{2/3} \right] + \frac{3}{4\pi N_d r_{sc} r_d^2} \approx \\ &= \frac{3}{4\pi N_d r_{sc} r_d^2} + O\left(\frac{1}{r_d^3}\right). \end{aligned}$$

Hence:

$$\begin{aligned} \langle J_d(R) \rangle &\approx -\frac{24\beta_d \Delta E_d}{\alpha_d^3} \cdot \frac{3}{4\pi N_d r_{sc} r_d^2} = \\ &= -\frac{18}{\pi N_d r_{sc}} \cdot \frac{\beta_d \Delta E_d}{\alpha_d^3 r_d^2} = \\ &= -\frac{18}{\pi N_d r_{sc}} \cdot \frac{4\pi}{3} N_d r_d^3 \cdot \frac{\Delta E_d(0) r_d(0)}{r_d} \cdot \frac{r_{sc}^3}{r_d^3} \cdot \frac{1}{r_d^2} \end{aligned}$$

thus giving:

$$\langle J_d(R) \rangle \approx -24 \Delta E_d(0) \frac{r_d(0) r_{sc}^2}{r_d^3} . \quad (4F.3)$$

Such a value tends to zero as r_d tends to infinity.

By using the coordination number z_d given by Eq. (4.16), in the same limiting case we have (see (4.4)):

$$\begin{aligned} W_d &= z_d \langle J_d(R) \rangle \approx \zeta \frac{4\pi}{3} N_d r_d^3 \cdot 24 \Delta E_d(0) \frac{r_d(0) r_{sc}^2}{r_d^3} = \\ &= 32\pi \zeta N_d r_d(0) r_{sc}^2 \Delta E_d(0) , \end{aligned}$$

i.e. Eq. (4.17).

Chapter 4

Appendix 4G. Ionization in an impurity band (Eq. (4.23)).

In Sec. 4.3 we assumed that (Eq. (4.20)):

$$N_D^+ = N_D^+(E < E_C) + N_D(E \geq E_C) , \quad (4G.1)$$

where (see Eqs. (4.21)):

$$N_D(E \geq E_C) = \int_{E_C}^{+\infty} \rho_D(E) dE \quad (4G.2a)$$

$$N_D^+(E < E_C) = \int_{-\infty}^{E_C} \frac{\rho_D(E)}{1 + g_D \exp\left(\frac{E_F - E}{k_B T}\right)} dE \quad (4G.2b)$$

and:

$$\rho_D(E) = \begin{cases} \frac{N_D}{2W_{D,eff}} & |E - E_D| \leq W_{D,eff} \\ 0 & |E - E_D| > W_{D,eff} \end{cases} . \quad (4G.3)$$

In calculating the integrals (4G.2), we have to distinguish three cases.

1) $E_D - E_C < -W_{D,eff}$.

In this case the impurity band lies entirely below the conduction band edge, thus:

$$N_D(E \geq E_C) = 0$$

and:

Chapter 4

$$N_D^+(E < E_C) = \frac{N_D}{2W_{D,eff}} \cdot \int_{E_D+W_{D,eff}}^{E_D+W_{D,eff}} \frac{dE}{1 + g_D \exp\left(\frac{E_F - E}{k_B T}\right)}$$

2) $|E_D - E_C| \leq W_{D,eff}$.

In this case the impurity band lies partly below and partly above the conduction band edge, thus:

$$\begin{aligned} N_D(E \geq E_C) &= \frac{N_D}{2W_{D,eff}} \cdot \int_{E_C}^{E_D+W_{D,eff}} dE = \\ &= \frac{N_D}{2W_{D,eff}} \cdot (E_D + W_{D,eff} - E_C) = \\ &= \frac{N_D}{2} \cdot \left(1 + \frac{E_D - E_C}{W_{D,eff}}\right) = \\ &= \frac{N_D}{2} \cdot \left(1 - \frac{\Delta E_D}{W_{D,eff}}\right) \end{aligned}$$

and:

$$N_D^+(E < E_C) = \frac{N_D}{2W_{D,eff}} \cdot \int_{E_D+W_{D,eff}}^{E_C} \frac{dE}{1 + g_D \exp\left(\frac{E_F - E}{k_B T}\right)}$$

3) $E_D - E_C > W_{D,eff}$.

In this case the impurity band lies entirely in the conduction band, thus:

$$N_D(E \geq E_C) = \frac{N_D}{2W_{D,eff}} \cdot \int_{E_D-W_{D,eff}}^{E_D+W_{D,eff}} dE = N_D$$

Inclusion of impurity bands in our model

and:

$$N_D^+(E < E_C) = 0 .$$

To calculate the concentration of ionized donors whose states lie below the conduction band, i.e. $N_D^+(E < E_C)$, we observe that:

$$\begin{aligned} \int \frac{dE}{1 + g_D \exp\left(\frac{E_F - E}{k_B T}\right)} &= \int \frac{\exp\left(\frac{E - E_F}{k_B T}\right) dE}{\exp\left(\frac{E - E_F}{k_B T}\right) + g_D} = \\ &= k_B T \cdot \ln \left[\exp\left(\frac{E - E_F}{k_B T}\right) + g_D \right] + const. \end{aligned}$$

Therefore, in the three cases we have distinguished:

$$1) E_D - E_C < -W_{D,eff} \quad \Leftrightarrow \quad \Delta E_D > W_{D,eff} :$$

$$\begin{aligned} N_D^+(E < E_C) &= \frac{N_D k_B T}{2W_{D,eff}} \cdot \ln \left[\frac{\exp\left(\frac{E_D + W_{D,eff} - E_F}{k_B T}\right) + g_D}{\exp\left(\frac{E_D - W_{D,eff} - E_F}{k_B T}\right) + g_D} \right] = \\ &= \frac{N_D k_B T}{2W_{D,eff}} \cdot \ln \left[\frac{\exp\left(\frac{W_{D,eff}}{k_B T}\right) \cdot \exp\left(\frac{E_D - E_C + E_C - E_F}{k_B T}\right) + g_D}{\exp\left(-\frac{W_{D,eff}}{k_B T}\right) \cdot \exp\left(\frac{E_D - E_C + E_C - E_F}{k_B T}\right) + g_D} \right] = \end{aligned}$$

Chapter 4

$$= \frac{N_D k_B T}{2W_{D,eff}} \cdot \ln \left[\frac{\exp\left(\frac{W_{D,eff}}{k_B T}\right) + g_D \exp\left(\frac{\Delta E_D + E_F - E_C}{k_B T}\right)}{\exp\left(-\frac{W_{D,eff}}{k_B T}\right) + g_D \exp\left(\frac{\Delta E_D + E_F - E_C}{k_B T}\right)} \right].$$

2) $|E_D - E_C| \leq W_{D,eff} \Leftrightarrow |\Delta E_D| \leq W_{D,eff} :$

$$\begin{aligned} N_D^+(E < E_C) &= \frac{N_D k_B T}{2W_{D,eff}} \cdot \ln \left[\frac{\exp\left(\frac{E_C - E_F}{k_B T}\right) + g_D}{\exp\left(\frac{E_D - W_{D,eff} - E_F}{k_B T}\right) + g_D} \right] = \\ &= \frac{N_D k_B T}{2W_{D,eff}} \cdot \ln \left[\frac{\exp\left(\frac{E_C - E_F}{k_B T}\right) + g_D}{\exp\left(-\frac{W_{D,eff}}{k_B T}\right) \cdot \exp\left(\frac{E_D - E_C + E_C - E_F}{k_B T}\right) + g_D} \right] = \\ &= \frac{N_D k_B T}{2W_{D,eff}} \cdot \ln \left[\frac{\exp\left(\frac{\Delta E_D}{k_B T}\right) + g_D \exp\left(\frac{\Delta E_D + E_F - E_C}{k_B T}\right)}{\exp\left(-\frac{W_{D,eff}}{k_B T}\right) + g_D \exp\left(\frac{\Delta E_D + E_F - E_C}{k_B T}\right)} \right] = \\ &= \frac{N_D k_B T}{2W_{D,eff}} \cdot \ln \left[\frac{\exp\left(\frac{\Delta E_D}{W_{D,eff}} \cdot \frac{W_{D,eff}}{k_B T}\right) + g_D \exp\left(\frac{\Delta E_D + E_F - E_C}{k_B T}\right)}{\exp\left(-\frac{W_{D,eff}}{k_B T}\right) + g_D \exp\left(\frac{\Delta E_D + E_F - E_C}{k_B T}\right)} \right]. \end{aligned}$$

3) $E_D - E_C > W_{D,eff} \Leftrightarrow \Delta E_D < -W_{D,eff} :$

We can write:

Inclusion of impurity bands in our model

$$N_D^+(E < E_C) = 0 = \frac{N_D k_B T}{2W_{D,eff}} \cdot \ln(1) =$$

$$= \frac{N_D k_B T}{2W_{D,eff}} \cdot \ln \left[\frac{\exp\left(-\frac{W_{D,eff}}{k_B T}\right) + g_D \exp\left(\frac{\Delta E_D + E_F - E_C}{k_B T}\right)}{\exp\left(-\frac{W_{D,eff}}{k_B T}\right) + g_D \exp\left(\frac{\Delta E_D + E_F - E_C}{k_B T}\right)} \right].$$

By introducing the dimensionless function (4.22):

$$F(x) \equiv \begin{cases} 1 & x > 1 \\ x & |x| \leq 1 \\ -1 & x < -1 \end{cases}$$

we can summarize our results in the compact form:

$$N_D(E \geq E_C) = \frac{N_D}{2} \cdot \left[1 - F\left(\frac{\Delta E_D}{W_{D,eff}}\right) \right]$$

$$N_D^+(E < E_C) =$$

$$= \frac{N_D k_B T}{2W_{D,eff}} \cdot \ln \left\{ \frac{\exp\left[\frac{W_{D,eff}}{k_B T} \cdot F\left(\frac{\Delta E_D}{W_{D,eff}}\right)\right] + g_D \exp\left(\frac{\Delta E_D + E_F - E_C}{k_B T}\right)}{\exp\left(-\frac{W_{D,eff}}{k_B T}\right) + g_D \exp\left(\frac{\Delta E_D + E_F - E_C}{k_B T}\right)} \right\}.$$

Eq. (4.23) follows immediately from (4G.1).

Chapter 4

Conclusions.

In this work we have established a model for simulating the incomplete ionization of substitutional dopants in homogeneous Silicon Carbide samples at thermal equilibrium. Our model is based on the solution of the Charge Neutrality Equation (CNE) and takes into account: 1) the presence of non-equivalent lattice sites in almost all SiC polytypes, which gives rise to more than one energy level in the bandgap for each dopant species, thus requiring in general a numerical solution of the CNE; 2) Fermi-Dirac statistics for free electrons and holes in the conduction and valence band, respectively, instead of the easier Boltzmann statistics, in order to study also heavily doped SiC samples; 3) the screening of the Coulomb potential around each dopant ion mainly by the “sea” of free carriers, causing the variation of the dopant ionization energy; 4) the formation of impurity bands by the splitting of the discrete dopant energy levels with increasing concentration.

Coulomb screening has required to replace the usual hydrogenic model for dopant atoms with the solution of Schrödinger equation with a screened Coulomb potential, which is not analytically solvable. The eigenvalues of such an equation furnish the ionization energy of dopants as a function of the screening radius. We obtained an approximate expression of such a function. We have then obtained an expression for the screening radius which takes into account both free carriers and ionized impurities, thus generalizing a well known formula to the case of more than one kind of impurity center. The CNE and the screening problem have to be solved self-consistently: we wrote a program which gives the desired solution. We have then established a relatively simple model for the impurity band density of states, which can be applied also to the case of heavily doped samples while most of the literature on this topic is limited to the moderate doping case. We have then written

Conclusions

a program which implements such a model and made a preliminary comparison of our results with the experimental ones available in the literature.

We have found a ionization degree of about 0.5 for high doping levels which compares well with the experimental value. Moreover, our model has shown to be able to describe the metallic behavior observed in 4H-SiC samples heavily doped with Phosphorus without requiring the onset of impurity conduction. This fact makes possible the use of our program for the analysis of temperature dependent Hall effect data also in the cases in which a heavy doping doesn't permit to use the standard procedures, as we have shown for three 4H-SiC:P samples. However, our model has to be further refined in order to obtain a complete agreement with the experimental results.

Bibliography.

- [Achatz08] : P. Achatz, J. Pernot, C. Marcenat, J. Kacmarcik, G. Ferro, and E. Bustarret, “Doping-induced metal-insulator transition in aluminum-doped 4H silicon carbide”, *Appl. Phys. Lett.* **92** (2008) 072103.
- [Afanas'ev96] : V. V. Afanas'ev, M. Bassler, G. Pensl, M. J. Schulz, and E. S. von Kamienski, “Band offsets and electronic structure of Si/SiO₂ interfaces”, *J. Appl. Phys.* **79** (1996) 3108.
- [Alampi10] : D. Alampi, “Simulation and technology of fabrication of a 4H-SiC BMFET”, dissertation, Mediterranean University of Studies, Reggio Calabria, 2010.
- [AymerichHumet81] : X. Aymerich-Humet, F. Serra Mestres, and J. Millán, “An analytical approximation for the Fermi-Dirac integral $F_{3/2}(\eta)$ ”, *Solid-State Electron.* **24** (1981) 981.
- [AymerichHumet83] : X. Aymerich-Humet, F. Serra Mestres, and J. Millán, “A generalized approximation of the Fermi-Dirac integrals”, *J. Appl. Phys.* **54** (1983) 2850.
- [Blakemore62] : J. S. Blakemore, *Semiconductor Statistics*, Pergamon Press, London, 1962.
- [Blood92] : P. Blood, and J. W. Orton, *The Electrical Characterization of Semiconductors: Majority Carriers and Electron States*, Academic Press, New York, 1992.

Bibliography

- [Cloutman89] : L. D. Cloutman, “Numerical evaluation of the Fermi-Dirac integrals”, *Astrophys. J. Suppl. Ser.* **71** (1989) 677.
- [CREE11] : CREE Press Room, “Cree Launches Industry’s First Commercial Silicon Carbide Power MOSFET; Destined to Replace Silicon Devices in High-Voltage (≥ 1200 -V) Power Electronics”:
http://www.cree.com/press/press_detail.asp?i=1295272745318
- [Diaz91] : C. G. Diaz, F. M. Fernández, and E. A. Castro, “Critical screening parameters for screened Coulomb potential”, *J. Phys. A: Math. Gen.* **24** (1991) 2061.
- [FerreiraDaSilva06] : A. Ferreira da Silva, J. Pernot, S. Contreras, Bo E. Sernelius, C. Persson, and J. Camassel, “Electrical resistivity and metal-nonmetal transition in n -type doped $4H$ -SiC”, *Phys. Rev. B* **74** (2006) 245201.
- [Fistul’69] : V. I. Fistul’, *Heavily Doped Semiconductors*, Plenum Press, New York, 1969.
- [Goano93] : M. Goano, “Series expansion of the Fermi-Dirac integral $\mathcal{F}_j(x)$ over the entire domain of real j and x ”, *Solid-State Electron.* **36** (1993) 217.
- [Götz93] : W. Götz, A. Schöner, G. Pensl, W. Suttrop, W. J. Choyke, R. Stein, and S. Leibenzeder, “Nitrogen donors in $4H$ -silicon carbide”, *J. Appl. Phys.* **73** (1993) 3332.
- [GreulichWeber97] : S. Greulich-Weber, “EPR and ENDOR Investigations of Shallow Impurities in SiC Polytypes”, *phys. stat. sol. (a)* **162** (1997) 95.
- [Handy00] : E. M. Handy, M. V. Rao, O. W. Holland, K. A. Jones, M. A. Derenge, and N. Papanicolaou, “Variable-dose (10^{17} – 10^{20} cm $^{-3}$) phosphorus ion implantation into $4H$ -SiC”, *J. Appl. Phys.* **88** (2000) 5630.

Bibliography

- [Harrison99] : W. A. Harrison, *Elementary Electronic Structure*, World Scientific, Singapore, 1999.
- [Holubec90] : A. Holubec, A. D. Stauffer, P. Acacia, and J. A. Stauffer, “Asymptotic shooting method for the solution of differential equations”, *J. Phys. A: Math. Gen.* **23** (1990) 4081.
- [Hung50] : C. S. Hung, “Theory of Resistivity and Hall effect at Very Low Temperatures”, *Phys. Rev.* **79** (1950) 727.
- [Hung54] : C. S. Hung, and J. R. Gliessman, “Resistivity and Hall Effect of Germanium at Low Temperatures”, *Phys. Rev.* **96** (1954) 1226.
- [Ikeda79] : M. Ikeda, H. Matsunami, and T. Tanaka, “Site-dependent donor and acceptor levels in 6H-SiC”, *J. Lumin.* **20** (1979) 111.
- [Ikeda80] : M. Ikeda, H. Matsunami, and T. Tanaka, “Site effect on the impurity levels in 4H, 6H, and 15R SiC”, *Phys. Rev. B* **22** (1980) 2842.
- [ISE04] : *ISE TCAD Release 10.0. DESSIS manual*, Integrated System Engineering AG, Zurich, 2004.
- [Ivanov05] : I. G. Ivanov, A. Henry, and E. Janzén, “Ionization energies of phosphorus and nitrogen donors and aluminum acceptors in 4H silicon carbide from the donor-acceptor pair emission”, *Phys. Rev. B* **71** (2005) 241201.
- [Jog79] : S. D. Jog, “Expansions and approximations for Fermi-Dirac integrals of arbitrary order”, *Phys. Lett.* **72A** (1979) 303.
- [Kagamihara04] : S. Kagamihara, H. Matsuura, T. Hatakeyama, T. Watanabe, M. Kushibe, T. Shinohe, and K. Arai, “Parameters required to simulate electric characteristics of SiC devices for *n*-type 4H-SiC”, *J. Appl. Phys.* **96** (2004) 5601.

Bibliography

- [Kane63] : E. O. Kane, “Thomas-Fermi Approach to Impure Semiconductor Band Structure”, *Phys. Rev.* **131** (1963) 79.
- [Kittel80] : C. Kittel, and H. Kroemer, *Thermal Physics*, W.H. Freeman & Company, San Francisco, 1980.
- [Koizumi09] : A. Koizumi, J. Suda, and T. Kimoto, “Temperature and doping dependencies of electrical properties in Al-doped 4H-SiC epitaxial layers”, *J. Appl. Phys.* **106** (2009) 013716.
- [Kronig31] : R. D. Kronig, and W. G. Penney, “Quantum Mechanics of Electrons in Crystal Lattices”, *Proc. Roy. Soc. London A* **130** (1931) 499.
- [Laube02] : M. Laube, F. Schmid, G. Pensl, G. Wagner, M. Linnarsson, and M. Maier, “Electrical activation of high concentrations of N⁺ and P⁺ ions implanted into 4H-SiC”, *J. Appl. Phys.* **92** (2002) 549.
- [Lee75] : T. F. Lee, and T. C. McGill, “Variation of impurity-to-band activation energies with impurity density”, *J. Appl. Phys.* **46** (1975) 373.
- [Lehman55] : G. W. Lehman, and H. M. James, “Interaction of Impurities and Mobile Carriers in Semiconductors”, *Phys. Rev.* **100** (1955) 1698.
- [Leloup78] : J. Leloup, H. Djerassi, J. H. Albany, and J. B. Mullin, “Hall effect in *n*-type InP crystals: Thermal activation energy and influence of compensation”, *J. Appl. Phys.* **49** (1978) 3359.
- [Lether00] : F. G. Lether, “Analytical Expansion and Numerical Approximation of the Fermi-Dirac Integrals $\mathcal{F}_j(x)$ of Order $j = -1/2$ and $j = 1/2$ ”, *J. Sci. Comput.* **15** (2000) 479.

Bibliography

- [Linddefelt98] : U. Linddefelt, “Doping-induced band edge displacements and band gap narrowing in 3C-, 4H-, 6H-SiC, and Si”, *J. Appl. Phys.* **84** (1998) 2628.
- [MacLeod98] : A. J. MacLeod, “Algorithm 779: Fermi-Dirac Functions of Order $-1/2, 1/2, 3/2, 5/2$ ”, *ACM Trans. Math. Softw.* **24** (1998) 1.
- [Martinez02] : A. Martinez, U. Linddefelt, M. Hjelm, and H.-E. Nilsson, “Monte Carlo study of hole mobility in Al-doped 4H-SiC” *J. Appl. Phys.* **91** (2002) 1359.
- [Matsuura02] : H. Matsuura, “The influence of excited states of deep dopants on majority-carrier concentration in a wide-bandgap semiconductor”, *New. J. Phys.* **4** (2002) 12.
- [Milnes73] : A. G. Milnes, *Deep Impurities in Semiconductors*, Wiley-Interscience, New York, 1973.
- [Morgan65] : T. N. Morgan, “Broadening of Impurity Bands in Heavily Doped Semiconductors”, *Phys. Rev.* **139** (1965) A343.
- [Mott74] : N. F. Mott, *Metal-Insulator Transitions*, Taylor & Francis, London, 1974.
- [NSM] : NSM archive, *SiC: Effective Masses and Densities of States*, Ioffe Physical Technical Institute, St. Petersburg:
<http://www.ioffe.ru/SVA/NSM/Semicond/SiC/bandstr.html#Masses>
- [Ozpineci02] : B. Ozpineci, “System impact of silicon carbide power electronics on hybrid electric vehicle applications”, Ph.D. dissertation, The University of Tennessee, Knoxville, 2002.
- [Patrick62] : L. Patrick, “Inequivalent Sites and Multiple Donor and Acceptor Levels in SiC polytypes”, *Phys. Rev.* **127** (1962) 1878.

Bibliography

- [Pearson49] : G. L. Pearson, and J. Bardeen, “Electrical Properties of Pure Silicon and Silicon Alloys Containing Boron and Phosphorus”, *Phys. Rev.* **75** (1949) 865.
- [Pearson50] : G. L. Pearson, and J. Bardeen, “Erratum: Electrical properties of Pure Silicon and Silicon Alloys”, *Phys. Rev.* **77** (1950) 303.
- [Pensl93] : G. Pensl, and W. J. Choyke, “Electrical and optical characterization of SiC”, *Physica B* **185** (1993) 264.
- [Pernot01] : J. Pernot, W. Zawadzki, S. Contreras, J. L. Robert, E. Neyret, and L. Di Cioccio, “Electrical transport in *n*-type 4H silicon carbide”, *J. Appl. Phys.* **90** (2001) 1869.
- [Persson97] : C. Persson, and U. Lindelfelt, “Relativistic band structure calculation of cubic and hexagonal SiC polytypes”, *J. Appl. Phys.* **82** (1997) 5496.
- [Rao06] : S. Rao, T. P. Chow, and I. Bhat, “Dependence of the Ionization Energy of Phosphorus Donor in 4H-SiC on Doping Concentration”, *Mater. Sci. Forum* **527-529** (2006) 597.
- [Rogers70] : F. J. Rogers, H. C. Graboske, Jr., and D. J. Harwood, “Bound Eigenstates of the Static Screened Coulomb Potential”, *Phys. Rev. A* **1** (1970) 1577.
- [Rozen08] : J. Rozen, “Electronic properties and reliability of the SiO₂/SiC interface”, Ph.D. dissertation, Vanderbilt University, Nashville, 2008.
- [Ruff94] : M. Ruff, H. Mitlehner, and R. Helbig, “SiC Devices: Physics and Numerical Simulation”, *IEEE Trans. Electron Devices* **41** (1994) 1040.
- [Sagar91] : R. P. Sagar, “On the evaluation of the Fermi-Dirac integrals”, *Astrophys. J.* **376** (1991) 364.

Bibliography

- [Scaburri] : R. Scaburri, A. Desalvo, and R. Nipoti, "Simulation of the incomplete ionization of the n -type dopant Phosphorus in 4H-SiC, including screening by free carriers", *Mater. Sci. Forum* (in press).
- [Segall86] : B. Segall, S. A. Alterovitz, E. J. Haugland, and L. G. Matus, "Compensation in epitaxial cubic SiC films", *Appl. Phys. Lett.* **49** (1986) 584.
- [Shklovskii80] : B. I. Shklovskii, and A. L. Éfros, "Structure of impurity band in lightly doped semiconductors (review)", *Sov. Phys. Semicond.* **14** (1980) 487.
- [Shklovskii84] : B. I. Shklovskii, and A. L. Efros, *Electronic Properties of Doped Semiconductors*, Springer-Verlag, Berlin, 1984.
- [SILVACO00] : *ATLAS User's manual* (2 vol.), SILVACO International, Santa Clara, 2000.
- [Singh84] : D. Singh, and Y. P. Varshni, "Comparative study of the bound states of static screened Coulomb and cut-off Coulomb potentials", *Phys. Rev. A* **29** (1984) 2895.
- [Smith64] : C. R. Smith, "Bound States in a Debye-Hückel Potential", *Phys. Rev.* **134** (1964) A1235.
- [Sze07] : S. M. Sze, and K. K. Ng, *Physics of Semiconductor Devices*, Wiley-Interscience, Hoboken, 2007.
- [VanCong91] : H. Van Cong, "New series representation of Fermi-Dirac integral F_j ($-\infty < a \ll \infty$) for arbitrary $j > -1$, and its effect on $F_j(a \geq 0_+)$ for integer $j \geq 0$ ", *Solid-State Electron.* **34** (1991) 489.

Bibliography

- [VanCong92] : H. Van Cong, and B. Doan-Khanh, “Simple accurate general expression of the Fermi-Dirac integral $F_j(a)$ for arbitrary a and $j > -1$ ”, *Solid-State Electron.* **35** (1992) 949.
- [VanHalen85] : P. Van Halen, and D. L. Pulfrey, “Accurate, short series approximations to Fermi-Dirac integrals of order $-1/2$, $1/2$, 1 , $3/2$, 2 , $5/2$, 3 , and $7/2$ ”, *J. Appl. Phys.* **57** (1985) 5271.
- [Wang02] : R. Wang, I. B. Bhat, and T. P. Chow, “Epitaxial growth of n -type SiC using phosphine and nitrogen as the precursors”, *J. Appl. Phys.* **92** (2002) 7587.
- [Wellenhofer97] : G. Wellenhofer, and U. Rössler, “Global Band Structure and Near-Band-Edge States”, *phys. stat. sol. (b)* **202** (1997) 107.
- [Wigner33] : E. Wigner, and F. Seitz, "On the Constitution of Metallic Sodium", *Phys. Rev.* **43** (1933) 804.

Acknowledgements.

Firstly, I wish to thank my family, first of all my grandfather Pietro who made me appreciate the great beauty of science, starting from mathematics, when I was only a child. Unfortunately, he died before seeing me getting a degree in Physics: he would be proud of me if he were here. Then, I would like to thank my supervisors Maria Chiara Bignozzi, Agostino Desalvo and Roberta Nipoti for their professional and human qualities, for having had faith in me and patience in difficulties, for their continuous critiques and suggestions which were indispensable to this work. I thank the institute CNR-IMM, Bologna, for having fully granted this thesis and for the beautiful persons I met there. I thank also my colleague Anindya Nath, who demonstrated great humanity and professionalism: it was really stimulating working with him, when he was at IMM in Bologna. I would like to thank also all my friends for having encouraged and borne me, but the list would be too long and the risk to forget someone too great.